Biological Band-Aids: Design and Application of a Glycosaminoglycan-Peptide Conjugate to Regulate Cell-Cell Interactions During Acute Inflammation

By

TIMA DEHGHANI
DISSERTATION

Submitted in partial satisfaction of the requirements for the degree of

DOCTOR OF PHILOSOPHY

in

Biomedical Engineering

in the

OFFICE OF GRADUATE STUDIES

of the

UNIVERSITY OF CALIFORNIA

DAVIS

Approved:

_____

Alyssa Panitch, Chair

_____

Steven George

_____

Richard Perez

Committee in Charge

2021

For my parents, who taught me to be ambitious and resilient

ACKNOWLEDGEMENTS

This work would have not been possible without the support, encouragement, and mentorship of my family, friends, and academic advisors. While it would be impossible to list everyone who has supported me along the way, I'd like to highlight several whose contributions have been integral.

First, I'd like to thank my parents Ardavan and Kittrene for their never-ending encouragement, for fostering my curiosity for science, and for passing down the gene for relentless stubbornness and determination. I also thank my brothers Matt and Joe for their continual support and enthusiasm, and for finding the perfect word – coddiwomple – to describe my academic pursuits. Finally, thank you to my fiancé Scott for his endless encouragement, patience, and for believing in me even when I didn't believe in myself.

I would especially like to thank my advisor, Dr. Alyssa Panitch, for always believing in my project – and me – amid confusing or discouraging data. Thank you for trusting in my ability to tackle difficult problems, and for encouraging me to pursue my (sometime scattered) ideas. This degree would not have been possible without your support, patience, and guidance. I would also like to thank my other committee members, Dr. Steven George and Dr. Richard Perez for their expertise and guidance in my training, and for their critical and insightful feedback.

This work would have not been possible without my many collaborators, including Dr. Angela Haczku, Dr. Vasilios Morikis, Dr. James Wodicka, Dr. Scott Simon, Dr. Aijun Wang, Dr. Nipavan Chiamvimonvat, Dr. Phung Thai, Dr. Kit Lam, Chris Pivetti, and Ivonne Palma. Your expertise and contributions made complex experimental pursuits possible, and made an invaluable impact on my growth as a scientist and critical thinker.

UC Davis has been an incredible place to pursue a PhD. To the Biomedical Engineering Student Association (BESA), thank you for creating such a welcoming and fun environment for all students. To

Christal Wintersmith, I cannot thank you enough for your help and guidance over the years, and for all the work you do for the grad group.

There are several people I'd like to thank for their support, encouragement, feedback, and friendship throughout my time at UC Davis. Thank you to my friend and former labmate Dr. Tanaya Walimbe for helping me reason through experimental planning, for your words of encouragement, and for enabling my love of coffee. Thank you to my current and former labmates Laney Casella, Hark Sodhi, Katelyn Wiseman, Dr. Marcus Deloney, and Dr. Nelda Vazquez Portalatin for making our lab group such a fun and welcoming place. I am also grateful to my friends Dr. Amy Becker, Dr. Nuala del Piccolo, Dr. Charlotte Vorwald, Sarah Gaffney, and Matt Favetti for making Davis such an amazing place to live. Your friendship and adventures have made the past five years unforgettable.

Finally, I would like to acknowledge my funding sources that have supported my graduate work: TRDRP Predoctoral Fellowship, NSF PEGS 21, UC Davis STAIR Grant, Biomedical Engineering Graduate Fellowship, and Earle C. Anthony Fellowship.

ABSTRACT

After an acute inflammatory event such as a heart attack, stroke, or organ transplant, blood vessels and circulating immune cells take on a complex phenotype that, if dysregulated, can perpetuate disease. Adverse changes in endothelial phenotype, including glycocalyx shedding and upregulation of immune cell adhesion molecules (i.e., selectins), facilitate the recruitment and adhesion of circulating leukocytes (i.e., neutrophils) and platelets to the vessel walls. In some cases, this otherwise restorative physiological response devolves into a proinflammatory feedback loop; this process is shared among organ systems, enabling disease-agnostic drug discovery. Selectins are an attractive therapeutic target to inhibit the proinflammatory feedback loop; however, their low affinity for monovalent binding ligands and pivotal role in restorative inflammatory mechanisms has created a barrier to drug development. In addition, glycosaminoglycans such as dermatan sulfate (DS) have inherent anti-inflammatory properties that, if localized to a pro-inflammatory environment, can indirectly regulate immune cell adhesion by creating a steric, band-aid-like surface along inflamed endothelial cells.

Through the chapters of this dissertation, we introduce a novel selectin-binding glycosaminoglycan-peptide conjugate (DS-IkL) as a molecular "band-aid" to address multiple elements of endothelial dysfunction, including: selectin upregulation, glycocalyx shedding, and aberrant immune cell adhesion and influx. We show that DS-IkL localizes to inflamed vasculature, interferes with selectin-mediated cell complexing, reduces neutrophil extravasation into tissue, and has short- and long-term cardioprotective effects following an acute myocardial infarction. This work details the (i) discovery of a novel selectin-targeting peptide comprised of both L- and D-amino acids and its tunable conjugation to a DS polymer; (ii) functional characterization of DS-IkL's capacity to curb neutrophil binding, platelet activation, and fibrotic remodeling in *in vitro* and *in vivo* models; and (iii) preliminary exploration of the molecule's ability to interfere with the formation of platelet-neutrophil and platelet-neutrophil-endothelial cell aggregates. Overall, this work serves as a proof-of-concept demonstrating the potential of DS-IkL as a multifunctional anti-inflammatory therapeutic.

TABLE OF CONTENTS

LIST OF FIGURES

LIST OF TABLES

CHAPTER 1: INTRODUCTION

This chapter consists of a manuscript published by Dehghani T and Panitch A in *Open Biology*, Volume 10, Issue 10, 2020, https://doi.org/10.1098/rsob.200161.

1.1 Background and Significance

Severe fibrotic and thrombotic events permeate the healthcare system, causing suffering for millions of patients with inflammatory disorders. As late-state consequences of chronic inflammation, fibrosis and thrombosis are the culmination of pathological interactions of activated endothelium, neutrophils, and platelets after vessel injury. Coupling of these three cell types ensures a pro-coagulant, cytokine-rich environment that promotes the capture, activation, and proliferation of circulating immune cells and recruitment of key pro-fibrotic cell types such as myofibroblasts. As the first responders to sterile inflammatory injury, it is important to understand how endothelial cells, neutrophils, and platelets help create this environment. There has been a growing interest in this intersection over the past decade that has helped shape the development of therapeutics to target these processes. In this thesis, we review recent insights into how neutrophils, platelets, and endothelial cells guide the development of pathological vessel repair that can also result in underlying tissue fibrosis. We further discuss recent efforts that have been made to translate this knowledge into therapeutics, including the design and characterization of a novel selectin-targeted glycosaminoglycan-peptide conjugate, and provide perspective as to how compound or combination therapeutics may be most efficacious when tackling fibrosis and thrombosis that is brought upon by chronic inflammation.

1.2 Endothelial cells, neutrophils, and platelets as drivers of fibrosis

The peripheral vasculature is a complex continuum made up in part by a collagenous tunica externa, an elastic and smooth muscle-lined tunica media, and an endothelial monolayer making up the tunica

intima, or inner vessel lining. This structure differs slightly in the capillaries, which are composed of a tunica intima and basement membrane. Vascular integrity relies on a coordinated homeostasis of these dynamic components. As the inner lining of the blood vessel, the endothelium provides an interface between circulating blood components and the adjacent tissues and plays a particularly pivotal role in tissue damage and fibrosis. In response to vascular damage, metabolic disorders, or inflammation, endothelial cells prompt the recruitment of key inflammatory cells: platelets and neutrophils. Changes to endothelial morphology, chemokine production, and surface proteins foster a pro-inflammatory environment that mediates the mobilization of circulating immune cells such as polymorphonuclear neutrophils and platelets. In many circumstances, interactions between recruited neutrophils, platelets, and the endothelium lead to the resolution of vessel damage; indeed, inflammatory events are vial for proper wound healing (1). However, if inflammatory stimuli are persistent these interactions can tip the balance toward fibrotic healing.

The fibrotic response is the culmination of many chronic inflammatory diseases. Fibrosis is characterized as the accumulation of excess extracellular matrix (ECM) proteins, such as collagen and fibronectin. Although ECM deposition is a vital and largely self-restorative part of wound healing, repetitive or severe damage can cause pathological dysregulation of this process leading to fibrosis. Inflammation mediated by the innate immune response is a critical trigger of pathological fibrosis (2). In response to vascular damage or systemic and local inflammation, endothelium transitions from a quiescent state to a state called endothelial dysfunction, which in its severe form causes the exposure of underlying ECM such as collagen (3). Soluble pro-inflammatory factors such as reactive oxygen species (ROS) and matrix metalloproteinases (MMPs) are released by the endothelium (4, 5), recruiting circulating neutrophils to the scene. Neutrophils and circulating platelets tether to upregulated cell adhesion molecules that are expressed on inflamed endothelium, such as E-selectin, P-selectin, and von Willebrand Factor (vWF). This tethering initiates an inflammatory cascade that, if persistent, culminates as thrombotic vessel occlusion or fibrotic myofibroblast proliferation and ECM deposition. Left unchecked, excessive ECM deposition can result in impaired organ function and, in some cases, end-stage organ failure and death.

Given the influential roles endothelial cells, neutrophils, and platelets play in aberrant inflammation, thrombosis, and fibrosis, many studies have focused on elucidating mechanisms behind profibrotic and prothrombotic events in order to develop targeted therapeutics that interfere with these processes. These cell types have been of growing interest over the past decade, as is evidenced by the steady increase in relevant literature (**Figure 1-1)**. In this work, we detail how disruptions to the endothelium and its protective ECM layer, the glycocalyx, contribute to endothelial cell dysfunction, neutrophil and platelet dysregulation, thrombosis, and fibrosis. We discuss the promise and limitations of therapeutic strategies for limiting neutrophil and platelet mediated fibrosis.

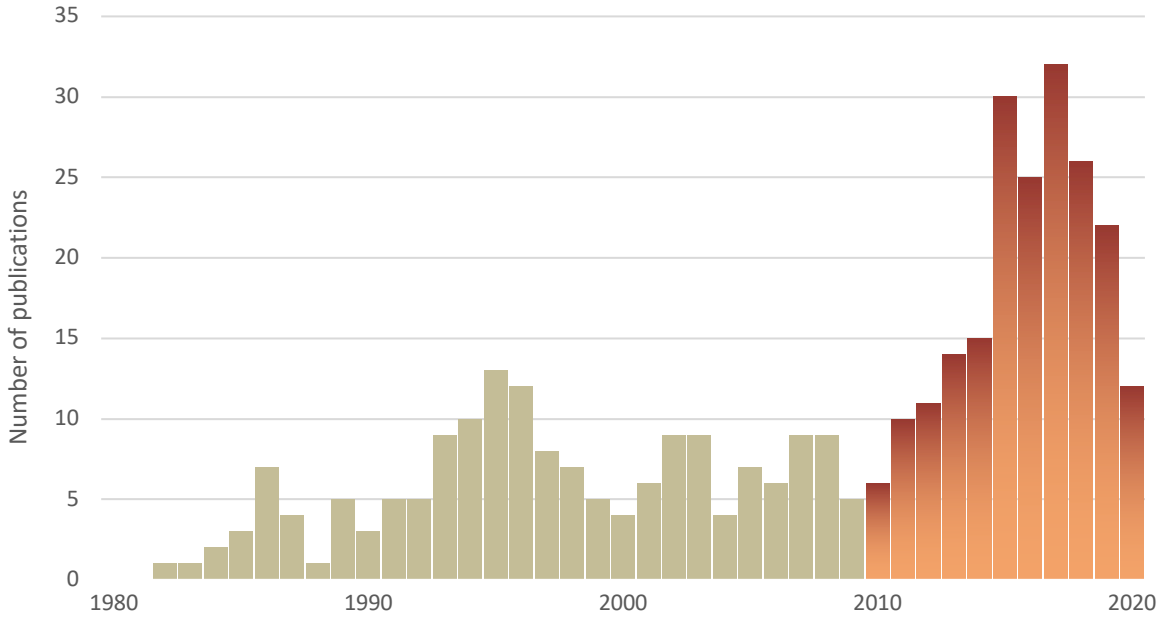

Figure 1-1 PubMed search results since 1980. A PubMed literature search for the years 1980-2020 was conducted for the following key terms: neutrophil, platelet, endothelial, and thrombosis or fibrosis. Results were further narrowed down to the years 2010-2020, during which the number of publications per year steadily increased. Publications were screened for titles relevant to topics discussed in this review.

1.2.1 Endothelial Dysfunction Within the Scope of Inflammation

The blood vessels are a conduit for immune cell trafficking in response to tissue damage. Amid differences in vessel composition, elasticity, size, and stiffness, all blood vessels are lined by an inner layer of endothelium. The vascular endothelium is made up of a heterogenous continuum of individual

endothelial cells that reside on a bed of collagen-rich ECM (6). As its most basic function, the endothelium acts as a physical barrier between circulating fluids and the surrounding tissues. For many years, this was believed to be the sole purpose of the endothelium. It is now well accepted that the endothelium is a complex, bioactive cell layer that regulates immune cell function and tissue access, vasoreactivity, and the extravasation of macromolecules, solutes, hormones, and fluids (7). Endothelial cell health plays a precarious role in chronic inflammatory and thrombogenic diseases, including diabetes (8), atherosclerosis (4, 9), acute respiratory distress syndrome (10), cystic fibrosis (11), and liver cirrhosis (12). Damage to the endothelium initiates and sustains inflammation and thrombogenesis (7), with endothelial cells themselves providing a platform to fast-track thrombosis during dysregulated haemostasis, and fibrosis during pathological wound repair.

The endothelium is lined by a thin, glycosaminoglycan-rich barrier called the endothelial glycocalyx. The glycocalyx is a dynamic participant in endothelial cell barrier function and immune regulation (13). Structurally, the glycocalyx ranges from nanometres to several micrometres thick, depending on the vessel type, location within a vessel, conditions, and the imaging technique used (14, 15). Even within one vessel, the glycocalyx is a heterogenous structure (16). The glycocalyx is comprised of a glycoprotein or proteoglycan core protein anchored to underlying actin cytoskeletal filaments at the endothelial surface (13, 17). While the luminal portion of a glycoprotein is decorated with small sugar residues, the proteoglycan core, primarily from the syndecan and glypican families (16, 18), extends into the vessel lumen and is decorated with glycosaminoglycans (GAGs) such as heparan sulphate, chondroitin sulphate, hyaluronan, and dermatan sulphate. GAG components, particularly heparan sulphate and dermatan sulphate, possess anticoagulant and antithrombotic qualities (19, 20) that have been leveraged as therapeutics (21-24). Though heparan sulphate makes the greatest contribution to glycocalyx thickness, heterogeneity within the glycocalyx suggests that each GAG contributes to glycocalyx function and vessel permeability (25).

Under healthy conditions, the glycocalyx exists in dynamic equilibrium with circulating blood, changing its composition and thickness in response to hemodynamic forces and cues from soluble factors (26) in order to maintain equilibrium between hydrostatic and oncotic forces in the vessel (27). Changes to the rheological environment are detected by the glycocalyx (28) and transduced to the underlying endothelium via actin anchoring. The actin cytoskeleton and the glycocalyx exist in a dynamic equilibrium with one another, each being modified in response to changes in the other to control endothelial barrier properties (29, 30). Indeed, mechanical stress has been shown to alter GAG and proteoglycan synthesis and remodelling in vascular endothelial cells (31, 32), lending insight into how pathological stretch and disturbed flow can influence endothelial cell behaviour and function.

After physical, local, or systemic inflammatory insult, damaged endothelium exhibit signs of endothelial dysfunction. Endothelial dysfunction is a complex phenomenon involving heightened reactive oxygen species (ROS) production, altered nitric oxide (NO) production and disruptions to vascular tone; production of MMPs and pro-inflammatory cytokines; and upregulation of cell adhesion molecules such as E-selectin, P-selectin, and intracellular adhesion molecule-1 (ICAM-1) (4, 5, 33, 34). MMPs and ROS facilitate glycocalyx degradation and shedding, causing impaired mechanosensing and altering cell behaviour (22, 28, 35) to enable immune cell capture and trafficking (26, 36-39). Compromised mechanosensing can in turn perpetuate reductions in shear-sensitive NO secretion and augment vascular permeability. Paired with the release of sequestered chemokines and the exposure of immune cell adhesion molecules along the endothelial surface, glycocalyx degeneration facilitates inflammation, thrombosis, and eventual fibrosis by promoting immune cell migration into the underlying tissue (40, 41).

Dysfunctional endothelium plays an interesting role in perpetual inflammation. While in a dysfunctional state, endothelial cell senescence is accelerated and migration is hindered (31, 42). In damaged vessels, the inability to replenish the endothelial layer with healthy cells results in a prolonged inflammatory attack. Even when reendothelialization can occur, newly formed glycocalyx is fragile and less responsive to shear (26), and readily concedes to the inflammatory state. Further exacerbating the

dysfunctional state, circulating platelets bind to collagen, which normally resides below the surface of the endothelium (6, 43), but is exposed between contracting cells (44) or is revealed after vessel denudation (45). In some cases, adherent platelets induce a pro-fibrotic cascade involving platelet-mediated leukocyte recruitment, tissue factor secretion, and fibrin(ogen) deposition (46, 47).

1.3 Drivers of platelet-neutrophil aggregation, endothelial dysfunction, and fibrosis

Inflammatory stimulus and vessel choice influence the relative contributions of platelets, neutrophils, and endothelial cells to inflammation, thrombosis, and fibrosis (48) (**Figure 1-1**). Here we discuss recent insights into how these three cell types collaborate to exacerbate inflammation, thrombosis, and fibrosis.

1.3.1 Endothelial Cells

As the lining of the conduits of blood components, metabolites, and immune cells, the vascular endothelium is often on the front line in an inflammatory insult. A major source of endothelial inflammation is the overproduction of reactive oxygen species (ROS), whose aetiology can range from diet, to hormone dysregulation, to cellular by-products such as those produced during macrophage digestion of apoptotic debris and foreign substances (34). Excess ROS inactivates nitric oxide (NO) production – a known mediator of vascular tone. Reduced NO enhances vessel stiffness and contractility, both of which contribute to endothelial dysfunction (4). Paradoxically, NO overproduction can likewise induce cellular inflammation and apoptosis (57), highlighting the importance of maintaining tight regulation of homeostasis.

Table 1-1 Endothelial injury methods and outcomes

VESSEL OR CELL TYPE	INJURY METHOD	KEY OBSERVATIONS	REFERENCES
Cremaster arteriole	Laser activation	Laser activated endothelial cells trigger thrombus formation; neutrophil slow rolling on thrombus mediated by P-selectin/PSGL-1	(49)
Cremaster arteriole and HUVEC	Laser activation	Endothelial activation precedes platelet accumulation; normal fibrin formation observed in Par4$^{-/-}$ mice	(50)
Cremaster arteriole	Laser activation	Prothrombinase found on activated endothelial cells	(51)
Cremaster arteriole	Laser activation	Neutrophils contain and express tissue factor at the site of laser injury; neutrophils accumulated before platelets	(52)
Venule	TNF-α	TNF-α activated endothelial cells recruit neutrophils; platelets bind adherent neutrophils rather than endothelium	(49)
Artery and HUVEC	TNF-α and IFN-γ	Fractalkine causes degranulation, activation, and expression of platelet P-selectin on adherent platelets, mediating neutrophil recruitment	(53)
HUVEC	TNF-α	Endothelial TF drives fibrin deposition and coagulation; upregulated ICAM can be targeted for delivering recombinant thrombomodulin to inflamed cells	(47)
Cremaster arteriole	CCL2, TNF-α, IL-1β, or IFN-γ	Platelets guide neutrophils to extravasation points via P-selectin/PSGL-1 and CD40/CD40L	(54)
Artery and HUVEC	ApoE$^{-/-}$ mice	Increased endothelial stiffness causes enhanced leukocyte transendothelial migration	(55)
Artery	ApoE$^{-/-}$ mice	Reduced glycocalyx thickness and increased platelet adhesion occur at bifurcation point	(56)
Artery	ApoE$^{-/-}$ mice	Endothelial dysfunction and glycocalyx impairment coincide with endothelial-dependent vasodilation, permeability, and increases in atherosclerotic biomarkers	(4)

HUVEC, human umbilical vein endothelial cells; PSGL-1, P-selectin glycoprotein ligand-1; Par4, protease activated receptor 4; TNF-α, tumour necrosis factor alpha; IFN-γ, interferon gamma; CCL-2, C-C motif chemokine ligand 2; IL-1β, interleukin-1 beta; ApoE, apolipoprotein E, TF: tissue factor.

Endothelial cytoskeletal structure and stiffness play a critical role in leukocyte recruitment and fibrosis. TNF-α stimulated endothelial cells present a cortical stiffness gradient to slow-rolling neutrophils, guiding them to transmigration sites (55). This effect is augmented on stiff matrices (55, 58), consistent with neutrophil recruitment and extravasation in atherosclerotic vessels (9). Pro-fibrotic cellular pathways

such as the autotaxin/lysophosphatidic acid axis likewise stimulate endothelial actin rearrangement and cell contractility, causing vascular leak and aiding in the migration of fibroblasts in the underlying tissue (59). Structural alterations of the cytoskeleton affect glycocalyx distribution and function (29), further exacerbating endothelial dysfunction and vascular damage.

Dysfunctional endothelial cells are known initiators of fibrosis. In response to noxious stimuli such as excess ROS, lipopolysaccharide (LPS), bleomycin, or physical damage, dysfunctional endothelial cells secrete a milieu of pro-inflammatory cytokines including TNF-α, IL-1β, and IL-6 (2). TNF-α initiates a signalling cascade that can lead to endothelial apoptosis or necrosis (60). Surviving endothelial cells begin to shed their glycocalyx, unmasking upregulated selectins and integrin-binding ligands embedded within the cell membrane (61). In the venules, selectins act as the initial point of neutrophil capture (62), which can then act as secondary capture sites for circulating platelets (49). Bleomycin-induced pulmonary fibrosis exemplifies the potential pathological response once the endothelium becomes inflamed. In one representative study, bleomycin-induced pulmonary endothelial inflammation resulted in a peak in endothelial inflammation at 7 days post-bleomycin instillation; enhanced vWF, plasminogen activator inhibitor-1, MMP-12, and NO led to increased collagen deposition and pulmonary fibrosis, peaking at day 21, clearly delineating the link between endothelial dysfunction and fibrosis (57).

Similarly, studies using alternative stimuli have evidenced endothelial cells as sources of tissue factor (TF) (47, 50, 63), a protein that is primarily secreted by activated monocytes to initiate platelet deposition and thrombin formation (64) and thereby actuate thrombogenesis and tissue fibrosis (65, 66). Endothelial derived TF has been reported in response to TNF-α (47, 63) and laser activation (50, 51), a technique which can elicit endothelial activation without vessel denudation that has been used as a model of vascular thrombosis and atherosclerosis (67). Endothelial TF has been shown to cause fibrin deposition, upregulation of ICAM-1 and VCAM-1, and increased platelet binding. Atkinson et al. demonstrated that endothelial activation, calcium mobilization, and granule secretion precede platelet accumulation in cremaster arterioles (50). Notably, fibrin production persisted on activated HUVECs upon treatment with

platelet depleted plasma, further validating endothelial cells as a source of TF. Ivanciu and colleagues later observed enhanced prothrombinase activity on similarly activated endothelium, reinforcing the idea that activated endothelium forms a pro-coagulant surface that supports thrombus formation after injury (51).

Link to the Inflammatory Triangle

Despite similar methods of endothelial activation, there is a lack of consensus regarding the main source of TF produced in response to vessel damage. Contrary to the results described above, leukocytes have been demonstrated as the first responders to endothelial activation. Adherent leukocytes express TF and create a platform for platelet binding (52). In a separate study, neutrophil rolling and adhesion was observed only after platelet thrombi had formed, with rolling mediated by platelet P-selectin and neutrophil P-selectin glycoprotein ligand-1 (PSGL-1) (49), suggesting multiple factors are likely at play, orchestrating the timing and sequence of events.

While it is clear all three cell types work in coordination to address vessel damage, more studies are needed to elucidate mechanisms behind thrombo-inflammation in models of cytokine, bacterial, and physical damage. Understanding these mechanisms may allow for the development of more targeted therapeutics to combat vascular inflammation and fibrosis, for example targeting endothelial – but not leukocyte or platelet – derived TF, or selectively upregulated cell adhesion molecules. Further investigation into these mechanisms from the perspective of neutrophils and platelets follows.

1.3.2 Neutrophils

Neutrophils play a paradoxical role in inflammation. The neutrophil recruitment cascade is a conserved process that is integral to the resolution of inflammation, infection, and wound healing (68). However, pathological activation of neutrophils perpetuates acute and chronic inflammatory diseases. Pathological neutrophilia in response to cytokine storm is observed in rheumatic diseases, as well as infectious diseases such as coronavirus pneumonia seen in severe acute respiratory syndrome (SARS),

Middle East respiratory syndrome (MERS), and coronavirus disease 2019 (COVID-19) (69, 70), leading to irreversible tissue fibrosis or necrosis.

We have known for decades that neutrophil engagement exacerbates endothelial activation (71) and collagen synthesis (72). Neutrophils are recruited to the endothelial surface in response to endothelial cues after cellular activation. As previously described, endothelial cells release a milieu of pro-inflammatory stimuli upon damage such as ROS, TNF-α, IL-1β, and MMPs that degrade the endothelial glycocalyx and recruit circulating neutrophils to the damaged area. Tethered neutrophils roll along the endothelial surface, stabilized by shear-strengthening, transient catch bonds between endothelial E/P-selectin, CD44, and neutrophil PSGL-1 (61, 73). E/P-selectin engagement directs neutrophil signalling by stimulating an intracellular neutrophil calcium burst (74, 75) and augments chemokine signalling to activate neutrophil β2 integrins, leading to cell arrest, migration into the underlying tissue, and further neutrophil recruitment.

With the exception of the pulmonary system, in which cell recruitment occurs at the capillaries (76, 77), veins and post-capillary venules act as the primary capture sites for neutrophils during inflammatory damage, though arterial recruitment has been observed after physical vessel damage by laser activation (49-52, 78). This unequal involvement is perhaps due to differences in junctional proteins that result in increased intrinsic leakiness within the venules, selectin and ICAM-1 expression, shear stress and flow mechanics, and gene expression (7, 79). In the venules, TNF-α and LPS activation quickly result in neutrophil adhesion to the vessel wall (48, 49, 80, 81). Adherent and activated neutrophils secrete endothelial barrier disrupting molecules such as ROS and release of neutrophil degranulation products including myeloperoxidase, elastase, and metalloproteases (82), facilitating migration through the endothelium.

Further damage can be caused by neutrophil extracellular trap (NET) production. Coordinated PSGL-1 (83) and CXCR2 (73) signalling leads to enhanced neutrophil adhesion, NET formation, and flow restriction. While their primary function is to trap pathogens, NETs have been shown to enhance

inflammation and endothelial permeability and have been implicated in several inflammatory diseases (82). Further, NETs are known to trap platelets, red blood cells, and fibrin, fostering the growth of pathological thrombi. NETs are drivers of vascular damage, venous thrombosis (73, 84), and virus-induced organ damage and mortality, as is seen in severe COVID-19 (69, 85).

Link to the Inflammatory Triangle

Neutrophil-mediated fibrin deposition and thrombosis can occur even in the absence of exogenous inflammatory stimuli or direct endothelial cell damage, such as in a murine stenosis model of deep vein thrombosis (DVT). In this model, the endothelium remains intact and the underlying collagen-rich ECM unexposed, but altered blood flow by partial vessel occlusion is enough to cause cooperative signalling by neutrophils at the endothelial surface that initiates fibrin formation and propagates venous thrombosis (73, 84). Once bound to the endothelium, neutrophils physically alter the rheological environment within the vasculature by creating an altered flow pattern near the vessel wall (48). Drag forces grab circulating platelets and bring them toward the surface of the neutrophil, allowing molecular interactions between platelet and neutrophil. Interestingly, NETs have also been implicated in DVT and likely exacerbate neutrophil-mediated thrombosis (86).

This relationship between rheological haemostasis and thrombosis aligns with atherosusceptible vascular regions such as vessel branches, where blood flow patterns are disturbed (87). However, rather than disturbed flow causing endothelial activation, activated neutrophils cause rheological changes that promote platelet adhesion and vessel activation. It is evident that the interplay between neutrophil, endothelial, and platelet activation cannot be reduced to a single initiator of thrombosis, vessel stenosis, or tissue fibrosis. Therefore, while blocking neutrophil-vessel interactions has shown therapeutic promise in reducing neutrophil-mediated vessel damage (81, 88-92), pro-inflammatory neutrophil-platelet interactions are a compelling target for emerging therapeutics (93).

1.3.3 Platelets

Platelets are cell fragments of megakaryocytes that govern the haemostatic resolution of vascular wounds (94, 95). Thrombocytopenia and platelet depletion caused by genetic deficiencies or anticoagulants can provoke disorders such as haemophilia and interfere with the proper resolution of infection (96) and inflammation (97-99). More recently, platelets have been recognized as drivers of inflammatory damage, working alongside circulating neutrophils to perpetuate inflammation (93, 100, 101). During severe vessel damage, endothelial cell death (102) or vessel denudation (45) causes the exposure of underlying ECM. Circulating platelets readily bind to and activate on exposed collagen-rich ECM that lies beneath the endothelial layer to create a platelet plug.

While platelet plugs are vital for maintaining haemostasis within an injured vessel (103), in some cases the haemostatic response can quickly become imbalanced by infiltrating immune cells, shifting the plug from haemostatic to thrombotic. In a haemostatic platelet plug, densely packed P-selectin positive platelets and a fibrin network form an ultra-dense thrombus core surrounded by more loosely packed P-selectin negative, minimally activated platelets at the luminal surface (103, 104). Once the healing cascade is compromised and thrombus formation becomes pathogenic, smaller vessels such as arterioles, capillaries, and post-capillary venules are at a greater risk of occlusion and resultant tissue ischemia due to thrombi taking up a larger relative proportion of the vessel (7, 46, 105). Platelet thrombi formed after traumatic or ischemia-reperfusion injury can release the α-granule chemokine neutrophil-activating peptide 2 (NAP-2) to recruit circulating neutrophils to the injury site. These thrombi then act as migration points for circulating neutrophils (106), driving tissue fibrosis.

Link to the Inflammatory Triangle

Adherent platelets have also been shown to guide neutrophils to inflammatory sites (54, 107) or act as anchor points for secondary capture of circulating neutrophils (49, 53, 108-110). This is especially apparent in arteries, where adherent platelets may be necessary for neutrophil recruitment (53), perhaps due

to high shear forces in the artery (7). In addition to facilitating capture, activated platelets and platelet derived soluble factors such as extracellular vesicles (111) can act as drivers of neutrophil and endothelial activation (83, 102, 110, 112-114) and affect their migration behaviour (115). Platelet-neutrophil-endothelial cell interactions are influenced by several factors, including the P-selectin-PSGL-1 axis (49, 53, 73, 114, 116-118) via phosphodiesterase type-4 (109) or Src family kinases (110, 119), and the vWF-Glycoprotein Ibα axis (48, 84). Similar to endothelial cells and neutrophils, shear stress seems to be a critical factor in achieving physiologically relevant platelet activation (120).

Upon activation, endothelial cells release Weibel-Palade bodies to the vascular surface. Weibel-Palade bodies are secretory granules that store platelet adhesion ligands P-selectin and vWF. Now available, P-selectin and vWF recruit additional circulating neutrophils and platelets (118), causing greater platelet and neutrophil recruitment and further aggravating the endothelium. In regions of endothelial denudation, this recruitment can be beneficial for wound healing (99); however, when uncontrolled it can also lead to irreversible fibrotic damage.

1.3.4 Implications in Tissue Fibrosis

Paradoxically, immune cells recruited for repair can potentiate damage if the inflammatory stimulus is not resolved. Activated leukocytes, platelets, and leukocyte-platelet complexes have been implicated as drivers of pulmonary and cardiovascular fibrotic diseases (121, 122). While not typically considered centre stage in fibrosis, dysregulated platelet and neutrophil accumulation play a critical role in aberrant tissue repair (123). Platelet activation and degranulation is associated with myofibroblast proliferation and the overactive deposition of ECM components that results in tissue fibrosis (124). Furthermore, activated platelets secrete large quantities of chemokines that are chemotactic for neutrophils and monocytes, triggering immune cells to migrate, activate, and produce additional cytokines and enzymes that stimulate the production of transforming growth factor-β (TGF- β), a key mediator of myofibroblast formation, collagen deposition, and fibrosis (125, 126).

Neutrophil migration along activated endothelium is one of the first steps toward the resolution of acute inflammation; however, without proper clearance, neutrophil accumulation causes sustained, chronic inflammation. Extravasating neutrophils are activated by ECM proteins, leading to injury and remodelling of the surrounding tissue (127), as is seen in chronic obstructive pulmonary disease and atherosclerosis (128). Excessive neutrophil activation, degranulation, and respiratory burst activity damages surrounding tissues (129), in part by the release of matrix degrading MMPs, toxic mediators such as ROS and reactive nitrogen species (2), and pro-inflammatory cytokines that activate and recruit other immune cells such as macrophages and T-lymphocytes. The reparative action by myofibroblasts in response to matrix degradation leads to formation of a dense, disorganized fibrotic tissue (124).

1.4 Clinical Manifestations

Several profibrotic diseases have been linked to perturbations in the proposed inflammatory triangle. Select disease states are briefly discussed below.

1.4.1 Lung Disease

The lungs are a particularly interesting platform for studying aberrant neutrophil-platelet interactions. Platelets have been shown to support recruitment and activation of neutrophils in the pulmonary capillaries in abdominal sepsis (123), acute lung injury (124), acute respiratory distress syndrome (124)(130, 131), and allergic inflammation (125). Elevated platelet activation indices have been reported in idiopathic pulmonary fibrosis (IPF) patients (139), with anti-platelet drugs showing promise in alleviating IPF by reducing platelet activation and platelet-mediated neutrophil infiltration (140). Recent insights into IPF have suggested that imbalanced endothelial activation plays a vital role in disease pathogenesis. Activated endothelium has been shown to secrete microparticles (132) and chemokines such

as IL-8 into circulation, augmenting neutrophil recruitment and activation (133). While the mechanisms underlying IPF are still unknown, vascular contributors such as these are an encouraging target.

1.4.2 Neointimal Hyperplasia

Endothelial denudation, as occurs after balloon angioplasty and severe inflammatory damage (102), presents a unique environment for platelet-neutrophil interactions. Under these conditions, circulating platelets bind to and activate on exposed collagen (44, 46, 109, 134, 135) and release extracellular vesicles that have been shown to influence neutrophil activation states, causing upregulation of platelet receptor CD41 (111). Intimal hyperplasia, or fibrosis within the artery itself, has been clearly linked with increased inflammation (136). This, in conjunction with studies relating platelet-mediated neutrophil binding and activation with thrombosis (49, 54, 102, 108, 109), suggests that more complex or combinatorial therapeutics are needed to reduce platelet- and neutrophil-mediated tissue damage.

1.4.3 COVID-19

Vascular inflammation and associated cytokine storm are known contributors to COVID-19 morbidities. These events are in part characterized by immune cell infiltration, NET formation (85), and dysregulated platelet activation (137), leading to hypercoagulopathy and vascular complications. Despite their role in hypercoagulopathy and the formation of pathogenic platelet-neutrophil complexes in this disease, platelets have paradoxically been shown to preserve endothelial integrity in severe COVID-19, with thrombocytopenia being associated with the impairment of platelet-dependent endothelium-protective mechanisms (138, 139). Therefore, as we learn more about this disease it will be important to distinguish between restorative and noxious immune cell activation states when developing treatments.

Ventilator-induced damage likewise imbalances the inflammatory triangle. Severe COVID-19 patients that have developed ARDS require mechanical ventilation; while a necessary therapy, mechanical ventilation has been associated with exacerbated lung damage, referred to as ventilator-induced lung injury

(VILI) (140, 141). Neutrophil infiltration and NET formation are elevated in patients with VILI (140), in part due to platelet-endothelial interactions. Platelets have been reported to contribute to neutrophil recruitment in VILI by presenting leukocyte-binding proteins at the endothelial surface (142, 143). It is likely that ventilator-induced lung injury and inflammation-induced damage go hand-in-hand in these patients, with platelet-neutrophil interactions exacerbating cytokine storm related morbidities.

1.5 Therapeutic Advances

As initiators of the fibrotic cascade, neutrophils, platelets, and activated endothelium have been investigated as potential therapeutic targets to combat vascular injury and occlusion and prevent the progression of fibrosis. For other vascular indications, established therapeutics such as rosuvastatin (statin; slows cholesterol production) (144) and ticagrelor (blood thinner; anti-platelet medication) (145) have exhibited a capacity to limit neutrophil binding, platelet aggregation, and neutrophil-platelet aggregates and are discussed elsewhere (145-148). Here we focus on efforts to protect or regenerate the glycocalyx, and select mediators of endothelial, neutrophil, and platelet induced inflammatory damage.

1.5.1 Glycocalyx Protection

While essential for healing processes, the inflammatory response can be devastating for damaged endothelium and underlying tissue if not kept under control. A pathological inflammatory response can lead to immune cell influx, altered vascular and tissue remodelling, and irreversible fibrotic damage, as is seen in ischemia reperfusion injury (149) and acute lung injury (150). As a regulator of endothelial health, the inflammatory response, and vascular permeability to macromolecules and immune cells, the endothelial glycocalyx presents a promising therapeutic target for a wide range of diseases without sacrificing the healing component of inflammation (151). Here we discuss recent efforts at preserving the glycocalyx that

have shown promise in reducing vascular and underlying tissue damage. For a comprehensive review on glycocalyx preserving molecules, we refer the reader elsewhere (152, 153).

Established drugs have been repurposed to combat glycocalyx damage and subsequent leukocyte and platelet adhesion, as is the case with the general anaesthetic sevoflurane. This drug is thought to function in part through upregulation of sialyltranferase, which in turn catalyses the transfer of sialic acid, an important mediator of oxidative stress (38, 154). Sevoflurane has shown promise in glycocalyx preservation in animal models of pulmonary ischemia reperfusion during lung transplant (155), cardiac ischemia/reperfusion (156), and aortic damage by H_2O_2 (154), although limited efficacy has been shown in humans (157, 158).

GAGs and proteoglycans such as heparin and heparan sulphate have shown promise as glycocalyx protecting therapeutics for many years (159). Unfractionated and low molecular weight heparin are best known for their anticoagulant properties and use in treating or preventing thrombotic events by activating antithrombin III (160). However, heparin has further been shown to possess anti-inflammatory properties, lending to improved vascular outcomes after inflammatory damage by limiting vascular permeability (161), neutrophil adherence and migration (63, 162), and platelet adhesion (163), fibrin deposition (63), and thrombus formation (92, 164, 165). As one of the oldest anticoagulants in clinical medicine, heparin and heparin-like products have been heavily studied (165-169). More recently, low molecular weight heparin has been used to treat coagulopathy seen in severe COVID-19 patients (97, 170, 171), and nebulised unfractionated heparin is currently being evaluated in clinical trials for acute lung injury (171) and COVID-19 (ACCORD 2: A Multicentre, Seamless, Phase 2 Adaptive Randomisation Platform Study to Assess the Efficacy and Safety of Multiple Candidate Agents for the Treatment of COVID 19 in Hospitalised Patients, EudraCT number 2020-001736-95) (171). While risks of thrombocytopenia and haemorrhagic shock limit the clinical use of this drug for inflammatory indications in its standard form, non-anticoagulant mechanisms of heparin are a promising pivot point for heparin-derived therapeutics (172).

Other promising molecules include sphingosine-1-phosphate and sulodexide. The signalling triggered by sphingolipid sphingosine-1-phosphate has been described as glycocalyx protective (173). When paired with heparan sulphate, sphingosine-1-phosphate has been shown to regenerate the glycocalyx and restore inter-endothelial communication (21). Sphingosine-1-phosphate analogues and receptor modulators have been tested clinically for a range of autoimmune and inflammatory diseases, including multiple sclerosis, psoriasis, acute stroke, and inflammatory bowel disease (174, 175). However, prolonged exposure to sphingosine-1-phosphate has also been shown to enhance vascular leak and fibrosis after lung injury (176), therefore caution should be taken before employing sphingosine-1-phosphate modulating drugs to different organ systems and disease indications.

Sulodexide is a decades-old glycosaminoglycan mixture made up of 80% fast-moving heparin (iduronylglycosaminoglycan) and 20% dermatan sulphate that mitigates the bleeding risk of heparin-only therapeutics while maintaining antithrombotic potential (177, 178). Originally used for cardiac indications such as myocardial infarction (179), Sulodexide has since been extended to other vascular disorders that manifest as endothelial dysfunction and glycocalyx damage, such as in type-2 diabetes mellitus patients (180) and in patients with venous ulcers (181). Sulodexide has been shown to promote glycocalyx regeneration and improve animal survival after severe sepsis (22) and reduce the levels of collagen degrading MMP9 in patients with chronic vascular disease (24).

Taken together, the benefits seen with this class of molecules with respect to decreased neutrophil and platelet adhesion further suggest that restoring function of the critical endothelial glycocalyx barrier can improve outcomes for fibrotic and thrombotic diseases that result from overexuberant interactions between endothelial cells, platelets, and neutrophils.

1.5.2 Cytokine inhibitors

Recombinant human cytokines and cytokine receptors have been used as therapeutic targets to modulate inflammatory activity, driven in part by the pain patients experience as a result of acute and

chronic inflammatory diseases (182, 183). Three core pro-inflammatory cytokines have been of particular interest in this realm: TNF-α, IL-1β, and IL-6. These cytokines act as key inducers of endothelial activation, neutrophil accumulation and activation, and platelet adhesion and degranulation, suggesting potential benefit of inhibitors in regulating endothelial activation and the downstream consequences of endothelial dysfunction. There are currently several FDA approved TNF-α, IL-1, and IL-6 inhibitors for clinical indications such as rheumatic diseases, Crohn's disease, and Cryopyrin-Associated Periodic Syndromes (CAPS) (184).

TNF-α blockers have been successfully employed to combat fibrotic indications such rheumatoid arthritis and psoriasis (185, 186); unfortunately these benefits are not ubiquitous for all fibrotic diseases, as was evidenced by their ineffectiveness against idiopathic pulmonary fibrosis (187). Anti-TNF-α therapies for chronic heart failure have likewise been tested in clinical trials with little success (188), and potential beneficial effects on endothelial function in patients with inflammatory arthropathies are inconsistent (189).

IL-1β antagonists have shown greater potential in vascular inflammatory disorders, perhaps in part due to the integral role of IL-1 in leukocyte and endothelial signalling. The FDA approved IL-1 agonists canakinumab (originally approved for CAPS), anakinra (originally approved for rheumatoid arthritis), and rilonacept (originally approved for CAPS) have shown promise in clinical trials of cardiovascular conditions such as pericarditis and recurrent ischemic events after myocardial infarction (190, 191), but thus far none have been approved for these indications.

IL-6 is known to promote endothelial cell dysfunction and regulate leukocyte recruitment to the vascular wall (192); therefore, it is unsurprising that FDA approved IL-6 blockers for arthritic conditions are of interest for treating off-label inflammatory conditions such as systemic sclerosis. Clinical trials of tocilizumab and sarilumab have recently begun as treatment for "cytokine storm" related morbidities in severe SARS-CoV-2 patients (70, 193). The anti-IL-6 receptor tocilizumab is particularly promising, as it has been shown to cause transient neutropenia without impairing host defence (194).

While cytokine inhibitors and cytokine receptor blockers may be beneficial in certain inflammatory conditions, the mixed results of this class of molecules suggests the need for combination therapies, or therapies more directed at the key cellular interactions.

1.5.3 Collagen Protection

Severe endothelial damage can cause the exposure of the underlying collagen matrix, prompting rapid platelet adhesion. As described in this review, activated endothelium and collagen-adherent platelets provide an adhesive surface for neutrophil recruitment, eventually leading to tissue fibrosis; therefore, targeting exposed collagen could enhance anti-neutrophil/platelet therapies.

Several groups have designed collagen-targeting therapeutics to discourage platelet and/or neutrophil accumulation. Paderi and colleagues designed a proteoglycan mimetic consisting of collagen binding peptides conjugated to a dermatan sulphate backbone that bound collagen, but not endothelium, of denuded arteries after balloon angioplasty (45). Their therapeutic reduced *in vivo* platelet-induced vasospasm in the femoral artery as well as whole blood and platelet binding *in vitro*. Further, their studies showed that reduced platelet binding the arterial wall correlated with reduced fibrosis or neointimal hyperplasia *in vivo*.

Similarly, McMasters et al. designed a thermoresponsive collagen-binding nanoparticle for effective systemic delivery of a mitogen-activated protein kinase activated protein kinase 2 (MK2) anti-inflammatory peptide (43). The authors show that nanoparticle delivery of the MK2 inhibitor *in vitro* reduced cellular binding to collagen surfaces, IL-6 levels in endothelial cells and smooth muscle cells, and platelet activation on a collagen matrix. Additional nanostructures have been developed to aid in drug delivery to exposed collagen. Collagen IV targeting nanoburrs (195) and nanofibers (196, 197) have been designed to target angioplasty injured vasculature (195) and atherosclerotic plaques (197).

1.5.4 P- and E-Selectin

Rather than targeting platelet deposition on denuded endothelium, Totani et al. have focused on preventing neutrophil deposition on adherent platelets (109), thereby reducing the likelihood of thrombosis within the vessel. Blockade of phosphodiesterase type-4 by rolipram, originally an anti-depressant drug, caused a reduction in neutrophil binding to fixed, activated platelets *in vitro* as well as adherent neutrophils along the denuded femoral artery *in vivo*. Adhesion was likewise lost on untreated P-selectin deficient platelets, further suggesting P-selectin as a mediator of platelet-neutrophil interactions.

P-selectin has been a focal point in anti-inflammatory therapeutics due to the substantial role it plays in endothelial signalling, neutrophil and platelet recruitment to inflamed endothelium, and the formation of platelet-leukocyte aggregates. Competitive inhibitors of P- and E-selectin and their binding partners, PSGL-1, CD44, and E-selectin ligand 1, have been investigated as antagonists to neutrophil and platelet-mediated vascular damage. Monoclonal antibody therapy to P- and E-selectin have shown promise in combating platelet and neutrophil mediated injury (198-200), as is seen with the FDA approved P-selectin antibody crizanlizumab, designed to address vaso-occlusive crises in sickle cell anaemia (201). However, clinical trials of Inclacumab, the monoclonal antibody designed to bind P-selectin, evidenced that a major limitation of antibody therapy is the need for high doses for therapeutic effects (90, 202), leading to high production costs (203, 204).

Because of the role E- and P-selectin play in vaso-occlusive processes, small molecule inhibitors of these ligands are also under various stages of development. The pan-selectin antagonist Rivepansel (GMI-1070) was designed to combat vaso-occlusive crises in severe sickle cell anaemia by preventing the interaction of leukocytes and endothelium (205), but unfortunately failed to meet its phase 3 clinical trial endpoints. Clinical trials for GMI-1271, a small molecule inhibitor of E-selectin, is currently underway for treating venous thrombosis (206). Exogenous recombinant human vimentin, a cytoskeletal structural protein and CD44 binding partner (207), has been shown to act as a competitive inhibitor of neutrophil

binding to platelets and endothelial cells in a P-selectin dependent manner (88). Treatment with recombinant human vimentin reduced neutrophilia and acute lung injury scores in mice treated with sub-lethal doses of LPS. Clinical trials assessing the role of vimentin in sepsis, rheumatoid arthritis, and renal transplant are currently underway. However, given that both increases and deficiencies of this protein can lead to vascular abnormalities (207, 208), the effects of exogenous systemic administration will need to be extensively studied before vimentin is used as a therapeutic.

Selectins have been used as targeting modalities for glycan and polysaccharide-based molecules. Glycomimetics designed to bind selectins or selectin tetrasaccharide sialyl-Lewis^x are a new perspective on anti-inflammatory therapeutics (209), in part because of the anti-inflammatory nature of polysaccharides, glycosaminoglycans, and proteoglycans. Recently, a selectin-targeting dermatan sulphate conjugate has been reported as reducing neutrophil and platelet interactions with inflamed endothelial cell *in vitro*, and reduced thrombus formation *in vivo* (91, 164). Similarly, glycopeptide analogues of PSGL-1 effectively reduced neutrophil-platelet aggregates (80).

Polymer microcapsules coated with fucoidan, a complex polysaccharide that has been shown to slow blood clotting, have been proposed as a drug delivery tool to inflamed vessels expressing P-selectin under high shear (210). Polymer, glycosaminoglycan, and polysaccharide-based therapeutics present indirect benefits in addition to competing for selectin binding. Bulky therapeutics could provide a steric boundary limiting neutrophil and platelet interactions with inflamed endothelium and exposed collagen. Dual targeting to inflamed endothelium and exposed collagen could likewise prevent pathological accumulation of neutrophils, platelets, and neutrophil-platelet aggregated in damaged vessels and thereby reduce immunothrombus and tissue fibrosis.

As the initial points of capture for both neutrophils and platelets, selectin inhibition may provide a way to modulate thrombosis and fibrosis early on in disease progression. Therapeutics that blanket the adhesive endothelium, such as polymer-based molecules and glycoconjugates that are targeted toward

upregulated selectins, may overcome limitations of monoclonal antibodies and recombinant proteins. Nonetheless, therapeutics will need to be studied on a case-by-case basis to maximize their efficacy as anti-inflammatory, anti-thrombotic, or anti-fibrotic therapies.

1.6 Conclusions and Perspective

Neutrophils, platelets, and activated endothelial cells each make substantial contributions to the initiation and perpetuation of vascular dysfunction. As such, many studies have been conducted to establish the relative contribution each of these makes to downstream thrombosis and fibrosis. When physiological redundancies are considered, it is likely that the relative contributions shift depending on the vascular environment in a coordinated effort to resolve an inflammatory stimulus (**Figure 1-2**). Endothelial activation initiates the secretion of pro-inflammatory cytokines and shedding of glycocalyx components, prompting the recruitment of circulating immune cells. Upregulated endothelial E- and P-selectin capture circulating platelets and neutrophils. Adhesion of these inflammatory regulators propels further recruitment, eventually overwhelming the vessel's capacity for self-restoration and shifting the cellular environment toward thrombotic or fibrotic. Captured and rolling neutrophils capitalize on contracting, leaky endothelium, which presents extravasation points that facilitate neutrophil migration into the underlying tissue. Neutrophil activation augments endothelial activation through the release of degranulation products and, in severe cases, NET formation.

Severe endothelial activation exposes the underlying collagen-rich ECM, causing platelet recruitment beyond that triggered by selectin upregulation. Activated adherent platelets express platelet P-selectin, which can act as a congregation point for additional platelets or a secondary capture point for circulating neutrophils. Accumulation of platelets alone or platelet-neutrophil aggregates can result in vessel thrombosis and, in severe cases, vessel occlusion and tissue ischemia. In vessels more susceptible to

fibrosis, platelet activation stimulates the production of pro-fibrotic cytokine TGF-β, pathological ECM secretion, and downstream fibrosis.

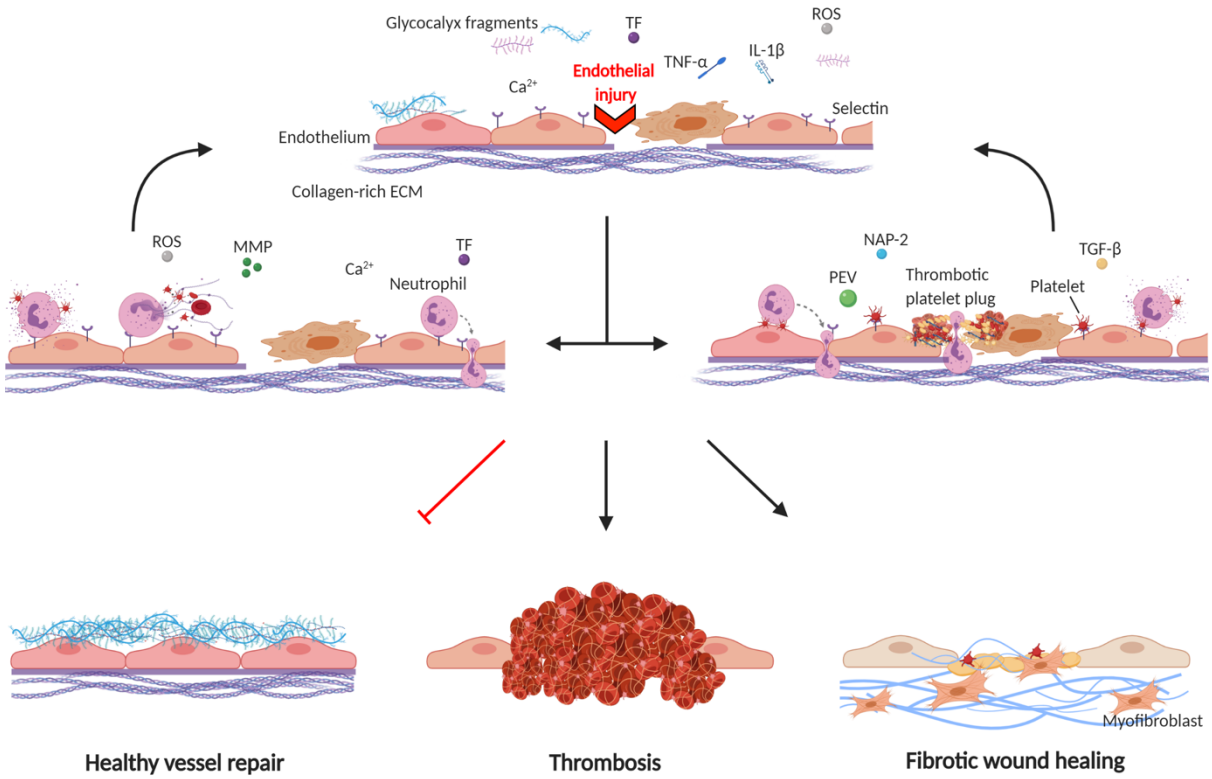

Figure 1-2 Neutrophil, platelet, and endothelial contributions to vessel repair. In response to vessel injury, endothelial cells shed their protective glycosaminoglycan rich layer, the endothelial glycocalyx, exposing upregulated selectins that have been mobilized to the cell surface. Activated endothelial cells secrete pro-inflammatory cytokines such as TNF-α and IL-1β that recruit circulating neutrophils and platelets to the damaged region. ROS production and dysregulated calcium homeostasis causes reductions in NO, enhanced cell contraction, vessel leakiness, and the exposure of the underlying collagen-rich ECM. In some cases, neutrophils captured by upregulated selectins degranulate, releasing additional ROS and matrix degrading MMPs. Adherent neutrophils act as secondary capture points for circulating platelets. Neutrophils undergoing NETosis capture red blood cells, platelets, and fibrin, facilitating thrombosis development. Neutrophil activation results in further endothelial activation, which can lead to apoptosis of endothelial cells. In other cases, platelets anchor to upregulated vWF and P-selectin on the endothelial surface via GPIIbIIIa and PSGL-1. Adherent platelets secrete factors such as NAP-2, TGF-β, and platelet extracellular vesicles (PEVs) that cause further endothelial activation, neutrophil recruitment, and promote the migration and proliferation of collagen-producing myofibroblasts. Platelets form a platelet plug at regions with severe endothelial damage, where denudation has occurred. Neutrophils infiltrate the platelet plug, causing an imbalance in the haemostatic response that shifts plug formation toward thrombotic. Activated platelets help guide crawling neutrophils through the thrombus or endothelium. Persistent or unresolved endothelial damage causes continued recruitment and activation of platelets and neutrophils, overwhelming the vessel and shifting the repair process toward thrombosis and fibrotic wound healing.

Several therapeutic strategies have been implemented to combat the downstream effects of endothelial dysfunction. Each approach primarily targets one interaction to halt what appears to be a highly coupled group of interactions that, when unbalanced, results in pathological thrombosis and/or fibrosis. Conflicting outcomes suggest that no one therapeutic will be a panacea that resets the balance toward healthy regeneration and healing. Based on our current understanding of the coordination of endothelial cells, neutrophils, and platelets when the endothelium becomes dysfunctional, combination therapeutics or complex therapies that target multiple adhesion axes simultaneously may be most efficacious in treating thrombotic and fibrotic conditions.

Deeper understanding of these complex pathways is needed to develop therapeutic strategies for what is surely a large number of distinct pathological states that result from sterile inflammation, diffuse dysfunction that exists with metabolic syndrome, and the sudden and severe response to cytokine storm, like that seen as a result of severe COVID-19 infections, among others. Key discoveries such as the role of NO and ROS in endothelial vasoreactivity or, more recently, the role of platelets as drivers of thrombosis, inflammation, and fibrosis, have been integral in strengthening our understanding of these complex phenomena. Furthermore, elucidating how interactions between neutrophils and endothelial cells can result in NET formation and eventual thrombus formation provides a new foundation from which to innovate and think about disease and healing. The community needs to remain open to the fact that the mechanisms involved in endothelial dysfunction, coupled with platelet and neutrophil interactions, are multipronged; therefore, combinatorial approaches to treatment may well be required. This mode of thinking will expand the potential of targeting not just intercellular signalling cascades, but also cell-cell and cell-ECM interactions to quickly alter the biological response to injury and disease.

1.7 Thesis Overview

After an acute inflammatory event (e.g., heart attack or stroke), blood vessels and circulating immune cells take on a complex phenotype that can perpetuate disease. First responders such as platelets, neutrophils, and the endothelial cell lining of affected blood vessels play a pivotal and cooperative role in mediating the balance between restoration and chronic inflammation after an injury. With these interactions in mind, our lab has designed multifunctional targeted glycosaminoglycan-peptide conjugate molecules that influence outcomes of acute inflammation by regulating immune cell interactions with inflamed the vasculature (45, 91, 211). This thesis describes the design, synthesis, and functional characterization of novel selectin-targeted glycan therapeutic, DS-IkL.

Chapter 2 details the design and construction of a one-bead-one-compound combinatorial peptide library that was weighted toward a known selectin-binding sequence from the literature (164, 212). We first created a one-bead-one-compound library that incorporated D- and unnatural amino acids into the peptide sequence to render the peptide less susceptible to enzymatic degradation *in vivo*. We identified four lead sequences from up to 30^7 unique sequences in this library, which were further reduced to a single lead peptide, IkLLpOR ("IkL"). IkL includes multiple D-enantiomers and a more neutral charge than the parent sequence, IELLQAR. Our next efforts focused on validating that IkL could be successfully conjugated to a dermatan sulfate glycosaminoglycan backbone using any of three conjugation chemistries. One chemistry, in which 4-(4,6-Dimethoxy-1,3,5-triazin-2-yl)-4-methylmorpholinium chloride (DMTMM) was used to activate carboxylic acids on the DS polymer, exhibited the best conjugation efficiency of the three chemistries tested and was selected for future work.

In Chapter 3 we describe the synthesis and characterization of our lead molecule, termed DS-IkL. Given the prominent role selectin-mediated immune cell interactions play in ischemia-reperfusion injury (IRI) (149, 213, 214), we were interested in evaluating the therapeutic capacity of DS-IkL against downstream effects of IRI, namely neutrophil infiltration, fibrotic remodelling, and impaired organ

function. This chapter explores the *in vitro* binding characteristics of DS-IkL, as well as *in vivo* efficacy in a murine model of cardiac IRI by acute myocardial infarction.

The *in vitro* elements of Chapter 3 emphasize the effects of DS-IkL on reducing immune cell interactions with inflamed endothelial cells. However, platelet-neutrophil and platelet-neutrophil-endothelial complexing is known to perpetuate inflammation and organ dysfunction in sterile inflammatory disease (100, 215-217). Chapter 4 describes preliminary work investigating the effect DS-IkL may have on these complex cell interactions by assessing platelet-neutrophil complex formation, proinflammatory cytokine expression, and neutrophil extracellular trap release in the presence of platelet activation factors. This chapter further characterizes the anti-inflammatory, non-anticoagulative properties of our glycan therapeutic.

Finally, Chapter 5 summarizes the findings from each of the previous chapters and gives perspective into future work.

1.8 References

1. Eming SA, Krieg T, Davidson JM. Inflammation in Wound Repair: Molecular and Cellular Mechanisms. Journal of Investigative Dermatology. 2007;127(3):514-25.
2. Wynn TA, Ramalingam TR. Mechanisms of fibrosis: therapeutic translation for fibrotic disease. Nat Med. 2012;18(7):1028-40.
3. Woywodt A, Bahlmann FH, de Groot K, Haller H, Haubitz M. Circulating endothelial cells: life, death, detachment and repair of the endothelial cell layer. Nephrology Dialysis Transplantation. 2002;17(10):1728-30.
4. Bar A, Targosz-Korecka M, Suraj J, Proniewski B, Jasztal A, Marczyk B, et al. Degradation of Glycocalyx and Multiple Manifestations of Endothelial Dysfunction Coincide in the Early Phase of Endothelial Dysfunction Before Atherosclerotic Plaque Development in Apolipoprotein E/Low-Density Lipoprotein Receptor-Deficient Mice. J Am Heart Assoc. 2019;8(6):e011171.
5. Park KH, Park WJ. Endothelial dysfunction: Clinical implications in cardiovascular disease and therapeutic approaches. Journal of Korean Medical Science. 2015;30:1213-25.
6. Xu J, Shi G-P. Vascular wall extracellular matrix proteins and vascular diseases. Biochimica et biophysica acta. 2014;1842(11):2106-19.
7. Krüger-Genge A, Blocki A, Franke R-P, Jung F. Vascular Endothelial Cell Biology: An Update. International journal of molecular sciences. 2019;20(18):4411.
8. Altabas V. Diabetes, Endothelial Dysfunction, and Vascular Repair: What Should a Diabetologist Keep His Eye on? International Journal of Endocrinology. 2015;2015:848272.
9. Huynh J, Nishimura N, Rana K, Peloquin JM, Califano JP, Montague CR, et al. Age-Related Intimal Stiffening Enhances Endothelial Permeability and Leukocyte Transmigration. Science Translational Medicine. 2011;3(112):112ra22.
10. Wanner A, Mendes ES. Airway Endothelial Dysfunction in Asthma and Chronic Obstructive Pulmonary Disease. American Journal of Respiratory and Critical Care Medicine. 2010;182(11):1344-51.
11. Totani L, Plebani R, Piccoli A, Di Silvestre S, Lanuti P, Recchiuti A, et al. Mechanisms of endothelial cell dysfunction in cystic fibrosis. Biochimica et Biophysica Acta (BBA) - Molecular Basis of Disease. 2017;1863(12):3243-53.
12. Stoy S, Patel VC, Sturgeon JP, Manakkat Vijay GK, Lisman T, Bernal W, et al. Platelet-leucocyte aggregation is augmented in cirrhosis and further increased by platelet transfusion. Aliment Pharmacol Ther. 2018;47(10):1375-86.
13. Weinbaum S, Tarbell JM, Damiano ER. The Structure and Function of the Endothelial Glycocalyx Layer. Annual Review of Biomedical Engineering. 2007;9(1):121-67.
14. Barker AL, Konopatskaya O, Neal CR, Macpherson JV, Whatmore JL, Winlove CP, et al. Observation and characterisation of the glycocalyx of viable human endothelial cells using confocal laser scanning microscopy. Physical Chemistry Chemical Physics. 2004;6(5):1006-11.
15. Cao RN, Tang L, Xia ZY, Xia R. Endothelial glycocalyx as a potential theriapeutic target in organ injuries. Lippincott Williams and Wilkins; 2019. p. 963-75.
16. Curry FE. The Molecular Structure of the Endothelial Glycocalyx Layer (EGL) and Surface Layers (ESL) Modulation of Transvascular Exchange. Adv Exp Med Biol. 2018;1097:29-49.
17. Kundra P, Goswami S. Endothelial glycocalyx: Role in body fluid homeostasis and fluid management. Indian J Anaesth. 2019;63(1):6-14.
18. Betteridge KB, Arkill KP, Neal CR, Harper SJ, Foster RR, Satchell SC, et al. Sialic acids regulate microvessel permeability, revealed by novel in vivo studies of endothelial glycocalyx structure and function. The Journal of Physiology. 2017;595(15):5015-35.
19. Trowbridge JM, Gallo RL. Dermatan sulfate: new functions from an old glycosaminoglycan. Glycobiology. 2002;12(9):117R-25R.
20. Tovar AMF, de Mattos DA, Stelling MP, Sarcinelli-Luz BSL, Nazareth RA, Mourão PAS. Dermatan sulfate is the predominant antithrombotic glycosaminoglycan in vessel walls: Implications for a possible physiological function of heparin cofactor II. Biochimica et Biophysica Acta (BBA) - Molecular Basis of Disease. 2005;1740(1):45-53.
21. Mensah SA, Cheng MJ, Homayoni H, Plouffe BD, Coury AJ, Ebong EE. Regeneration of glycocalyx by heparan sulfate and sphingosine 1-phosphate restores inter-endothelial communication. PLoS One. 2017;12(10):e0186116.

22. Song JW, Zullo JA, Liveris D, Dragovich M, Zhang XF, Goligorsky MS. Therapeutic Restoration of Endothelial Glycocalyx in Sepsis. Journal of Pharmacology and Experimental Therapeutics. 2017;361(1):115-21.
23. Lipowsky HH, Lescanic A. Inhibition of inflammation induced shedding of the endothelial glycocalyx with low molecular weight heparin. Microvasc Res. 2017;112:72-8.
24. Mannello F, Medda V, Ligi D, Raffetto JD. Glycosaminoglycan sulodexide inhibition of MMP-9 gelatinase secretion and activity: possible pharmacological role against collagen degradation in vascular chronic diseases. Curr Vasc Pharmacol. 2013;11(3):354-65.
25. Gao L, Lipowsky HH. Composition of the endothelial glycocalyx and its relation to its thickness and diffusion of small solutes. Microvascular Research. 2010;80(3):394-401.
26. Bai K, Wang W. Shear stress-induced redistribution of the glycocalyx on endothelial cells in vitro. Biomechanics and Modeling in Mechanobiology. 2014;13(2):303-11.
27. Hu X, Adamson RH, Liu B, Curry FE, Weinbaum S. Starling forces that oppose filtration after tissue oncotic pressure is increased. American Journal of Physiology-Heart and Circulatory Physiology. 2000;279(4):H1724-H36.
28. Harding IC, Mitra R, Mensah SA, Nersesyan A, Bal NN, Ebong EE. Endothelial barrier reinforcement relies on flow-regulated glycocalyx, a potential therapeutic target. Biorheology. 2019;56(2-3):131-49.
29. Li W, Wang W. Structural alteration of the endothelial glycocalyx: contribution of the actin cytoskeleton. Biomechanics and modeling in mechanobiology. 2018;17(1):147-58.
30. Thi MM, Tarbell JM, Weinbaum S, Spray DC. The role of the glycocalyx in reorganization of the actin cytoskeleton under fluid shear stress: a "bumper-car" model. Proceedings of the National Academy of Sciences of the United States of America. 2004;101(47):16483-8.
31. Russo TA, Stoll D, Nader HB, Dreyfuss JL. Mechanical stretch implications for vascular endothelial cells: Altered extracellular matrix synthesis and remodeling in pathological conditions. Life Sciences. 2018;213:214-25.
32. Yao Y, Rabodzey A, C. Forbes Dewey J. Glycocalyx modulates the motility and proliferative response of vascular endothelium to fluid shear stress. American Journal of Physiology-Heart and Circulatory Physiology. 2007;293(2):H1023-H30.
33. Yu H, Kalogeris T, Korthuis RJ. Reactive species-induced microvascular dysfunction in ischemia/reperfusion. Free Radic Biol Med. 2019;135:182-97.
34. Cai H, Harrison DG. Endothelial Dysfunction in Cardiovascular Diseases: The Role of Oxidant Stress. Circulation Research. 2000;87(10):840-4.
35. Curry FE, Michel CC. A fiber matrix model of capillary permeability. Microvasc Res. 1980;20(1):96-9.
36. Uchimido R, Schmidt EP, Shapiro NI. The glycocalyx: a novel diagnostic and therapeutic target in sepsis. Critical Care. 2019;23(1):16.
37. Rehm M, Bruegger D, Christ F, Conzen P, Thiel M, Jacob M, et al. Shedding of the endothelial glycocalyx in patients undergoing major vascular surgery with global and regional ischemia. Circulation. 2007;116(17):1896-906.
38. Chappell D, Heindl B, Jacob M, Annecke T, Chen C, Rehm M, et al. Sevoflurane reduces leukocyte and platelet adhesion after ischemia-reperfusion by protecting the endothelial glycocalyx. Anesthesiology. 2011;115(3):483-91.
39. McDonald KK, Cooper S, Danielzak L, Leask RL. Glycocalyx Degradation Induces a Proinflammatory Phenotype and Increased Leukocyte Adhesion in Cultured Endothelial Cells under Flow. PLoS One. 2016;11(12):e0167576.
40. Kolarova H, Ambruzova B, Svihalkova Sindlerova L, Klinke A, Kubala L. Modulation of endothelial glycocalyx structure under inflammatory conditions. Mediators Inflamm. 2014;2014:694312.
41. Becker BF, Jacob M, Leipert S, Salmon AHJ, Chappell D. Degradation of the endothelial glycocalyx in clinical settings: Searching for the sheddases. British Journal of Clinical Pharmacology. 2015;80(3):389-402.
42. Buijs JOd, Musters M, Verrips T, Post JA, Braam B, Riel Nv. Mathematical modeling of vascular endothelial layer maintenance: the role of endothelial cell division, progenitor cell homing, and telomere shortening. American Journal of Physiology-Heart and Circulatory Physiology. 2004;287(6):H2651-H8.
43. McMasters J, Panitch A. Collagen-binding nanoparticles for extracellular anti-inflammatory peptide delivery decrease platelet activation, promote endothelial migration, and suppress inflammation. Acta Biomaterialia. 2017;49:78-88.
44. Brouns SLN, Provenzale I, van Geffen JP, van der Meijden PEJ, Heemskerk JWM. Localized endothelial-based control of platelet aggregation and coagulation under flow: A proof-of-principle vessel-on-a-chip study. Journal of Thrombosis and Haemostasis. 2020;18(4):931-41.
45. Paderi JE, Stuart K, Sturek M, Park K, Panitch A. The inhibition of platelet adhesion and activation on collagen during balloon angioplasty by collagen-binding peptidoglycans. Biomaterials. 2011;32(10):2516-23.

46. Kuijpers MJ, Munnix IC, Cosemans JM, Vlijmen BV, Reutelingsperger CP, Egbrink MO, et al. Key role of platelet procoagulant activity in tissue factor-and collagen-dependent thrombus formation in arterioles and venules in vivo differential sensitivity to thrombin inhibition. Microcirculation. 2008;15(4):269-82.
47. Greineder CF, Johnston IH, Villa CH, Gollomp K, Esmon CT, Cines DB, et al. ICAM-1-targeted thrombomodulin mitigates tissue factor-driven inflammatory thrombosis in a human endothelialized microfluidic model. Blood advances. 2017;1(18):1452-65.
48. Puhr-Westerheide D, Schink SJ, Fabritius M, Mittmann L, Hessenauer MET, Pircher J, et al. Neutrophils promote venular thrombosis by shaping the rheological environment for platelet aggregation. Sci Rep. 2019;9(1):15932.
49. Kim KH, Barazia A, Cho J. Real-time imaging of heterotypic platelet-neutrophil interactions on the activated endothelium during vascular inflammation and thrombus Formation in live mice. J Vis Exp. 2013(74):50329.
50. Atkinson BT, Jasuja R, Chen VM, Nandivada P, Furie B, Furie BC. Laser-induced endothelial cell activation supports fibrin formation. Blood. 2010;116(22):4675-83.
51. Ivanciu L, Krishnaswamy S, Camire RM. New insights into the spatiotemporal localization of prothrombinase in vivo. Blood. 2014;124(11):1705-14.
52. Darbousset R, Thomas GM, Mezouar S, Frère C, Bonier R, Mackman N, et al. Tissue factor–positive neutrophils bind to injured endothelial wall and initiate thrombus formation. Blood. 2012;120(10):2133-43.
53. Schulz C, Schäfer A, Stolla M, Kerstan S, Lorenz M, Brühl M-Lv, et al. Chemokine Fractalkine Mediates Leukocyte Recruitment to Inflammatory Endothelial Cells in Flowing Whole Blood. Circulation. 2007;116(7):764-73.
54. Zuchtriegel G, Uhl B, Puhr-Westerheide D, Pörnbacher M, Lauber K, Krombach F, et al. Platelets Guide Leukocytes to Their Sites of Extravasation. 2016;14(5):e1002459.
55. Schaefer A, Te Riet J, Ritz K, Hoogenboezem M, Anthony EC, Mul FP, et al. Actin-binding proteins differentially regulate endothelial cell stiffness, ICAM-1 function and neutrophil transmigration. J Cell Sci. 2014;127(Pt 20):4470-82.
56. Reitsma S, Oude Egbrink MG, Heijnen VV, Megens RT, Engels W, Vink H, et al. Endothelial glycocalyx thickness and platelet-vessel wall interactions during atherogenesis. Thromb Haemost. 2011;106(5):939-46.
57. Kato S, Inui N, Hakamata A, Suzuki Y, Enomoto N, Fujisawa T, et al. Changes in pulmonary endothelial cell properties during bleomycin-induced pulmonary fibrosis. Respir Res. 2018;19(1):127.
58. Stroka KM, Aranda-Espinoza H. Endothelial cell substrate stiffness influences neutrophil transmigration via myosin light chain kinase-dependent cell contraction. Blood. 2011;118(6):1632-40.
59. Sakai N, Bain G, Furuichi K, Iwata Y, Nakamura M, Hara A, et al. The involvement of autotaxin in renal interstitial fibrosis through regulation of fibroblast functions and induction of vascular leakage. Sci Rep. 2019;9(1):7414.
60. Idriss HT, Naismith JH. TNFα and the TNF receptor superfamily: Structure-function relationship(s). Microscopy Research and Technique. 2000;50(3):184-95.
61. Morikis VA, Simon SI. Neutrophil Mechanosignaling Promotes Integrin Engagement With Endothelial Cells and Motility Within Inflamed Vessels. Front Immunol. 2018;9:2774.
62. Ley K, Laudanna C, Cybulsky MI, Nourshargh S. Getting to the site of inflammation: the leukocyte adhesion cascade updated. Nature Reviews Immunology. 2007;7(9):678-.
63. Kirchhofer D, Tschopp TB, Hadváry P, Baumgartner HR. Endothelial cells stimulated with tumor necrosis factor-alpha express varying amounts of tissue factor resulting in inhomogenous fibrin deposition in a native blood flow system. Effects of thrombin inhibitors. The Journal of Clinical Investigation. 1994;93(5):2073-83.
64. Grover SP, Mackman N. Tissue Factor. Arteriosclerosis, Thrombosis, and Vascular Biology. 2018;38(4):709-25.
65. Mercer PF, Chambers RC. Coagulation and coagulation signalling in fibrosis. Biochimica et Biophysica Acta (BBA) - Molecular Basis of Disease. 2013;1832(7):1018-27.
66. Chrysanthopoulou A, Mitroulis I, Kambas K, Skendros P, Kourtzelis I, Vradelis S, et al. Tissue factor–thrombin signaling enhances the fibrotic activity of myofibroblasts in systemic sclerosis through up-regulation of endothelin receptor A. Arthritis & Rheumatism. 2011;63(11):3586-97.
67. Westrick RJ, Winn ME, Eitzman DT. Murine Models of Vascular Thrombosis. Arteriosclerosis, Thrombosis, and Vascular Biology. 2007;27(10):2079-93.
68. Calvente CJ, Tameda M, Johnson CD, del Pilar H, Lin YC, Adronikou N, et al. Neutrophils contribute to spontaneous resolution of liver inflammation and fibrosis via microRNA-223. The Journal of Clinical Investigation. 2019;129(10):4091-109.

69. Narasaraju T, Tang B, Herrmann M, Muller S, Chow VTK, Radic M. Neutrophilia and NETopathy as Key Pathologic Drivers of Progressive Lung Impairment in Patients with COVID-19. OSF Preprints. 2020.
70. Chen C, Zhang XR, Ju ZY, He WF. [Advances in the research of cytokine storm mechanism induced by Corona Virus Disease 2019 and the corresponding immunotherapies]. Zhonghua Shao Shang Za Zhi. 2020;36(0):E005.
71. Mesri M, Altieri DC. Endothelial Cell Activation by Leukocyte Microparticles. The Journal of Immunology. 1998;161(8):4382-7.
72. Kay EP, Nimni M, Smith RE. Modulation of endothelial cell morphology and collagen synthesis by polymorphonuclear leukocytes. Investigative Ophthalmology & Visual Science. 1984;25:502-12.
73. Yago T, Zhang N, Zhao L, Abrams CS, McEver RP. Selectins and chemokines use shared and distinct signals to activate beta2 integrins in neutrophils. Blood Adv. 2018;2(7):731-44.
74. Schaff UY, Yamayoshi I, Tse T, Griffin D, Kibathi L, Simon SI. Calcium Flux in Neutrophils Synchronizes β2 Integrin Adhesive and Signaling Events that Guide Inflammatory Recruitment. Annals of Biomedical Engineering. 2008;36(4):632-46.
75. Huang B, Ling Y, Lin J, Du X, Fang Y, Wu J. Force-dependent calcium signaling and its pathway of human neutrophils on P-selectin in flow. Protein & Cell. 2017;8(2):103-13.
76. Downey GP, Worthen GS, Henson PM, Hyde DM. Neutrophil sequestration and migration in localized pulmonary inflammation. Capillary localization and migration across the interalveolar septum. Am Rev Respir Dis. 1993;147(1):168-76.
77. DOERSCHUK CM. Mechanisms of Leukocyte Sequestration in Inflamed Lungs. Microcirculation. 2001;8(2):71-88.
78. Park SA, Choe YH, Park E, Hyun Y-M. Real-time dynamics of neutrophil clustering in response to phototoxicity-induced cell death and tissue damage in mouse ear dermis. Cell Adh Migr. 2018;12(5):424-31.
79. Pober JS, Sessa WC. Inflammation and the blood microvascular system. Cold Spring Harbor Perspectives in Biology. 2015;7(1).
80. Krishnamurthy VR, Sardar MYR, Ying Y, Song X, Haller C, Dai E, et al. Glycopeptide analogues of PSGL-1 inhibit P-selectin in vitro and in vivo. Nat Commun. 2015;6:6387-.
81. Gong Y, Zhang Y, Feng S, Liu X, Lu S, Long M. Dynamic contributions of P- and E-selectins to beta2-integrin-induced neutrophil transmigration. FASEB J. 2017;31(1):212-23.
82. Ma Y, Yang X, Chatterjee V, Meegan JE, Beard RS, Jr., Yuan SY. Role of Neutrophil Extracellular Traps and Vesicles in Regulating Vascular Endothelial Permeability. Front Immunol. 2019;10:1037.
83. Etulain J, Martinod K, Wong SL, Cifuni SM, Schattner M, Wagner DD. P-selectin promotes neutrophil extracellular trap formation in mice. Blood. 2015;126(2):242-6.
84. von Brühl M-L, Stark K, Steinhart A, Chandraratne S, Konrad I, Lorenz M, et al. Monocytes, neutrophils, and platelets cooperate to initiate and propagate venous thrombosis in mice in vivo. J Exp Med. 2012;209(4):819-35.
85. Barnes BJ, Adrover JM, Baxter-Stoltzfus A, Borczuk A, Cools-Lartigue J, Crawford JM, et al. Targeting potential drivers of COVID-19: Neutrophil extracellular traps. J Exp Med. 2020;217(6):e20200652.
86. Fuchs TA, Brill A, Wagner DD. Neutrophil Extracellular Trap (NET) Impact on Deep Vein Thrombosis. Arteriosclerosis, Thrombosis, and Vascular Biology. 2012;32(8):1777-83.
87. Green JP, Souilhol C, Xanthis I, Martinez-Campesino L, Bowden NP, Evans PC, et al. Atheroprone flow activates inflammation via endothelial ATP-dependent P2X7-p38 signalling. Cardiovascular research. 2018;114(2):324-35.
88. Lam FW, Da Q, Guillory B, Cruz MA. Recombinant Human Vimentin Binds to P-Selectin and Blocks Neutrophil Capture and Rolling on Platelets and Endothelium. The Journal of Immunology. 2018;200(5):1718-26.
89. Telen MJ, Wun T, McCavit TL, De Castro LM, Krishnamurti L, Lanzkron S, et al. Randomized phase 2 study of GMI-1070 in SCD: reduction in time to resolution of vaso-occlusive events and decreased opioid use. Blood. 2015;125(17):2656-64.
90. Stahli BE, Gebhard C, Duchatelle V, Cournoyer D, Petroni T, Tanguay JF, et al. Effects of the P-Selectin Antagonist Inclacumab on Myocardial Damage After Percutaneous Coronary Intervention According to Timing of Infusion: Insights From the SELECT-ACS Trial. J Am Heart Assoc. 2016;5(11):e004255.
91. Wodicka JR, Morikis VA, Dehghani T, Simon SI, Panitch A. Selectin-targeting peptide-glycosaminoglycan conjugates modulate neutrophil-endothelial interactions. Cellular and Molecular Bioengineering. 2018.
92. Culmer DL, Dunbar ML, Hawley AE, Sood S, Sigler RE, Henke PK, et al. E-selectin inhibition with GMI-1271 decreases venous thrombosis without profoundly affecting tail vein bleeding in a mouse model. Thromb Haemost. 2017;117(6):1171-81.

93. Ramirez GA, Manfredi AA, Maugeri N. Misunderstandings Between Platelets and Neutrophils Build in Chronic Inflammation. Frontiers in immunology. 2019;10:2491-.
94. Baimukanova G, Miyazawa B, Potter DR, Muench MO, Bruhn R, Gibb SL, et al. Platelets regulate vascular endothelial stability: assessing the storage lesion and donor variability of apheresis platelets. Transfusion. 2016;56 Suppl 1(Suppl 1):S65-S75.
95. Ghoshal K, Bhattacharyya M. Overview of platelet physiology: its hemostatic and nonhemostatic role in disease pathogenesis. ScientificWorldJournal. 2014;2014:781857-.
96. Amison RT, O'Shaughnessy BG, Arnold S, Cleary SJ, Nandi M, Pitchford SC, et al. Platelet Depletion Impairs Host Defense to Pulmonary Infection with Pseudomonas aeruginosa in Mice. American Journal of Respiratory Cell and Molecular Biology. 2018;58(3):331-40.
97. Zhou X, Li Y, Yang Q. Antiplatelet Therapy After Percutaneous Coronary Intervention in Patients With COVID-19: Implications From Clinical Features to Pathologic Findings. Circulation. 2020;141(22):1736-8.
98. Gros A, Syvannarath V, Lamrani L, Ollivier V, Loyau S, Goerge T, et al. Single platelets seal neutrophil-induced vascular breaches via GPVI during immune-complex-mediated inflammation in mice. Blood. 2015;126(8):1017-26.
99. Slaba I, Wang J, Kolaczkowska E, McDonald B, Lee W-Y, Kubes P. Imaging the dynamic platelet-neutrophil response in sterile liver injury and repair in mice. Hepatology. 2015;62(5):1593-605.
100. Gros A, Ollivier V, Ho-Tin-Noe B. Platelets in inflammation: regulation of leukocyte activities and vascular repair. Front Immunol. 2014;5(678):678.
101. Lindberg U, Svensson L, Hellmark T, Segelmark M, Shannon O. Increased platelet activation occurs in cystic fibrosis patients and correlates to clinical status. Thrombosis Research. 2018;162:32-7.
102. Maugeri N, Rovere-Querini P, Baldini M, Baldissera E, Sabbadini MG, Bianchi ME, et al. Oxidative Stress Elicits Platelet/Leukocyte Inflammatory Interactions via HMGB1: A Candidate for Microvessel Injury in Sytemic Sclerosis. Antioxidants & Redox Signaling. 2013;20(7):1060-74.
103. Tomaiuolo M, Matzko CN, Poventud-Fuentes I, Weisel JW, Brass LF, Stalker TJ. Interrelationships between structure and function during the hemostatic response to injury. Proceedings of the National Academy of Sciences. 2019;116(6):2243-52.
104. Stalker TJ, Traxler EA, Wu J, Wannemacher KM, Cermignano SL, Voronov R, et al. Hierarchical organization in the hemostatic response and its relationship to the platelet-signaling network. Blood. 2013;121(10):1875-85.
105. Welsh JD, Poventud-Fuentes I, Sampietro S, Diamond SL, Stalker TJ, Brass LF. Hierarchical organization of the hemostatic response to penetrating injuries in the mouse macrovasculature. J Thromb Haemost. 2017;15(3):526-37.
106. Ghasemzadeh M, Kaplan ZS, Alwis I, Schoenwaelder SM, Ashworth KJ, Westein E, et al. The CXCR1/2 ligand NAP-2 promotes directed intravascular leukocyte migration through platelet thrombi. Blood. 2013;121(22):4555-66.
107. Pitchford S, Pan D, Welch HCE. Platelets in neutrophil recruitment to sites of inflammation. Lippincott Williams and Wilkins; 2017. p. 23-31.
108. Zwaginga JJ, Torres HIG, Lammers J-WJ, Sixma JJ, Koenderman L, Kuijper PHM. Minimal Platelet Deposition and Activation in Models of Injured Vessel Wall Ensure Optimal Neutrophil Adhesion Under Flow Conditions. Ateriosclerosis, Thrombosis, and Vascular Biology. 1999;19:1549-54.

109. Totani L, Piccoli A, Dell'Elba G, Concetta A, Di Santo A, Martelli N, et al. Phosphodiesterase type 4 blockade prevents platelet-mediated neutrophil recruitment at the site of vascular injury. Arterioscler Thromb Vasc Biol. 2014;34(8):1689-96.

110. Evangelista V, Pamuklar Z, Piccoli A, Manarini S, Dell'elba G, Pecce R, et al. Src family kinases mediate neutrophil adhesion to adherent platelets. Blood. 2007;109(6):2461-9.
111. Kuravi SJ, Harrison P, Rainger GE, Nash GB. Ability of Platelet-Derived Extracellular Vesicles to Promote Neutrophil-Endothelial Cell Interactions. Inflammation. 2019;42(1):290-305.
112. Dole VS, Bergmeier W, Mitchell HA, Eichenberger SC, Wagner DD. Activated platelets induce Weibel-Palade–body secretion and leukocyte rolling in vivo: role of P-selectin. Blood. 2005;106(7):2334-9.
113. Petri B, Broermann A, Li H, Khandoga AG, Zarbock A, Krombach F, et al. von Willebrand factor promotes leukocyte extravasation. Blood. 2010;116(22):4712-9.

114. Abdulla A, Awla D, Hartman H, Weiber H, Jeppsson B, Regnér S, et al. Platelets regulate P-selectin expression and leukocyte rolling in inflamed venules of the pancreas. European Journal of Pharmacology. 2012;682(1):153-60.
115. Frydman GH, Le A, Ellett F, Jorgensen J, Fox JG, Tompkins RG, et al. Technical Advance: Changes in neutrophil migration patterns upon contact with platelets in a microfluidic assay. J Leukoc Biol. 2017;101(3):797-806.
116. Maugeri N, Rovere-Querini P, Evangelista V, Covino C, Capobianco A, Bertilaccio MT, et al. Neutrophils phagocytose activated platelets in vivo: a phosphatidylserine, P-selectin, and {beta}2 integrin-dependent cell clearance program. Blood. 2009;113(21):5254-65.
117. Braun OÖ, Slotta JE, Menger MD, Erlinge D, Thorlacius H. Primary and secondary capture of platelets onto inflamed femoral artery endothelium is dependent on P-selectin and PSGL-1. European Journal of Pharmacology. 2008;592(1):128-32.
118. Gremmel T, Koppensteiner R, Kaider A, Eichelberger B, Mannhalter C, Panzer S. Impact of variables of the P-selectin - P-selectin glycoprotein ligand-1 axis on leukocyte-platelet interactions in cardiovascular disease. Thromb Haemost. 2015;113(4):806-12.
119. Xu T, Zhang L, Geng ZH, Wang H-B, Wang J-T, Chen M, et al. P-selectin cross-links PSGL-1 and enhances neutrophil adhesion to fibrinogen and ICAM-1 in a Src kinase-dependent, but GPCR-independent mechanism. Cell Adh Migr. 2007;1(3):115-23.
120. Delaney MK, Liu J, Kim K, Shen B, Stojanovic-Terpo A, Zheng Y, et al. Agonist-induced platelet procoagulant activity requires shear and a Rac1-dependent signaling mechanism. Blood. 2014;124(12):1957-67.
121. Fahim A, Crooks MG, Morice AH, Hart SP. Increased Platelet Binding to Circulating Monocytes in Idiopathic Pulmonary Fibrosis. Lung. 2014;192(2):277-84.
122. Raker V, Haub J, Stojanovic A, Cerwenka A, Schuppan D, Steinbrink K. Early inflammatory players in cutanous fibrosis. J Dermatol Sci. 2017;87(3):228-35.
123. Jia LX, Qi GM, Liu O, Li TT, Yang M, Cui W, et al. Inhibition of platelet activation by clopidogrel prevents hypertension-induced cardiac inflammation and fibrosis. Cardiovascular Drugs and Therapy. 2013;27(6):521-30.
124. Dees C, Akhmetshina A, Zerr P, Reich N, Palumbo K, Horn A, et al. Platelet-derived serotonin links vascular disease and tissue fibrosis. Journal of Experimental Medicine. 2011;208(5):961-72.
125. Cooley BC, Nevado J, Mellad J, Yang D, St. Hilaire C, Negro A, et al. TGF-β Signaling Mediates Endothelial-to-Mesenchymal Transition (EndMT) During Vein Graft Remodeling. Science Translational Medicine. 2014;6(227):227ra34-ra34.
126. Weiskirchen R, Weiskirchen S, Tacke F. Organ and tissue fibrosis: Molecular signals, cellular mechanisms and translational implications. Molecular Aspects of Medicine. 2019;65:2-15.
127. Mortaz E, Alipoor SD, Adcock IM, Mumby S, Koenderman L. Update on Neutrophil Function in Severe Inflammation. Front Immunol. 2018;9:2171.
128. Padmanabhan J, Gonzalez AL. The effects of extracellular matrix proteins on neutrophil-endothelial interaction--a roadway to multiple therapeutic opportunities. Yale J Biol Med. 2012;85(2):167-85.
129. Hoenderdos K, Lodge KM, Hirst RA, Chen C, Palazzo SGC, Emerenciana A, et al. Hypoxia upregulates neutrophil degranulation and potential for tissue injury. Thorax. 2016;71(11):1030-8.
130. Morales-Ortíz J, Deal V, Reyes F, Maldonado-Martínez G, Ledesma N, Staback F, et al. Platelet-derived TLT-1 is a prognostic indicator in ALI/ARDS and prevents tissue damage in the lungs in a mouse model. Blood. 2018;132(23):2495-505.
131. Chen C-M, Lu H-C, Tung Y-T, Chen W. Antiplatelet Therapy for Acute Respiratory Distress Syndrome. Biomedicines. 2020;8(7):230.
132. Bacha NC, Blandinieres A, Rossi E, Gendron N, Nevo N, Lecourt S, et al. Endothelial Microparticles are Associated to Pathogenesis of Idiopathic Pulmonary Fibrosis. Stem Cell Reviews and Reports. 2018;14(2):223-35.
133. Blandinières A, Gendron N, Bacha N, Bièche I, Chocron R, Nunes H, et al. Interleukin-8 release by endothelial colony-forming cells isolated from idiopathic pulmonary fibrosis patients might contribute to their pathogenicity. Angiogenesis. 2019;22(2):325-39.
134. Chan TR, Stahl PJ, Yu SM. Matrix-Bound VEGF Mimetic Peptides: Design and Endothelial Cell Activation in Collagen Scaffolds. Adv Funct Mater. 2011;21(22):4252-62.
135. Swieringa F, Baaten CC, Verdoold R, Mastenbroek TG, Rijnveld N, van der Laan KO, et al. Platelet Control of Fibrin Distribution and Microelasticity in Thrombus Formation Under Flow. Arterioscler Thromb Vasc Biol. 2016;36(4):692-9.
136. Tanguay J-F, Hammoud T, Geoffroy P, Merhi Y. Chronic Platelet and Neutrophil Adhesion: A Causal Role for Neointimal Hyperplasia in In-Stent Restenosis. Journal of Endovascular Therapy. 2003;10(5):968-77.

137. Varga Z, Flammer AJ, Steiger P, Haberecker M, Andermatt R, Zinkernagel AS, et al. Endothelial cell infection and endotheliitis in COVID-19. Lancet (London, England). 2020;395(10234):1417-8.
138. Smeda M, Chlopicki S. Endothelial barrier integrity in COVID-19-dependent hyperinflammation: does the protective facet of platelet function matter? Cardiovascular research. 2020;116(10):e118-e21.
139. Lippi G, Plebani M, Henry BM. Thrombocytopenia is associated with severe coronavirus disease 2019 (COVID-19) infections: A meta-analysis. Clin Chim Acta. 2020;506:145-8.
140. Li H, Pan P, Su X, Liu S, Zhang L, Wu D, et al. Neutrophil Extracellular Traps Are Pathogenic in Ventilator-Induced Lung Injury and Partially Dependent on TLR4. BioMed research international. 2017;2017:8272504-.
141. Curley GF, Laffey JG, Zhang H, Slutsky AS. Biotrauma and Ventilator-Induced Lung Injury: Clinical Implications. Chest. 2016;150(5):1109-17.
142. Yadav H, Kor DJ. Platelets in the pathogenesis of acute respiratory distress syndrome. American journal of physiology Lung cellular and molecular physiology. 2015;309(9):L915-23.
143. Yiming MT, Lederer DJ, Sun L, Huertas A, Issekutz AC, Bhattacharya S. Platelets enhance endothelial adhesiveness in high tidal volume ventilation. Am J Respir Cell Mol Biol. 2008;39(5):569-75.
144. Sexton TR, Wallace EL, Macaulay TE, Charnigo RJ, Evangelista V, Campbell CL, et al. The effect of rosuvastatin on thromboinflammation in the setting of acute coronary syndrome. J Thromb Thrombolysis. 2015;39(2):186-95.
145. Sexton TR, Zhang G, Macaulay TE, Callahan LA, Charnigo R, Vsevolozhskaya OA, et al. Ticagrelor Reduces Thromboinflammatory Markers in Patients With Pneumonia. JACC Basic Transl Sci. 2018;3(4):435-49.
146. Kubisa MJ, Jezewski MP, Gasecka A, Siller-Matula JM, Postuła M. Ticagrelor - toward more efficient platelet inhibition and beyond. Ther Clin Risk Manag. 2018;14:129-40.
147. Koushki K, Shahbaz SK, Mashayekhi K, Sadeghi M, Zayeri ZD, Taba MY, et al. Anti-inflammatory Action of Statins in Cardiovascular Disease: the Role of Inflammasome and Toll-Like Receptor Pathways. Clin Rev Allergy Immunol. 2020.
148. Birnbaum Y, Tran D, Chen H, Nylander S, Sampaio L, Ye Y. Ticagrelor Improves Remodeling, Reduces Apoptosis, Inflammation and Fibrosis and Increases the Number of Progenitor Stem Cells After Myocardial Infarction in a Rat Model of Ischemia Reperfusion. Cellular physiology and biochemistry : international journal of experimental cellular physiology, biochemistry, and pharmacology. 2019;53:961-81.
149. Yang Q, He GW, Underwood MJ, Yu CM. Cellular and molecular mechanisms of endothelial ischemia/reperfusion injury: perspectives and implications for postischemic myocardial protection. Am J Transl Res. 2016;8(2):765-77.
150. Wolfson RK, Chiang ET, Garcia JGN. HMGB1 induces human lung endothelial cell cytoskeletal rearrangement and barrier disruption. Microvascular Research. 2011;81(2):189-97.
151. Wang J, Wu A, Wu Y. Endothelial Glycocalyx Layer: A Possible Therapeutic Target for Acute Lung Injury during Lung Resection. Biomed Res Int. 2017;2017:5969657.
152. Tarbell JM, Cancel LM. The glycocalyx and its significance in human medicine. J Intern Med. 2016;280(1):97-113.
153. Cao RN, Tang L, Xia ZY, Xia R. Endothelial glycocalyx as a potential theriapeutic target in organ injuries. Chin Med J (Engl). 2019;132(8):963-75.
154. Kazuma S, Tokinaga Y, Kimizuka M, Azumaguchi R, Hamada K, Yamakage M. Sevoflurane Promotes Regeneration of the Endothelial Glycocalyx by Upregulating Sialyltransferase. Journal of Surgical Research. 2019;241:40-7.
155. Casanova J, Simon C, Vara E, Sanchez G, Rancan L, Abubakra S, et al. Sevoflurane anesthetic preconditioning protects the lung endothelial glycocalyx from ischemia reperfusion injury in an experimental lung autotransplant model. J Anesth. 2016;30(5):755-62.
156. Chen C, Chappell D, Annecke T, Conzen P, Jacob M, Welsch U, et al. Sevoflurane mitigates shedding of hyaluronan from the coronary endothelium, also during ischemia/reperfusion: an ex vivo animal study. Hypoxia (Auckl). 2016;4:81-90.
157. Nemme J, Krizhanovskii C, Ntika S, Sabelnikovs O, Vanags I, Hahn RG. Hypervolemia does not cause degradation of the endothelial glycocalyx layer during open hysterectomy performed under sevoflurane or propofol anesthesia. Acta Anaesthesiol Scand. 2020;64(4):538-45.
158. Kim HJ, Kim E, Baek SH, Kim HY, Kim JY, Park J, et al. Sevoflurane did not show better protective effect on endothelial glycocalyx layer compared to propofol during lung resection surgery with one lung ventilation. J Thorac Dis. 2018;10(3):1468-75.

159. Koenig A, Norgard-Sumnicht K, Linhardt R, Varki A. Differential interactions of heparin and heparan sulfate glycosaminoglycans with the selectins. Implications for the use of unfractionated and low molecular weight heparins as therapeutic agents. The Journal of clinical investigation. 1998;101(4):877-89.
160. Alquwaizani M, Buckley L, Adams C, Fanikos J. Anticoagulants: A Review of the Pharmacology, Dosing, and Complications. Curr Emerg Hosp Med Rep. 2013;1(2):83-97.
161. Schmidt EP, Yang Y, Janssen WJ, Gandjeva A, Perez MJ, Barthel L, et al. The pulmonary endothelial glycocalyx regulates neutrophil adhesion and lung injury during experimental sepsis. Nat Med. 2012;18(8):1217-23.
162. Massena S, Christoffersson G, Hjertström E, Zcharia E, Vlodavsky I, Ausmees N, et al. A chemotactic gradient sequestered on endothelial heparan sulfate induces directional intraluminal crawling of neutrophils. Blood. 2010;116(11):1924-31.
163. Riffo-Vasquez Y, Somani A, Man F, Amison R, Pitchford S, Page CP. A Non-Anticoagulant Fraction of Heparin Inhibits Leukocyte Diapedesis into the Lung by an Effect on Platelets. American Journal of Respiratory Cell and Molecular Biology. 2016;55(4):554-63.
164. Wodicka J, Chambers A, Sangha G, Goergen C, Panitch A. Development of a Glycosaminoglycan Derived, Selectin Targeting Anti-Adhesive Coating to Treat Endothelial Cell Dysfunction. Pharmaceuticals. 2017;10(4):36-.
165. Mousavi S, Moradi M, Khorshidahmad T, Motamedi M. Anti-Inflammatory Effects of Heparin and Its Derivatives: A Systematic Review. Adv Pharmacol Sci. 2015;2015:507151-.
166. Nutescu EA, Burnett A, Fanikos J, Spinler S, Wittkowsky A. Pharmacology of anticoagulants used in the treatment of venous thromboembolism. Journal of thrombosis and thrombolysis. 2016;41(1):15-31.
167. Aláez-Versón CR, Lantero E, Fernàndez-Busquets X. Heparin: new life for an old drug. Nanomedicine. 2017;12(14):1727-44.
168. Vaidyanathan D, Williams A, Dordick JS, Koffas MAG, Linhardt RJ. Engineered heparins as new anticoagulant drugs. Bioeng Transl Med. 2017;2(1):17-30.
169. Oduah EI, Linhardt RJ, Sharfstein ST. Heparin: Past, Present, and Future. Pharmaceuticals (Basel, Switzerland). 2016;9(3):38.
170. Kim SY, Jin W, Sood A, Montgomery DW, Grant OC, Fuster MM, et al. Characterization of heparin and severe acute respiratory syndrome-related coronavirus 2 (SARS-CoV-2) spike glycoprotein binding interactions. Antiviral Research. 2020;181:104873.
171. van Haren FMP, Page C, Laffey JG, Artigas A, Camprubi-Rimblas M, Nunes Q, et al. Nebulised heparin as a treatment for COVID-19: scientific rationale and a call for randomised evidence. Critical Care. 2020;24(1):454.
172. Buijsers B, Yanginlar C, Maciej-Hulme ML, de Mast Q, van der Vlag J. Beneficial non-anticoagulant mechanisms underlying heparin treatment of COVID-19 patients. EBioMedicine. 2020;59:102969-.
173. Zhang L, Zeng M, Fan J, Tarbell JM, Curry F-RE, Fu BM. Sphingosine-1-phosphate Maintains Normal Vascular Permeability by Preserving Endothelial Surface Glycocalyx in Intact Microvessels. Microcirculation (New York, NY : 1994). 2016;23(4):301-10.
174. Park S-J, Im D-S. Sphingosine 1-Phosphate Receptor Modulators and Drug Discovery. Biomol Ther (Seoul). 2017;25(1):80-90.
175. Peyrin-Biroulet L, Christopher R, Behan D, Lassen C. Modulation of sphingosine-1-phosphate in inflammatory bowel disease. Autoimmunity Reviews. 2017;16(5):495-503.
176. Shea BS, Brooks SF, Fontaine BA, Chun J, Luster AD, Tager AM. Prolonged exposure to sphingosine 1-phosphate receptor-1 agonists exacerbates vascular leak, fibrosis, and mortality after lung injury. American journal of respiratory cell and molecular biology. 2010;43(6):662-73.
177. Lauver DA, Lucchesi BR. Sulodexide: A renewed interest in this glycosaminoglycan. Cardiovascular Drug Reviews. 2006;24(3-4):214-26.
178. Bignamini AA, Matuska J. Sulodexide for the Symptoms and Signs of Chronic Venous Disease: A Systematic Review and Meta-analysis. Adv Ther. 2020;37(3):1013-33.
179. Condorelli M, Chiariello M, Dagianti A, Penco M, Volta SD, Pengo V, et al. IPO-V2: A prospective, multicenter, randomized, comparative clinical investigation of the effects of sulodexide in preventing cardiovascular accidents in the first year after acute myocardial infarction. Journal of the American College of Cardiology. 1994;23(1):27-34.
180. Broekhuizen LN, Lemkes BA, Mooij HL, Meuwese MC, Verberne H, Holleman F, et al. Effect of sulodexide on endothelial glycocalyx and vascular permeability in patients with type 2 diabetes mellitus. Diabetologia. 2010;53(12):2646-55.
181. Coccheri S, Mannello F. Development and use of sulodexide in vascular diseases: implications for treatment. Drug Des Devel Ther. 2013;8:49-65.

182. Vanderwall AG, Milligan ED. Cytokines in Pain: Harnessing Endogenous Anti-Inflammatory Signaling for Improved Pain Management. Front Immunol. 2019;10:3009.
183. Borthwick LA, Wynn TA, Fisher AJ. Cytokine mediated tissue fibrosis. Biochimica et biophysica acta. 2013;1832(7):1049-60.
184. Rider P, Carmi Y, Cohen I. Biologics for Targeting Inflammatory Cytokines, Clinical Uses, and Limitations. Int J Cell Biol. 2016;2016:9259646-.
185. Haraoui B, Bykerk V. Etanercept in the treatment of rheumatoid arthritis. Ther Clin Risk Manag. 2007;3(1):99-105.
186. Campanati A, Giuliodori K, Ganzetti G, Liberati G, Offidani AM. A patient with psoriasis and vitiligo treated with etanercept. Am J Clin Dermatol. 2010;11 Suppl 1:46-8.
187. Raghu G, Brown KK, Costabel U, Cottin V, du Bois RM, Lasky JA, et al. Treatment of Idiopathic Pulmonary Fibrosis with Etanercept. American Journal of Respiratory and Critical Care Medicine. 2008;178(9):948-55.
188. Anker SD, Coats AJS. How to RECOVER from RENAISSANCE? The significance of the results of RECOVER, RENAISSANCE, RENEWAL and ATTACH. International Journal of Cardiology. 2002;86(2):123-30.
189. Nguyen T, Wu JJ. Relationship between tumor necrosis factor-α inhibitors and cardiovascular disease in psoriasis: a review. Perm J. 2014;18(1):49-54.
190. Abbate A, Toldo S, Marchetti C, Kron J, Van Tassell BW, Dinarello CA. Interleukin-1 and the Inflammasome as Therapeutic Targets in Cardiovascular Disease. Circ Res. 2020;126(9):1260-80.
191. Szekely Y, Arbel Y. A Review of Interleukin-1 in Heart Disease: Where Do We Stand Today? Cardiol Ther. 2018;7(1):25-44.
192. Barnes TC, Anderson ME, Moots RJ. The many faces of interleukin-6: the role of IL-6 in inflammation, vasculopathy, and fibrosis in systemic sclerosis. Int J Rheumatol. 2011;2011:721608.
193. Anti-il6 Treatment of Serious COVID-19 Disease With Threatening Respiratory Failure. https://ClinicalTrials.gov/show/NCT04322773; 2020.
194. Wright HL, Cross AL, Edwards SW, Moots RJ. Effects of IL-6 and IL-6 blockade on neutrophil function in vitro and in vivo. Rheumatology. 2014;53(7):1321-31.
195. Chan JM, Zhang L, Tong R, Ghosh D, Gao W, Liao G, et al. Spatiotemporal controlled delivery of nanoparticles to injured vasculature. Proceedings of the National Academy of Sciences. 2010;107(5):2213-8.
196. Moyer TJ, Kassam HA, Bahnson ESM, Morgan CE, Tantakitti F, Chew TL, et al. Shape-Dependent Targeting of Injured Blood Vessels by Peptide Amphiphile Supramolecular Nanostructures. Small. 2015;11(23):2750-5.
197. So MM, Mansukhani NA, Peters EB, Albaghdadi MS, Wang Z, Rubert Pérez CM, et al. Peptide Amphiphile Nanostructures for Targeting of Atherosclerotic Plaque and Drug Delivery. Advanced Biosystems. 2018;2(3):1700123.
198. Nigam A, Kopecky SL. Therapeutic Potential of Monoclonal Antibodies in Myocardial Reperfusion Injury. American Journal of Cardiovascular Drugs. 2002;2(6):367-76.
199. Weyrich AS, Ma XY, Lefer DJ, Albertine KH, Lefer AM. In vivo neutralization of P-selectin protects feline heart and endothelium in myocardial ischemia and reperfusion injury. J Clin Invest. 1993;91(6):2620-9.
200. Schmitt C, Abt M, Ciorciaro C, Kling D, Jamois C, Schick E, et al. First-in-Man Study With Inclacumab, a Human Monoclonal Antibody Against P-selectin. Journal of cardiovascular pharmacology. 2015;65(6):611-9.
201. Riley TR, Riley TT. Profile of crizanlizumab and its potential in the prevention of pain crises in sickle cell disease: evidence to date. J Blood Med. 2019;10:307-11.
202. Niwa R, Satoh M. The Current Status and Prospects of Antibody Engineering for Therapeutic Use: Focus on Glycoengineering Technology. Journal of Pharmaceutical Sciences. 2015;104(3):930-41.
203. Tardif JC, Tanguay JF, Wright SR, Duchatelle V, Petroni T, Gregoire JC, et al. Effects of the P-selectin antagonist inclacumab on myocardial damage after percutaneous coronary intervention for non-ST-segment elevation myocardial infarction: results of the SELECT-ACS trial. J Am Coll Cardiol. 2013;61(20):2048-55.
204. Chames P, Van Regenmortel M, Weiss E, Baty D. Therapeutic antibodies: successes, limitations and hopes for the future. Br J Pharmacol. 2009;157(2):220-33.
205. Efficacy and Safety of Rivipansel (GMI-1070) in the Treatment of Vaso-Occlusive Crisis in Hospitalized Subjects With Sickle Cell Disease. https://ClinicalTrials.gov/show/NCT02187003; 2015-2019.
206. Study to Assess Safety, Tolerability, and Efficacy of GMI-1271 in Patients With Calf-level Deep Venous Thrombosis (DVT). https://ClinicalTrials.gov/show/NCT02744833; 2016.
207. Langlois B, Belozertseva E, Parlakian A, Bourhim M, Gao-Li J, Blanc J, et al. Vimentin knockout results in increased expression of sub-endothelial basement membrane components and carotid stiffness in mice. Scientific reports. 2017;7(1):11628-.

208. Danielsson F, Peterson MK, Caldeira Araújo H, Lautenschläger F, Gad AKB. Vimentin Diversity in Health and Disease. Cells. 2018;7(10):147.
209. Moog KE, Barz M, Bartneck M, Beceren-Braun F, Mohr N, Wu Z, et al. Polymeric Selectin Ligands Mimicking Complex Carbohydrates: From Selectin Binders to Modifiers of Macrophage Migration. Angewandte Chemie International Edition. 2017;56(5):1416-21.
210. Li B, Juenet M, Aid-Launais R, Maire M, Ollivier V, Letourneur D, et al. Development of Polymer Microcapsules Functionalized with Fucoidan to Target P-Selectin Overexpressed in Cardiovascular Diseases. Adv Healthc Mater. 2017;6(4):1601200.
211. Wodicka JR, Morikis VA, Dehghani T, Simon SI, Panitch A. Selectin-Targeting Peptide-Glycosaminoglycan Conjugates Modulate Neutrophil-Endothelial Interactions. Cell Mol Bioeng. 2019;12(1):121-30.
212. Fukuda MN, Ohyama C, Lowitz K, Matsuo O, Pasqualini R, Ruoslahti E, et al. A Peptide Mimic of E-Selectin Ligand Inhibits Sialyl Lewis X-dependent Lung Colonization of Tumor Cells. Cancer Research. 2000;60(2):450 LP-6.
213. Salvadori M, Rosso G, Bertoni E. Update on ischemia-reperfusion injury in kidney transplantation: Pathogenesis and treatment. World J Transplant. 2015;5(2):52-67.
214. Singhal AK, Symons JD, Boudina S, Jaishy B, Shiu Y-TE. Role of Endothelial Cells in Myocardial Ischemia-Reperfusion Injury. Vascular Disease Prevention. 2014;7(1):1-14.
215. Singbartl K, Forlow SB, Ley K. Platelet, but not endothelial, P-selectin is critical for neutrophil-mediated acute postischemic renal failure. FASEB J. 2001;15(13):2337-44.
216. Schanze N, Bode C, Duerschmied D. Platelet Contributions to Myocardial Ischemia/Reperfusion Injury. Frontiers in Immunology. 2019;10:1260-.
217. Asaduzzaman M, Lavasani S, Rahman M, Zhang S, Braun OÖ, Jeppsson B, et al. Platelets support pulmonary recruitment of neutrophils in abdominal sepsis*. Critical Care Medicine. 2009;37(4):1389-96.

CHAPTER 2: DISCOVERY OF AN E-SELECTIN BINDING MOLECULE USING A ONE-BEAD-ONE-COMPOUND COMBINATORIAL PEPTIDE LIBRARY

2.1 Abstract

E- and P-selectin play a vital role in several disease processes, including cancer cell homing and leukocyte adhesion during inflammation, making these proteins desirable targets for drug discovery. Molecules that can interfere with native selectin-ligand interactions have the potential to make a lasting impact on patient health. To address this, we designed a one-bead-one-compound combinatorial peptide library weighted toward a known selectin binding peptide. This synthesis method allowed for the incorporation of D- and unnatural amino acids into the peptide library, lending enzymatic stability to potential lead sequences. In this work, we describe the methodology behind the library design, library screening, and eventual discovery of an E-selectin binding sequence containing multiple D-amino acids. Furthermore, we show that this peptide sequence can be readily conjugated to a glycosaminoglycan backbone, yielding a novel selectin binding molecule, DS-IkL.

2.2 Introduction

Selectins are desirable targets in drug discovery efforts in part due to their role in the leukocyte adhesion cascade (1, 2), mesenchymal stem cell homing (3), and cancer cell homing (4). We have shown previously that the selectin binding peptide-glycosaminoglycan conjugate termed “EC-SEAL” reduced neutrophil and platelet interactions with inflamed endothelium (5, 6). *In vivo,* treatment with this molecule reduced venous thrombosis to a similar extent as heparin – a medical gold standard – without significantly increasing bleeding time (5). Despite its success in these pre-clinical models, this molecule has several disadvantages that are addressed in the current work.

The primary limitations of EC-SEAL discussed in this work include the amino acid sequence of the selectin-binding peptide, and the conjugation chemistry used to link the peptide to the glycosaminoglycan backbone. The amino acid sequence, (L)Ile-(L)Glu-(L)Leu-(L)Leu-(L)Gln-(L)Ala-(L)Arg, consists only of L-amino acids as shown. Given that L-amino acids are the naturally occurring enantiomer, the peptide sequence is therefore highly susceptible to proteolytic degradation in human plasma (7).

To address enzymatic stability of the peptide sequence, we designed a one-bead-one-compound (OBOC) peptide library that included unnatural and D-amino acids. Over the past several decades, there has been a push to develop rapid and cost-effective tools to accelerate drug discovery. Among these are techniques such as the OBOC combinatorial peptide library synthesis method developed by Lam et al. (8, 9). This method has major advantages over biological techniques (e.g., filamentous phage or plasmids), including the ability to incorporate D-amino acids or unnatural building blocks into the library, the capacity to synthesize cyclic peptides, and the relative simplicity and speed of producing huge libraries of individual peptides of differing sequences. The OBOC method uses a solid support resin to build unique peptide sequences through sequential amino acid coupling steps. The solid support can be easily immobilized and visualized, allowing for rapid and simple screening without specialized equipment. Because of these characteristics and others, we chose to use the OBOC method to search for a novel E-selectin binding sequence.

Finally, we tested different conjugation chemistries to attach our novel peptide to a dermatan sulfate (DS) backbone. Previous work with EC-SEAL showed oxidation chemistry, achieved by reacting with sodium metaperiodate followed by a heterobifunctional crosslinker, allowed for tunable addition of peptides to DS. This work serves as a proof of concept for future studies to show DS can be similarly decorated with peptide using simpler, less destructive chemistries.

2.3 Methods

2.3.1 Peptide synthesis on TentaGel resin

Solid phase Fmoc peptide synthesis was used to synthesize the library. Ten-fold excess of amino acids (Aapptec, Bachem, Advanced ChemTech, or Propeptide) were used at each coupling step (**Table 2-1**). Ten-fold excess of each hydroxybenzotriazole (HOBt), 1H-Benzotriazolium 1-[bis(dimethyl-amino)methylene]-5-chloro-hexafluorophosphate (1-),3-oxide (HCTU), and N,N-Diisopropylethylamine (DIPEA) in DMF were added to each reaction vessel. In some cases, N, N′-Diisopropylcarbodiimide (DIC) and HOBt were used. Polypropylene columns or microcentrifuge tubes were used during coupling steps. Amino acid couplings occurred for 4h at 60°C or overnight at room temperature (RT) with agitation.

Coupling was confirmed using a ninhydrin test (Kaiser test) (ThermoFisher). For tubes in which coupling was incomplete, fresh Fmoc amino acid, HOBt, HCTU, and DIPEA were added, and the reaction allowed to occur at 60°C for 1 h with agitation. In most cases, double coupling was not needed. Fmoc deprotection was achieved by two 10-minute incubations with 20% piperidine (Sigma) in DMF with rotation. Resin was washed 3x with each DMF, dichloromethane (DCM), methanol (MeOH), and DMF after each incubation.

2.3.2 Library setup and synthesis

A peptide library containing D- and unnatural amino acids was designed (**Table 2-1**) and biased toward the parent sequence H_2N-I-E-L-L-Q-A-R-COOH (see Chapter 3, **Figure 3-1**). One gram of TentaGel S resin (90-130 uM, loading 0.31 mmol/g) was swollen overnight in 50% DMF/DCM in a polypropylene column before library synthesis. At each step, the resin suspension was split in half. One half was coupled to the next amino acid in the parent sequence; the remaining half was divided into 30-32 separate polypropylene columns and coupled to discrete amino acids. At the sixth coupling step, 25% of

the resin was coupled to Glu, 25% was coupled to Asp, and the rest was split evenly into the remaining columns. If coupling was complete, resin from all columns was combined and deprotected.

Table 2-1 Tentagel Focus Library

Parent sequence:		IELLQAR/IDLLMAR		0.155 mmol/29=0.0054
1	1-letter code	AA	MW	**X1-X7 10eq (mg)**
2	a	Fmoc-D-Ala-OH	311.33	119.86
3	R	Fmoc-Arg(pmf)-OH	662.80	255.18
4	n	Fmoc-D-Asn(Trt)-OH	596.70	229.73
5	D	Fmoc-Asp(OtBu)-OH	411.45	158.41
6	Q	Fmoc-Gln(Trt)-OH	610.70	235.12
7	e	Fmoc-D-Glu(OtBu)-OH	425.47	163.81
8	G	Fmoc-Gly-OH	297.31	114.46
9	I	Fmoc-Ile-OH	353.41	136.06
10	k	Fmoc-D-Lys(Boc)-OH	468.54	180.39
11	m	Fmoc-D-Met-OH	371.45	143.01
12	f	Fmoc-D-Phe-OH	387.43	149.16
13	p	Fmoc-D-Pro-OH	337.37	129.89
14	S	Fmoc-L-Ser(OtBu)-OH	383.44	147.62
15	h	Fmoc-D-His(Trt)-OH	619.70	238.58
16	w	Fmoc-D-Trp(Boc)-OH	526.58	202.73
17	Y	Fmoc-Tyr(OtBu)-OH	459.53	176.92
18	V	Fmoc-L-Val-OH	339.39	130.67
19	t	Fmoc-D-Thr(tBu)-OH	397.50	153.04
20		Fmoc-Nle-OH	353.40	136.06
21	O	Fmoc-Hyp(tBu)-OH	409.00	157.47
22		Fmoc-Aad(OtBu)-OH	439.60	169.25
23		Fmoc-D-3-Pal-OH	388.40	149.53
24		Fmoc-Dpr(Boc)-OH	426.40	164.16
25		Fmoc-D-Tyr(me)-OH	417.47	160.73
26		Fmoc-D-Phe(3-Cl)-OH	421.90	162.43
27		Fmoc-D-Chg-OH	379.40	146.07
28		Fmoc-Bpa-OH	491.50	189.23
29		Fmoc-D-Nal-2-OH	437.47	168.43
30		Fmoc-L-Nal-1-OH	437.47	168.43
31		Fmoc-Phe(3,4-diCl)-OH	456.40	175.71
50%		Fmoc-Cha-OH	393.48	151.49
50%	R	Fmoc-Arg(pmf)-OH	662.80	410.94
50%	A	Fmoc-Ala-OH	311.33	193.02
50%	Q	Fmoc-Gln(Trt)-OH	610.70	378.63
50%	L	Fmoc-Leu-OH	353.41	328.67
25%	L	Fmoc-Leu-OH	353.41	328.67
25%	E	Fmoc-Glu(OtBu)-OH	425.47	131.90
50%	D	Fmoc-Asp(OtBu)-OH	411.45	127.55
	I	Fmoc-Ile-OH	353.41	219.11
	DIC	0.815	126.2	**244.81**
	6-Cl-HOBt		169.57	**265.46**
	HCTU		413.69	
		0.742	129.24	

The cycle was repeated for a total of 7 couplings, producing a maximum of 31^7 unique peptide sequences (31 amino acids, 7 couplings). Resin underwent a final deprotection step before proceeding.

Deprotected resin was washed 3x each with DMF, DCM, MeOH, DMF, and DCM before drying overnight. The next day, protecting groups were cleaved from the resin with 82.5% trifluoroacetic acid (TFA), 5% ultrapure water, 5% phenol, 5% tris(hydroxymethyl)aminomethane (Tris), and 2.5% Triisopropyl silane (TIPS) for 4 hours at RT with rotation. The deprotected resin was washed at least 3x with DMF, neutralized with 10% DIPEA in DMF, washed at least 3x with DMF, and stored in 0.05% (w/v) sodium azide in ultrapure water at 4°C.

2.3.3 Library screening

Screening of the peptide library was performed in several iterations until 15 sequences were isolated. 300 uL of resin was immobilized in a polystyrene 12-well plate using 90% DMF in water such that 90% of each well was covered. Wells were washed with phosphate buffered saline (PBS) 3x to remove unbound resin. Resin was blocked with 5% bovine serum albumin (BSA) and human FC fragment (1:800) in PBS for 20 min at RT. Blocking solution was removed and wells treated with HRP anti-6X His tag antibody (Abcam) (1:1000 in PBS) for 1h at RT. Wells were washed 3x with PBS before adding 10% (v/v) 3,3'-diaminobenzidine (DAB) substrate in PBS for 5 minutes. Wells were washed 3x and visualized under 2X magnification using a dissecting microscope (see Chapter 3, **Figure 3-1**). Stained resin beads were removed from the wells using a 100 uL micropipette before proceeding with the full staining protocol.

Remaining resin was incubated with recombinant human E-selectin-6-His (R&D Systems) (1:1000) in PBS for 1 h at RT. Wells were washed 3x with PBS, blocked (5% BSA for 20 minutes), then incubated with HRP anti-6X His secondary antibody (1:7000) for 1 h at RT. Wells were washed 3x with PBS then incubated with 10% DAB substrate for 5 min. After 3x washes with PBS, resin was visualized under 2X magnification. In some cases, images were taken using a Dino-Eye Microscope Edge Eyepiece Camera (Dino-Lite).

Beads that stained positive after the full screening protocol were carefully removed with a micropipette and sequentially immersed in ultrapure water, 8 M guanidine hydrochloride for 20 min, then ultrapure water, before being isolated for microsequencing.

2.3.4 Peptide synthesis – 2-Cl-Trt-Cl

For DS conjugation, peptides were synthesized on 2-chlorotrityl chloride (2-Cl-Trt-Cl) resin (CEM Corporation) or purchased (Innopep). When synthesized, resin was functionalized with hydrazine hydrate prior to solid phase peptide synthesis. Resin was weighed into a 50 mL glass peptide synthesis vessel, washed 3x with each DMF, DCM, and DMF, then swollen in 50% DCM/DMF for 1 h with nitrogen or ambient air bubbling. The reaction vessel was drained then for every 1 g of resin, 10 mL of a 10% (v/v) solution of hydrazine hydrate (NH_2NH_2, 78-82%, Sigma) in DMF with 100 µL DIPEA was added. The reaction was bubbled with nitrogen or ambient air for 2 h at RT then drained. A fresh NH_2NH_2 + DIPEA solution was added for 1 h. Resin was then washed 3x with DMF for 1 min each, then washed 2x each DMF, DCM, DMF. Unreacted Cl groups were capped by nitrogen or ambient air bubbling with 10 mL of 10% (v/v) MeOH for 30 minutes. Resin was then washed 3x with DMF for 1 min each, then washed 2x each with DMF, DCM, DMF before amino acid coupling.

Four-fold excess of Fmoc-Glycine-OH (Aapptec) and OxymaPure were dissolved in DMF and added to the reaction vessel. DIPEA and DIC were added, and the reaction left bubbling with nitrogen or ambient air overnight. After one washing cycle, glycine was coupled once more for 4 h. Resin was washed once 3x with each DMF, DCM, DMF, and coupling confirmed by ninhydrin test. Resin was then coupled on a Liberty Blue Automated Peptide Synthesizer. A small amino acid spacer, COOH-(L)Gly-(L)Arg-(L)Gly-(D)Ser-NH_2, was coupled before the COOH-IkLLpOR-NH_2 sequence.

Once synthesized, resin was washed 3x with each DMF, DCM, DMF, DCM, then left to dry on a vacuum overnight. Dried resin was cleaved and precipitated using diethyl ether, dried, and purified using

reversed phase FPLC on a 1 h, 0-60% acetonitrile gradient against water. Peaks were collected and verified using matrix assisted laser desorption/ionization – time of flight (MALDI-ToF).

2.3.5 Peptide conjugation to DS

Peptides were conjugated to DS using one of three chemistries, oxidation, DMTMM, or EDC, as described below.

Oxidation: Sodium metaperiodate was dissolved at 12 mg/mL in 0.1 M acetate buffer. Dermatan sulfate (DS, MW 41816 Da, Celcus Labs) was dissolved at 20 mg/mL in 0.1 M acetate buffer. The solutions were combined and reacted with shaking for 2 h at RT. Oxidized DS was then purified against 1x phosphate buffered saline (PBS) using a Biogel P-6 size exclusion column (BioRad) on an aqueous FPLC. The DS peak was collected into a conical tube containing 7 mg of (N-β-maleimidopropionic acid hydrazide) (BMPH). The solution was reacted for 2 h at RT with shaking before undergoing a second purification. The DS-BMPH peak was collected, frozen, and lyophilized for the next conjugation step. The area under the curve was calculated using a standard curve to determine the number of BMPH crosslinkers present on the DS by subtracting unbound BPMH from total added.

Purified DS-BMPH was dissolved in ultrapure water. Half of a 5 mg/mL solution of IkLLpORGC was added dropwise with agitation. After 15 minutes of shaking, the second half was added dropwise with agitation. The solution was left shaking for 2 h at RT. After 2 h a solution of semicarbazide hydrochloride was added and reacted for 2 h at RT. The resulting solution was purified against ultrapure water using size exclusion FPLC, frozen, and lyophilized.

DMTMM: DS was dissolved in phosphate buffer (pH 4.54) and reacted with 45 equivalents of 4-(4,6-dimethoxy-1,3,5-triazin-2-yl)-4-methyl-morpholinium chloride (DMTMM) for 5 minutes. HyNic-GRGsIkLLpOR (InnoPep) or N_2H_3GRGsIkLLpOR was dissolved in phosphate buffer and added to the reaction. The reaction was left to complete for 48-60 hours at room temperature with end-over-end rotation, quenched with water, then filtered using tangential flow filtration. Purified molecules were frozen and

lyophilized. The number of peptides bound was quantified by reading absorbance at 280 nm (HyNic-GRGsIkLLpOR) or 205 nm (N_2H_3GRGsIkLLpOR) on a NanoDrop Microvolume Spectrophotometer (ThermoFisher Scientific) and comparing it to a standard curve of free peptide.

EDC: DS was dissolved in 2-ethanesulfonic acid (MES) buffer (pH 4.54) and reacted with 45 equivalents of 1-Ethyl-3-(3-dimethylaminopropyl)carbodiimide (EDC) for 5 minutes. HyNic-GRGsIkLLpOR (InnoPep) or N_2H_3GRGsIkLLpOR was dissolved in MES buffer and added to the reaction. The reaction was left to complete for 48-60 hours at room temperature with end-over-end rotation. The reaction was stopped by increasing to pH 8 and left shaking for 30 min, then purified against ultrapurewater using tangential flow filtration. Purified molecules were frozen and lyophilized. The number of peptides bound was quantified by reading absorbance at 280 nm (HyNic-GRGSsIkLLpOR) or 205 nm (N_2H_3GRGsIkLLpOR) on a NanoDrop Microvolume Spectrophotometer (ThermoFisher Scientific) and comparing it to a standard curve of free peptide.

2.4 Results

2.4.1 Sequence determination

After several microsequencing iterations, 15 sequences of interest were listed in random order in an Excel spreadsheet and compared (**Table 2-2**). Four lead sequences were chosen for further study based on incorporation of D-amino acids and presence of conserved amino acids (**Table 2-3**). Lead sequences were synthesized on TentaGel S-NH_2 resin using a Liberty Blue Automated Microwave Peptide Synthesizer (CEM Corporation) and immobilized in individual wells of a 12-well polystyrene plate. The screening protocol was repeated as described to compare relative background and positive E-selectin binding among the sequences. Background staining and E-selectin binding was visualized using a benchtop dissecting microscope at 2X magnification. The sequence with the least background staining and greatest positive full

staining, (L)Ile-(D)Lys-(L)Leu-(L)Leu-(D)Pro-(L)Hyp-(L)Arg, was selected for future studies (data not shown).

Table 2-2 E-selectin Binding Peptide Library: Sequences of Interest

X_1	X_2	X_3	X_4	X_5	X_6	X_7
s	E	L	L	R	Q	R
I	Y	L	n	Nle	Hyp	R
I	k	s	L	Q	Nle	R
Nle	Q	h	f	Q	h	R
h	D	L	Dpr	Q	Hyp	R
Y	R	Y	e	D	L	D
k	R	D	L	Q	A	R
R	h	f	m	p	g	R
Y	R	Y	e	D	L	D
I	R	L	L	Nle	n	A
I	D	h	Dpr	R	hyp	R
k	D-Tyr(Me)	L	L	k	Hyp	Nal-1
R	R	R	L	Q	A	w
I	a	p	L	Q	nal-2	R
I	D	L	L	m	Q	Bpa
D	nal-2	h	Bpa	t	f	Aad
Dpr	E	S	Bpa	Q	h	R
h	E	L	L	D	D	Nal-1
I	D	R	Phe(3,4-diCl)	V	Nal-1	k
I	R	D-Phe(3-Cl)	Phe(3,4-diCl)	k	D-Try(Me)	R
I	D-Phe(3-Cl)	L	L	R	k	p
I	k	L	L	p	Hyp	R
Nle	D-Tyr(Me)	I	w	Q	h	R
I	R	L	L	T	D-Nal-2	k
I	f	Phe(3,4-diCl)	R	Q	D	k
D-Chg	p	Dpr	L	Q	p	R
Cha	E	R	h	Q	Hyp	Bpa
I	n	L	Cha	t	Q	I
I	Nle	t	D	Q	D-Nal-2	R
D-Tyr(Me)	D-Chg	k	L	I	D-3-Pal	Cha

Blue: Unusual or unnatural amino acids. Red: D-amino acids. Letters denote one-letter codes of standard amino acids.

Table 2-3 Amino Acid Composition of Lead Sequences

Lead sequences*	**D-amino acids (red)**	**Unnatural or unusual amino acids (blue)**
k-R-D-L-Q-A-R	k: D-Lysine	
I-k-L-L-p-O-R	k: D-Lysine; p: D-Proline	
I-f-Phe-R-Q-D-k	f: D-Phenylalanine; k: D-Lysine	Phe: D-Phe(3-Cl)
k-Tyr-L-L-k-O-Nal	k: D-Lysine	Tyr: D-Tyr(me); Nal: L-Nal-1

**Parent sequence: I-E-L-L-Q-A-R*

2.4.2 Peptide conjugation to a dermatan sulfate backbone

As a proof-of-concept study, peptides were conjugated to dermatan sulfate (DS) using three different chemistries (**Table 2-4**). Oxidation chemistry was used to create a molecule similar to the parent molecule, EC-SEAL. In this iteration, we wanted to first verify that up to 30 peptides could be successfully added to the DS backbone. Oxidation by sodium metaperiodate works by cleaving the DS ring at vicinal diols, thereby creating a conjugation point for a heterobifunctional cross linker such as BMPH (**Figure 2-1A**). By creating more sites for peptide conjugation, the DS ring structure is increasingly damaged, rendering it vulnerable to random coil and reducing molecule stability (10).

To address this, we tested DMTMM and EDC as conjugation chemistries. DMTMM and EDC activate the carboxylic acid on the ring structure, thereby leaving the ring structure intact (**Figure 2-1**). We tested EDC and DMTMM conjugation efficiency by activating 45 of the approximately 100 carboxylic acids on the DS polymer. Fifteen equivalents of peptide were added for each reaction. As shown in **Table 2-4**, the EDC reaction was slightly less efficient than DMTMM, with only 11 peptides conjugating to the backbone compared to 15.

Table 2-4 EDC, DMTMM, and Oxidation chemistry calculations

Chemistry	Avg abs, 280 nm (DS-EDC or DS-DMTMM subtracted)	mg/ml peptide (from standard curve)	% Contribution to molecule weight	Avg # of peptides per DS
EDC	1.2841875	0.2693817704	0.2693817704	11.14415902
DMTMM	1.573791667	0.3312590361	0.3312590361	14.97198588
Chemistry	**Unbound BMPH (mg)**	**Bound BMPH**	**Ratio of BMPH to DS***	**Molar Ratio of DS:IkL to add**
Oxidation	3.522712701	3.491287299	**27.11853899**	32.64817374
Standard Curves	**HyNic-N2H3GRGsIkLLpOR**	**BMPH (unbound)**		
Equations	y = 4.6803x + 0.0468	y = 271.39x - 12.729		
**Theoretical maximum number of peptides that can be added to the modified DS*				

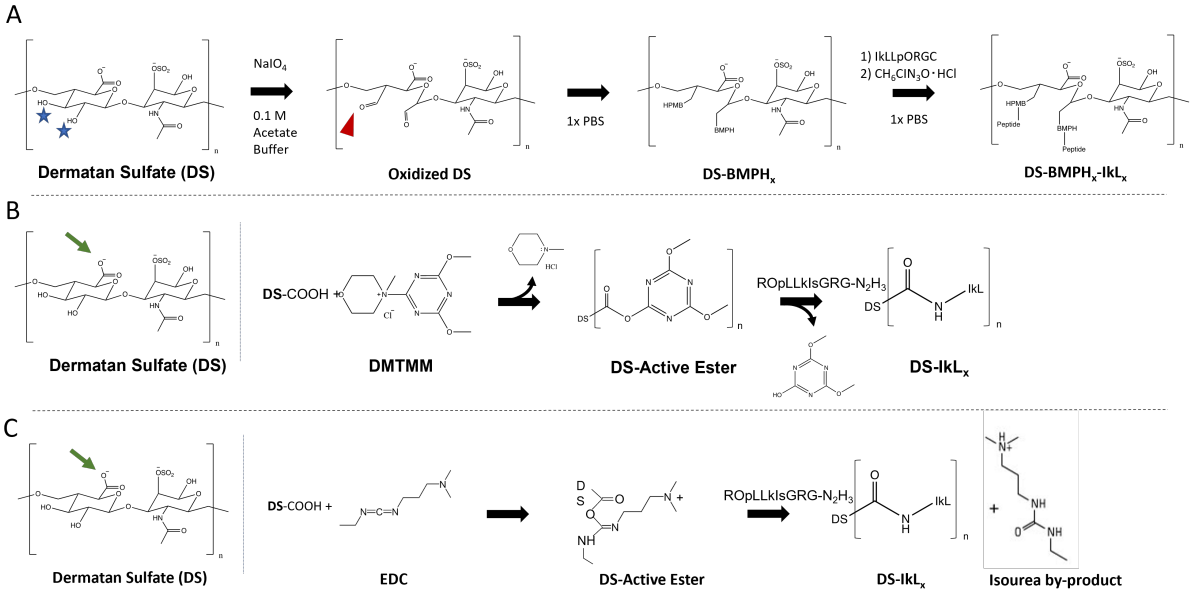

Figure 2-1 Conjugation chemistry used to link DS to DMTMM. Sodium metaperiodate cleaves the DS ring structure between two vicinal diols (blue stars) to create active aldehyde intermediates (red wedge) (**A**). During DMTMM conjugation, DMTMM reacts with a carboxylic acid (green arrow) to form an active ester intermediate (**B**). EDC works similarly to DMTMM but results in an isourea by-product (**C**).

2.5 Discussion

The one-bead-one-compound (OBOC) combinatorial peptide library synthesis method (8, 11) has been greatly influential in the discovery of disease targeting peptides and small molecules. This solid state synthesis format gives greater flexibility in the types of building blocks one can incorporate into the library,

including, but not limited to, D- and unusual amino acids (8). The OBOC method is compatible with most solid-state peptide synthesis resins, making it a highly adaptable tool for drug discovery.

In this work, TentaGel S-NH_2 resin was used to synthesize the peptide library. TentaGel S resin consists of a polystyrene bead attached to a polyethylene glycol (PEG) linker (**Figure 2-2**). This linkage is not acid labile, allowing for TFA cleavage of protecting groups from the final peptide after reaching a desired length – in this case, 7 mer – without cleaving the peptide from the solid support. The peptide-on-resin format allowed for the simple screening protocol described here. Screening was also facilitated by the PEG linker; PEG acts as a spacer, distancing the peptides from the resin bead.

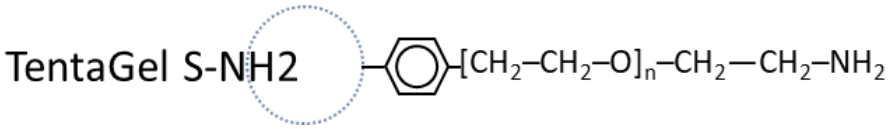

Figure 2-2 Structure of TentaGel S-NH2 resin

We have described the design of a OBOC peptide library for the discovery of a novel E-selectin binding peptide. Though several selectin binding peptides exist in the literature (5, 12), the vast majority are composed of L-amino acids – the more enzymatically vulnerable enantiomer (7). To address this, D- and unnatural amino acids were incorporated into the OBOC library (**Table 2-1**). Screening iterations yielded several sequences containing these building blocks (**Table 2-2**), suggesting selectin targeting may be achieved with more enzymatically resistant peptide sequences. However, given that D- and unnatural amino acids can influence peptide conformation and biological activity (13, 14), additional functional studies are needed to assess *in vivo* efficacy and safety.

The discovery of E-selectin binding sequences with high affinity has been historically difficult (15), in part due to the low affinity of E- and P-selectin for individual binding ligands (12, 15). A major advantage of the OBOC library is the multivalent nature of the peptide-bead, with each bead containing of 100-350 pmol or 10^{13} of copies of the same peptide on each bead. While the high density may increase the likelihood

of nonspecific binding to the peptide-bead due to phenomena such as charge-charge interactions or low affinity interactions within a high density of ligand (16), in our hands optimization of the antibody and protein treatments was sufficient to minimize background staining during the screening process. Multiple screening iterations yielded 15 peptide sequences of interest, which were further narrowed down to 4 sequences. After an additional screening step, wherein color development was monitored after background subtraction in the presence or absence of recombinant human E-selectin, a lead E-selectin binding sequence was determined: IkLLpOR.

To verify we could decorate DS with our peptide, we tested three different conjugation chemistries: oxidation, DMTMM, and EDC. Though oxidation chemistry is highly tunable, increasing amounts of modification interfere with the stability of the DS (10). By using a non-destructive chemistry such as DMTMM or EDC, which activate carboxylic acids on the DS backbone, we can modify the same number of DS monomers – 15 – with half the number of peptides. Our molecule would therefore remain multivalent while maintaining molecule stability. Of the non-destructive chemistries DMTMM and EDC, we saw better coupling efficiency with DMTMM after the 48-h conjugation period; therefore, we chose to move forward with this chemistry in future work.

In future studies using a peptide library, functional screening protocols after initial screening may be better suited to molecule discovery depending on the interaction of interest. One limitation of the screening protocol used in this work was the lack of a fluid shear component when binding to E-selectin. Selectins act as catch bonds, wherein the bonds strengthen as shear force is applied (17). Therefore, incorporation of a flow component into the screening protocol (e.g., by using a microfluidic device) may lead to sequences with greater binding affinity, particularly after lead sequences have been identified using the simple screening protocol described here.

2.6 Conclusions

In this work, we describe the design and synthesis of a peptide-bead combinatorial library using the OBOC split synthesis method. The library was biased toward a known E-selectin binding sequence (5, 12), and consisted of L, D-, and unnatural amino acids. A simple screening protocol requiring standard laboratory equipment was used to select beads of interest for microsequencing. Sequences were further assessed until a lead sequence, IkLLpOR, was selected for future studies. We proceeded to show this peptide can be conjugated to a dermatan sulfate backbone using any of three chemistries. Conjugation efficiency and degree of DS modification/ring cleavage were compared among oxidation, DMTMM, and EDC conjugation. Of the three, DMTMM showed the greatest conjugation efficiency without cleaving the ring structure and was therefore selected for future work.

2.7 Acknowledgements

We thank members of Dr. Kit Lam's lab at UC Davis for their help with the conceptualization and synthesis of the peptide library, including Dr. Xiaocen (Chris) Li and Dr. Ruiwu Liu. We would also like to thank the Combinatorial Chemistry and Chemical Biology Shared Resource at University of California Davis for assistance of synthesis and sequence decoding of OBOC peptide library, and the UC Davis Campus Mass Spectrometry Facilities (CMSF) for access to the MALDI-ToF Spectrometer.

2.8 References

1. Ley K, Laudanna C, Cybulsky MI, Nourshargh S. Getting to the site of inflammation: the leukocyte adhesion cascade updated. Nature Reviews Immunology. 2007;7(9):678-.
2. Dehghani T, Panitch A. Endothelial cells, neutrophils and platelets: getting to the bottom of an inflammatory triangle. Open Biol. 2020;10(10):200161.
3. Jiang L, Song XH, Liu P, Zeng CL, Huang ZS, Zhu LJ, et al. Platelet-mediated mesenchymal stem cells homing to the lung reduces monocrotaline-induced rat pulmonary hypertension. Cell Transplant. 2012;21(7):1463-75.
4. Natoni A, Macauley MS, O'Dwyer ME. Targeting Selectins and Their Ligands in Cancer. Frontiers in Oncology. 2016;6(93).
5. Wodicka J, Chambers A, Sangha G, Goergen C, Panitch A. Development of a Glycosaminoglycan Derived, Selectin Targeting Anti-Adhesive Coating to Treat Endothelial Cell Dysfunction. Pharmaceuticals. 2017;10(4):36-.
6. Wodicka JR, Morikis VA, Dehghani T, Simon SI, Panitch A. Selectin-Targeting Peptide-Glycosaminoglycan Conjugates Modulate Neutrophil-Endothelial Interactions. Cell Mol Bioeng. 2019;12(1):121-30.
7. Tugyi R, Uray K, Ivan D, Fellinger E, Perkins A, Hudecz F. Partial D-amino acid substitution: Improved enzymatic stability and preserved Ab recognition of a MUC2 epitope peptide. Proc Natl Acad Sci U S A. 2005;102(2):413-8.
8. Lam KS, Salmon SE, Hersh EM, Hruby VJ, Kazmierski WM, Knapp RJ. A new type of synthetic peptide library for identifying ligand-binding activity. Nature. 1991;354(6348):82-4.
9. Pei D, Appiah Kubi G. Developments with bead-based screening for novel drug discovery. Expert Opinion on Drug Discovery. 2019;14(11):1097-102.
10. Perlin AS. Glycol-Cleavage Oxidation. Academic Press Inc.; 2006. p. 183-250.
11. Lam KS, Lake D, Salmon SE, Smith J, Chen ML, Wade S, et al. A One-Bead One-Peptide Combinatorial Library Method for B-Cell Epitope Mapping. Methods. 1996;9(3):482-93.
12. Fukuda MN, Ohyama C, Lowitz K, Matsuo O, Pasqualini R, Ruoslahti E, et al. A Peptide Mimic of E-Selectin Ligand Inhibits Sialyl Lewis X-dependent Lung Colonization of Tumor Cells. Cancer Research. 2000;60(2):450 LP-6.
13. Gao W, Cho E, Liu Y, Lu Y. Advances and Challenges in Cell-Free Incorporation of Unnatural Amino Acids Into Proteins. Frontiers in Pharmacology. 2019;10(611).
14. Melchionna M, Styan KE, Marchesan S. The Unexpected Advantages of Using D-Amino Acids for Peptide Self- Assembly into Nanostructured Hydrogels for Medicine. Curr Top Med Chem. 2016;16(18):2009-18.
15. Kaila N, Thomas Iv BE. Design and synthesis of sialyl Lewisx mimics as E- and P-selectin inhibitors. Medicinal Research Reviews. 2002;22(6):566-601.
16. Chen X, Tan PH, Zhang Y, Pei D. On-Bead Screening of Combinatorial Libraries: Reduction of Nonspecific Binding by Decreasing Surface Ligand Density. Journal of Combinatorial Chemistry. 2009;11(4):604-11.
17. Morikis VA, Chase S, Wun T, Chaikof EL, Magnani JL, Simon SI. Selectin catch-bonds mechanotransduce integrin activation and neutrophil arrest on inflamed endothelium under shear flow. Blood. 2017;130(19):2101-10.

CHAPTER 3: SELECTIN-TARGETING GLYCOSAMINOGLYCAN-PEPTIDE CONJUGATE LIMITS NEUTROPHIL MEDIATED CARDIAC REPERFUSION INJURY

This chapter consists of a manuscript published by Dehghani T, Thai PN, Sodhi H, Ren L, Sirish P, Nader CE, Timofeyev V, Overton JL, Li X, Lam KS, Chiamvimonvat N, and Panitch P in *Cardiovascular Research*, 2020, https://doi.org/10.1093/cvr/cvaa312.

3.1 Abstract

Aims: One of the hallmarks of myocardial infarction (MI) is excessive inflammation. During an inflammatory insult, damaged endothelial cells shed their glycocalyx, a carbohydrate-rich layer on the cell surface which provides a regulatory interface to immune cell adhesion. Selectin-mediated neutrophilia occurs as a result of endothelial injury and inflammation. We recently designed a novel selectin-targeting glycocalyx mimetic (termed DS-IkL) capable of binding inflamed endothelial cells. This study examines the capacity of DS-IkL to limit neutrophil binding and platelet activation on inflamed endothelial cells, as well as the cardio-protective effects of DS-IkL after acute myocardial infarction.

Methods and Results: *In vitro*, DS-IkL diminished neutrophil interactions with both recombinant selectin and inflamed endothelial cells, and limited platelet activation on inflamed endothelial cells. Our data demonstrated that DS-IkL localized to regions of vascular inflammation *in vivo* after 45 minutes of left anterior descending coronary artery ligation induced MI. Further, findings from this study show DS-IkL treatment had short- and long-term cardioprotective effects after ischemia/reperfusion at the left anterior descending coronary artery. Mice treated with DS-IkL immediately after ischemia/reperfusion and 24 hours later exhibited reduced neutrophil extravasation, macrophage accumulation, fibroblast and endothelial cell proliferation, and fibrosis compared to saline controls.

Conclusions: Our findings suggest that DS-IkL has great therapeutic potential after MI by limiting reperfusion injury induced by the immune response.

3.2 Introduction

Cardiovascular disease remains the leading cause of mortality in the United States. Approximately 805,000 Americans will be diagnosed with coronary artery disease (CAD), the most common heart disease, this year (1). Approximately half of those diagnosed with CAD will be susceptible to acute myocardial infarction (MI), as well as complications that can lead to heart failure and sudden cardiac death (2). Although initial damage occurs during acute MI due to oxygen deprivation during the ischemic phase, it is well documented that further injury can result from reperfusion (3). The effects of reperfusion injury (RI) are complex. In the absence of oxygen, ischemic tissues experience severe disruptions to their homeostasis. A necessary shift from aerobic to anaerobic metabolism results in the accumulation of lactic acid, which contributes to a decline in intracellular pH, an impairment of ion exchange, and an increase in reactive oxygen species (ROS) production (3, 4), subsequently damaging cells within the vicinity. Paradoxically, the restoration of blood flow further contributes to cellular damage, partly due to inefficient oxidative phosphorylation that results in further production of ROS, reductions in nitric oxide (NO), and the recruitment of immune cells (5, 6).

Ischemia/reperfusion induced damage to vascular endothelial cells (EC) initiates an inflammatory cascade that recruits neutrophils and platelets to the sites of damage (5). Increased permeability of the vasculature potentiates RI by allowing the infiltration of immune cells into the tissue. Reperfused ECs experience disruptions to their Ca^{2+} homeostasis and begin to contract (7), giving rise to endothelial gaps that facilitate the extravasation of leukocytes being recruited by ROS and cytokines. Though these cells have vital cardioprotective functions, overaccumulation of leukocytes and activated platelets exacerbates myocardial damage, contributing to the overall infarct size.

During RI, ECs shed their glycocalyx, a carbohydrate-rich protective layer that resides on the surface of healthy endothelium (8, 9). The glycocalyx is known to play a role in many cellular processes, including mechanotransduction (10), microvascular permeability (11), and modulation of inflammatory

mediators (12). Diminution of the endothelial glycocalyx has been shown to contribute to vascular edema as well as neutrophil and platelet adhesion (10, 13). While the endothelial glycocalyx has been shown to recover from enzyme-induced damage, this recovery was inversely proportional to white blood cell count (14). The inflammatory response hence plays a critical role in RI with respect to the glycocalyx, with neutrophil influx (15, 16) and increased enzyme production (8, 17) likely delaying glycocalyx regeneration. Therefore, a molecule that provides a stable, stealthy interface with the capacity to down-regulate platelet activation and neutrophil capture could prevent inflammation-mediated RI.

To address this critical problem, we have designed a novel multivalent selectin-targeting carbohydrate conjugate (termed DS-IkL) that effectively abates neutrophil interactions within damaged regions of the vasculature. Given the elevated levels of matrix metalloproteinases and other proteolytic enzymes within the inflammatory zone, the glycosaminoglycan-derived backbone is conjugated to several selectin binding peptides consisting of D- or unnatural amino acids in order to increase the enzymatic stability of the molecule in the harsh inflammatory environment. We directly test the hypothesis that DS-IkL will significantly interfere with neutrophil capture and platelet activation on ECs *in vitro,* and provide beneficial effects *in vivo* in a preclinical model of MI by reducing neutrophil extravasation, macrophage accumulation, fibroblast and EC proliferation, and fibrosis.

Our study demonstrates that DS-IkL interfered with neutrophil capture and adhesion on E-selectin substrates and cytokine stimulated cardiac-derived ECs. DS-IkL provided a protective effect against platelet activation on ECs *in vitro*, maintaining a similar activation state as on unstimulated ECs. In corroboration with these findings, we observed cardioprotection after a left anterior descending coronary artery (LAD) ligation-induced MI in mice *in vivo*. Treatment with DS-IkL resulted in improved cardiac function, reduced fibrosis, and a significant decrease in neutrophil, macrophage, proliferative fibroblasts, and proliferative ECs in the infarcted region. Taken together, these findings establish a therapeutic role of DS-IkL after MI by reducing reperfusion injury mediated by the immune response.

3.3 Materials and Methods

For more detailed methods, please see **Supplementary Materials**.

3.3.1 Animal Model / IR Surgery

We used 10-16 week-old male and female C57Bl/6J mice for this study. All animal handling and laboratory procedures were performed in accordance with the approved protocols of the Institutional Animal Care and Use Committee of the University of California, Davis, which conforms to the Guide for the Care and Use of Laboratory Animals published by the US National Institutes of Health (8th Edition, 2011). Mice were selected to undergo either sham-operation, or ischemia followed by 24 hours [triphenyltetrazolium chloride (TTC) staining and cardiac troponin measurments], 36 hours [in vivo imaging (IVIS) and fluorescence assisted cell sorting (FACS) analysis], or 2 weeks (electrophysiology, histology, immunohistochemistry) of reperfusion (I/R). Mice were anesthetised with 80 mg/kg ketamine and 5 mg/kg xylazine, intraperitoneal, prior to surgery. After toe pinch and corneal reflexes were lost, ischemia was induced by ligating the proximal LAD coronary artery for 45 minutes. Anaesthesia was maintained by supplementing 1% isoflurane throughout the I/R procedure. Mice were injected with 100 µl of either 0.9% saline or 30 µM DS-IkL in saline via the tail vein immediately after reperfusion and at t=24 hours. Mice were randomly selected to receive either DS-IkL or saline. Mice were given buprenorphine twice daily for 48-72 hours post-operation (0.1 mg/kg subcutaneously). For euthanasia, mice were injected with 80 mg/kg ketamine and 5 mg/kg xylazine to achieve a surgical plane of anaesthesia followed by exsanguination upon removal of the heart. Cardiac structure and function, and neutrophil and macrophage aggregation, were assessed 2 weeks after surgery. For the *in vivo* imaging system and flow cytometry experiments, mice were allowed to recover for 36 hours after surgery. Animals were imaged on an IVIS Spectrum in vivo imaging system (Perkin Elmer) 1, 12, 24, and 36 hours after reperfusion prior to euthanasia. For TTC staining and troponin analysis, mice were euthanized 24 hours following reperfusion.

3.3.2 Peptide Library

A combinatorial peptide library biased toward a known 7-mer selectin-binding peptide sequence, Ile-Glu-Leu-Leu-Asp-Ala-Arg19, 20, was created using the one-bead-one-peptide split synthesis method21 on Tentagel S resin. The library was split a total of 7 times, yielding 317 unique sequences (**Figure 3-1**). Protecting groups were cleaved (82.5% trifluoroacetic acid, 5% phenol, 5% water, 5% thioanisole, 2.5% triisopropylsilane) and resin screened for binding to recombinant human E-selectin Fc chimera. One sequence, Ile-(D)Lys-Leu-Leu-(D)Pro-Hydroxyproline-Arg (IkL) was selected for use in the experiments described herein.

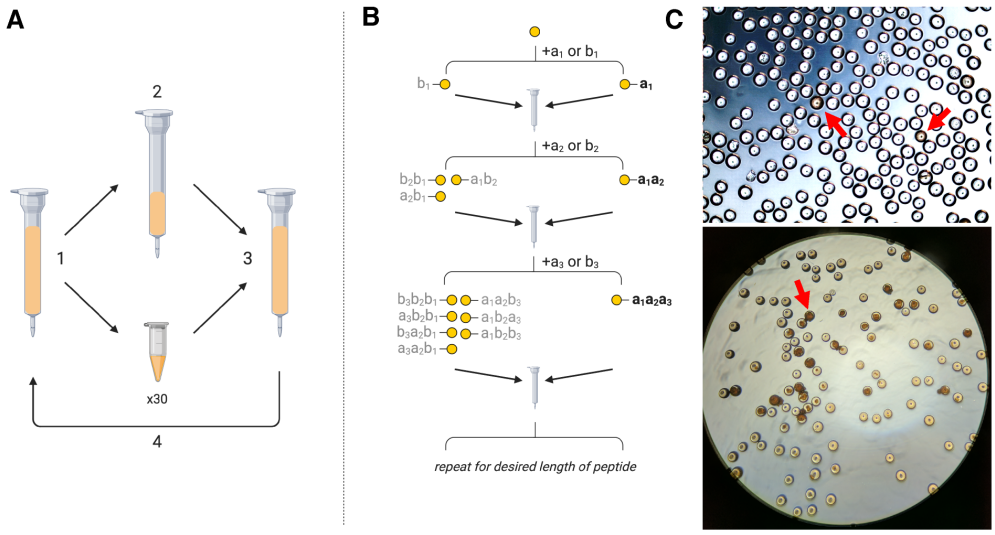

Figure 3-1 One-bead-one-peptide library synthesis. A) A combinatorial peptide library was designed using the split synthesis method of Lam et al. biased toward a known E-selectin binding sequence. (1) Resin was split in half; (2) half was coupled to the first amino acid of the selectin binding sequence and the other half divided evenly into 30 tubes, each containing a different amino acid. (3) After coupling was complete, resin was combined and deprotected. (4) The cycle was repeated for each amino acid in the selectin-binding sequence to create a library with 31^7 unique peptide sequences. **B**) In each step, resin is divided in two and coupled to a different amino acid, b_x or a_x. The cycle is repeated three times to create a library with 2^3 unique sequences. **C**) An example of the screening result is shown. Resin with peptide that bound E-selectin can be seen in brown (red arrows). This figure was created with BioRender.

3.3.3 DS-IkL Synthesis

Dermatan sulphate (DS, 41816 Da, Celsus Laboratories) was dissolved in phosphate buffer (pH 4.54) and reacted with 45 equivalents of 4-(4,6-dimethoxy-1,3,5-triazin-2-yl)-4-methyl-morpholinium chloride (DMTMM) for 5 minutes. HyNic-GRGsIkLLpHypR (IkL) (InnoPep) was dissolved in phosphate buffer and added to the reaction. The reaction was left to complete for 48-60 hours at room temperature with constant shaking, quenched with water, then filtered using tangential flow filtration. Purified molecules were frozen and lyophilized for future use. The number of peptides bound was quantified by reading absorbance at 280 nm on a NanoDrop Microvolume Spectrophotometer (ThermoFisher Scientific) and comparing it to a standard curve of free peptide. Unless otherwise stated, molecule with an average of 14-16 peptides bound per DS was used for the present studies. For fluorescent molecules, CF594 Dye Hydrazide (Biotum) was conjugated to DS using 2 equivalents of DMTMM and the complex purified before conjugation to IkL.

3.3.4 Cell Culture

Human cardiac microvascular endothelial cells (HCMEC, PromoCell) p4-6 were used. Stimulation media was prepared by diluting to 0.4 ng/ml tumour necrosis factor alpha (TNF-α) and 0.3 ng/ml interleukin 1 beta (IL-1β) in complete endothelial growth medium MV (PromoCell).

3.3.5 Neutrophil and Platelet Isolation

Human whole blood was collected into EDTA (neutrophil experiments) or sodium citrate (platelet experiments) tubes in accordance with approved protocols of the Institutional Review Board Administration at UC Davis, which conform to the principles outlined in the Declaration of Helsinki. All participants gave informed consent prior to participation in the study. Neutrophils were isolated using an EasyStep Direct Human Neutrophil Isolation Kit (Stem Cell Technologies) and used at 0.3-2x10^6 cells/ml in Hank's Balanced Salt Solution with calcium and magnesium ($HBSS^{+/+}$) supplemented with 0.1% human serum

albumin (HSA). For HCMEC binding experiments, neutrophils were stained with 1.5 nM Calcein-AM (BioLegend) for 30 minutes at 37˚C before use. For microsphere experiments, neutrophils were stained with AF488 anti-human CD11a/CD18 (clone m24) and PE anti-human CD15 (clone HI98) antibodies (BioLegend) for 20 minutes on ice. For platelet experiments, blood was separated by centrifugation for 20 minutes at 200 x g; the resultant platelet rich plasma (PRP) layer was collected and used.

3.3.6 Platelet Activation

HCMECs were grown to confluence on 96-well CellBind plates then treated with 30 μM DS-IkL, 450 μM IkL peptide, or 30 μM DS in stimulation media for 4 hours. Wells were rinsed 2x with $HBSS^{+/+}$ then treated with 100 μL of PRP at 37˚C. After 1 hour, 45 μL of PRP was removed from each well and added to tubes containing 5 μL of ETP [107 mM Ethylenediaminetetraacetic acid, disodium salt (EDTA), 12 mM Theophylline, and 2.8 μM Prostaglandin E1 in water]. Samples were briefly centrifuged and flash frozen.

3.3.7 NAP-2 and PF-4 ELISA

Unless otherwise stated, all incubations occurred at room temperature with shaking (700 RPM) and wells were rinsed 3x with PBS+0.05% Tween 20 (PBST) or 1% BSA in PBS between steps. Mouse monoclonal anti-hNAP-2 IgG and anti-hPF4 IgG_{2B} capture antibodies (R&D Systems) were coated on 96-well EIA/RIA high binding plates (Corning) at 2 μg/mL in 1x PBS and incubated at 4˚C overnight. Wells were then blocked for 1 hour with 1% BSA. Samples were thawed and centrifuged at 2000 x g for 20 minutes and supernatant diluted 1:5000 in 1% BSA. Blocking buffer was removed (no rinse) and samples added for 2 hours. Biotinylated polyclonal goat anti-hNAP-2 IgG and anti-hPF4 IgG detection antibodies (R&D systems) were added at 0.2 μg/ml in 1% BSA for 2 hours. Streptavidin-HRP (diluted 1:200 in PBS) was then added for 20 minutes. Colorimetric change was induced with 1:1 hydrogen perodide:tetramethylbenzidine solution for 20 minutes. The reaction was stopped by addition of 2N sulfuric acid and absorbance measured at 450 nm and 540 nm. Signals were subtracted to obtain a final absorbance.

3.3.8 Neutrophil Binding to E-selectin Coated Microspheres

Fluoresbrite 641 1.75 μm carboxylate microspheres were coated with 10 μg/ml E-selectin using a PolyLink coupling kit (PolySciences, Inc.). Functionalized microspheres were treated with $HBSS^{+/+}$ (vehicle), EC-SEAL (30 μM), DS-IkL_{10} (30 μM), or DS-IkL_{15} (30 μM) for one hour. Microspheres were pelleted at 1000xg and resuspended in stained isolated human neutrophils, then incubated for 30 minutes at room temperature with rotation. Samples were fixed in 4% paraformaldehyde (PFA) and read on an Attune NxT Flow Cytometer (Invitrogen). Data was analysed using FlowJo software.

3.3.9 Neutrophil Binding to HCMECs

HCMECs were grown to confluence in a tissue culture treated 96-well plate, stimulated for 4 hours, then treated with DS-IkL (30 μM), DS (30 μM), IkL alone (450 μM), or $HBSS^{+/+}$ containing 0.2% HSA (vehicle) for 1 hour. Cells were washed twice with $HBSS^{+/+}$ then treated with 50,000 Calcein-AM labelled neutrophils per well with rotation (150 RPM, 37˚C). After 30 minutes, cells were washed to remove non-adherent neutrophils and fluorescence read on a SpectraMax M5 plate reader (Molecular Devices).

3.3.10 CF594-DS-IkL Binding to Selectin Surfaces

Piranha etched glass coverslips were coated with 0.2 mg/ml protein A/G and 25 mM (bis(sulfosuccinimidyl)suberate) (BS3) overnight before being adhered to sticky-Slides VI 0.4-untreated (Ibidi). Channels were coated with E-selectin-FC or P-selectin-FC at 20 μg/ml (R&D Systems) for 1.5 hours with rocking, blocked with 0.2% HSA for 1 hour, then treated with serially diluted CF594-DS-IkL in $HBSS^{+/+}$ for 1 hour with rocking. Channels were rinsed and stored in $HBSS^{+/+}$ at 4˚C overnight before imaging to remove non-specifically bound molecule, then imaged on a Nikon TE2000 inverted microscope (Nikon, Minato, Tokyo, Japan). For each channel, five images were acquired in random locations and average fluorescence (mean grey value) within a two-dimensional region of interest (ROI) quantified using ImageJ.

3.3.11 Echocardiography

Cardiac structure and function were monitored using 2D echocardiography (VisualSonic Vevo 2100 with a MS 550D probe). All mice underwent echocardiography 2 weeks after either sham-operation or I/R surgery. Systolic function was recorded under conscious conditions, while diastolic function was recorded with isoflurane (~0.5-1%). Systolic function was acquired from 2-D M-mode images and B-mode videos at the short axis, and diastolic function was obtained from pulse-wave Doppler images.

3.3.12 Fibrosis Measurements

After 2 weeks, hearts from all four groups were fixed in 4% PFA solution in PBS, followed by paraffin embedding. Five micrometre sections were cut at the transverse plane of the heart, at the point of ligation. Sections were then deparaffinized in a series of xylene/alcohol (xylene, xylene, 1:1 xylene:ethanol, 100% ethanol, 100% ethanol, 95% ethanol, 70% ethanol, 50% ethanol; 3 minutes in each solution). These sections were stained for both Picrosirius Red and Masson's Trichrome, which provide information on the collagen level. Images were analysed in a blinded fashion.

3.3.13 Cell Isolation

Cells were isolated using a Langendorff perfusion system as previously described (18). After isolation, cells were fixed in 0.4% PFA, and then subjected to flow cytometry.

3.3.14 Flow Cytometric Analysis of Non-Myocyte Cells

Single cell suspension was obtained from 10- to 12-week-old C57BL/6 mice as described above. The cells were re-suspended in Ca^{2+} and Mg^{2+} free PBS, treated with phytoerythrin-conjugated anti-Thy1.2 (BD Bioscience, San Diego, CA), anti-CD11b, anti-Ly-6C, anti-Ly-6G (BD Bioscience), anti-CD31 (BD Bioscience), anti-MyHC (Developmental Studies Hybridoma Bank, created by NICHD of the NIH and maintained at The University of Iowa, Department of Biology, Iowa City, IA), and proliferation-specific

Ki67 antibodies (BD Bioscience). Cells were also stained with 40 µg/ml 7-amino- actinomycin D (7AAD, BD Bioscience, San Jose, CA) to measure the DNA content. Data was collected using a standard FACScan cytometer (BD Biosciences, San Jose, CA) upgraded to a dual laser system with the addition of a blue laser (15 mW at 488 nm) and a red laser (25 mW at 637 nm Cytek Development, Inc, Fremont, CA) or Becton Dickinson LSR-II Flow Cytometer. Data was acquired using CellQuest and DIVA 6.2 software (BD Bioscience). Cells stained with isotype-matched IgG antibodies were used as controls to determine the positive cell population. Data was analysed using FlowJo software (ver9.4 Treestar Inc., San Carlos).

3.3.15 IVIS Imaging

Mice were injected with 30 µM CF594-DS-IkL or free fluorophore in 0.9% saline after surgery and after 24 hours (100 µl via the tail vein). Prior to imaging, mice were anesthetized by isoflurane inhalation. Mice (n=6 per group) were imaged in an IVIS Spectrum Imaging System (PerkinElmer). Fluorescent images were taken 1, 12, and 24 hours after the initial injection, and 12 hours after the second injection (36 hours after the initial injection). Images were analysed using Living Image system software (PerkinElmer, version 4.3.1). Two-dimensional ROI circles were drawn around the heart to quantify fluorescence and a control ROI was drawn on the flank to quantify background. Fluorescence values were normalized to background by dividing average radiant efficiency of heart by that of background.

3.3.16 Immunohistochemistry (IHC)

Hearts were fixed in 4% PFA overnight then washed with PBS the following day. Hearts were paraffin embedded and sliced into 5 µm sections. The sections were deparaffinized with xylene and rehydrated in a descending grade of ethanol. Antigen retrieval was performed in Citrate Buffer (pH 6.0, 15 mins at 95°C). Sections were permeabilized with 0.25% Triton X-100 in PBS for 30 minutes at room temperature, and then blocked with 5% donkey serum diluted by 0.25% Triton X-100. For macrophage staining, sections were incubated with rat anti-F4/80 (BioLegend, monoclonal, 1:200) and mouse anti-α-Actinin (Sigma, monoclonal, 1:200) primary antibodies. For neutrophil staining, primary antibodies used

were rat anti-Ly6G (BioLegend, monoclonal, 1:200) and mouse anti-α-Actinin (Sigma, monoclonal, 1:200). Primary antibodies were diluted in blocking solution and sections incubated overnight at 4°C. Secondary antibodies used were donkey anti-mouse Alexa Fluor 488 (Invitrogen, 1:500) or donkey anti-rat Alexa Fluor 554 (Abcam, 1:500). Secondary antibodies were diluted in blocking solution and incubated for 1 hour at room temperature. Slides were mounted and then imaged using a Zeiss confocal LSM 700 microscope. Images were analysed by ImageJ.

3.3.17 TTC Staining

Hearts were embedded in 2% agarose gel in a heart matrix, then subsequently sliced into 1-1.5 mm sections. Sections were immersed in 1% TTC solution for 30 mins at 37°C. They were then fixed in 4% PFA for 20 minutes before images were taken under a dissection microscope connected to a Dino-Lite USB microscope.

3.3.18 Troponin I Measurements

Troponin I (CNTI) was measured using a commercial kit (Life Diagnostics) according to the manufacturer instructions. Sample concentrations were calculated from a standard curve generated in GraphPad Prism (San Diego, CA) using 4-parameter logistic regression. Sample concentrations were multiplied by their respective dilution factors to obtain final concentration values.

3.3.19 Statistics

All *in vitro* experiments were repeated at least 3 times for an $n \geq 3$. Each experiment was performed with 3-4 technical replicates. Data were analysed using one-way or two-way ANOVA with post-hoc Tukey multi-comparisons analysis. Data are represented as means ± SEM.

3.4 Results

3.4.1 Combinatorial peptide library screening generated the selectin-binding sequence, IkLLpHypR

Selectins mediate the initial capture of leukocytes to the vascular surface(15) and are therefore a promising target for modulating leukocyte recruitment. We first set out to create a combinatorial peptide library containing unnatural amino acids, biased toward the selectin binding sequence of EC-SEAL, a molecule we previously described(19, 20). We used the one-bead-one-compound combinatorial library method, which allows for the unrestricted incorporation of natural and unnatural amino acids (**Figure 3-1**) (21), to discover the sequence Ile-(D)Lys-Leu-Leu-(D)Pro-Hydroxyproline-Arg.

3.4.2 DS-IkL exhibited binding to E- and P-selectin coated surfaces and reduced neutrophil binding to E-selectin in solution

To confirm that DS-IkL binds selectins, P- and E-selectin coated surfaces were treated with increasing concentrations of DS-IkL or DS alone. Dermatan sulphate (DS) is a negatively charged proteoglycan that is known to interact with P-selectin (22). We directly determined if the addition of IkL would improve binding to P- or E-selectin compared to DS alone. **Figure 3-2** shows that DS-IkL exhibited significantly enhanced binding to both selectins with increasing concentrations of molecule, which is not observed in the DS group. The ability of DS-IkL to interfere with E-selectin binding to neutrophils in suspension was further confirmed in **Supplementary Figure 3-1**. Treatment with DS-IkL inhibited neutrophil binding to E-selectin, but not P-selectin, at 5-30 μM concentrations by up to 35%. These reductions were similar to those seen on endothelial cell surfaces (**Figure 3-3D**). Higher concentrations were needed to reduce P-selectin binding. Similarly, in the presence of DS-IkL, stimulated neutrophils bound less E-selectin, but not intercellular adhesion molecule-1 (ICAM-1) (**Supplementary Table 3-1**), suggesting DS-IkL preferentially binds E-selectin.

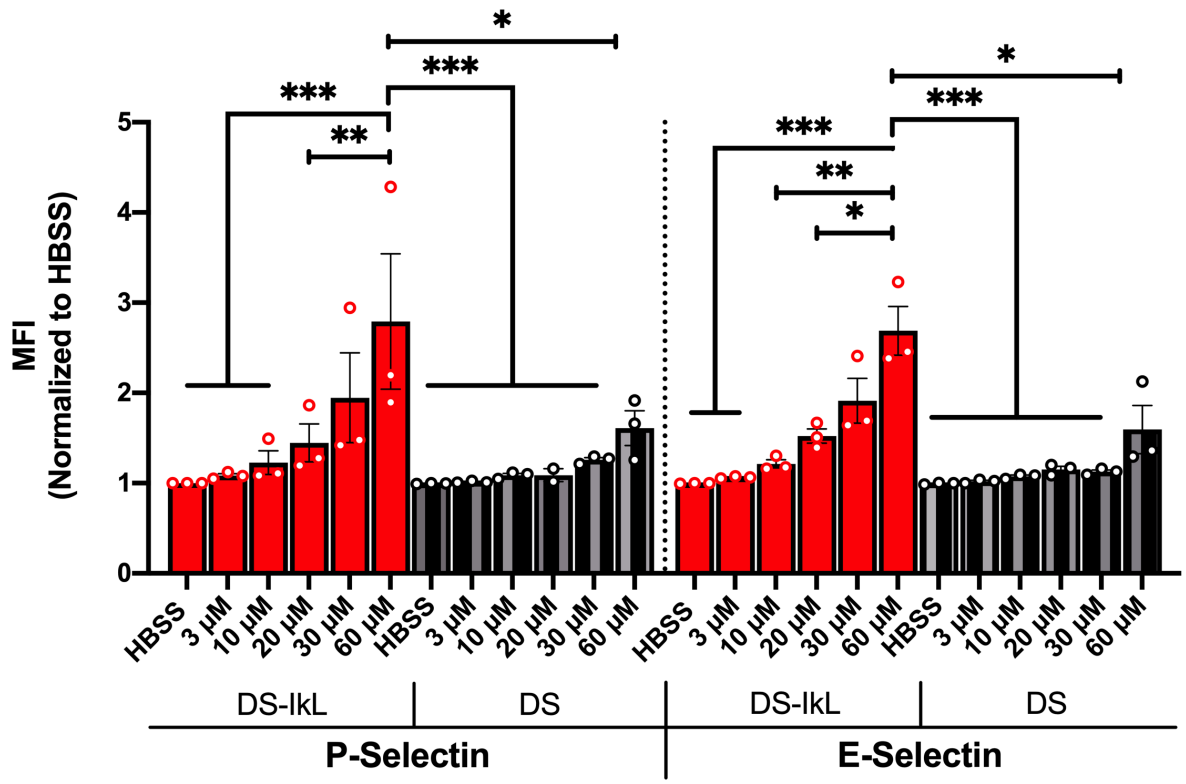

Figure 3-2 Improved binding to immobilized selectin surfaces with DS-IkL. P- and E-selectin coated surfaces were treated with CF594-DS-IkL (30 µM, red) or CF594-DS (30 µM, black). CF594-DS-IkL binding increased with increasing concentration, as assessed by mean fluorescence intensity (MFI) normalized to vehicle (HBSS). Data are represented as means ± SEM of 3 biological replicates. * $p<0.05$, ** $p<0.01$, *** $p<0.001$ by two-way ANOVA with post-hoc Tukey test.

3.4.3 Treatment with DS-IkL significantly reduced platelet activation on stimulated endothelial cells

Enhanced platelet activation and binding have been implicated in a multitude of chronic inflammatory diseases, including acute coronary and pulmonary syndromes (23). Activated platelets release cytokines such as platelet factor 4 (PF-4) and neutrophil activating peptide 2 (NAP-2) that can in turn activate neutrophils (24). Given their contributions to neutrophil recruitment to sites of inflammation, we aimed to test if treatment of inflamed ECs with DS-IkL could reduce PF-4 and NAP-2 activation of platelets. Platelets were allowed to interact with stimulated HCMECs under standard culture conditions for 1 hour

before supernatant was collected. Levels of PF-4 and NAP-2 that accumulated in the supernatant during this time were significantly diminished in DS-IkL treated cells ($p<0.05$), as shown in **Figure 3-3A-B**. Notably, DS-IkL reduced NAP-2 activation on stimulated HCMECs to levels similar to unstimulated controls, implying our molecule has the potential to act as a barrier to platelet-induced neutrophil activation.

3.4.4 DS-IkL reduced neutrophil arrest on E-selectin coated microspheres and stimulated endothelial cells

The neutrophil adhesion cascade begins with initial capture and slow rolling along selectins that are upregulated on inflamed endothelium and activated platelets; therefore, interfering with this initial capture could prove therapeutically beneficial. To test our molecule's ability to block neutrophil-selectin interactions, E-selectin coated microspheres were treated with DS (30 μM), IkL peptide (450 μM), DS-IkL (30 μM), DS-IkL_{10} (30 μM), or vehicle prior to incubation with isolated human neutrophils. Only IkL peptide and DS-IkL were able to reduce neutrophil adhesion to microspheres to approximately 75% of control ($p<0.05$, **Figure 3-3C**), with DS and DS-IkL_{10} exhibiting similar neutrophil-microsphere colocalization as control. Given the importance of tightly regulated neutrophil capture and activation in proper wound healing (25), this slight reduction could be the tipping point back toward a restorative state.

We next sought to investigate if the effect of DS-IkL on neutrophil-selectin interactions was retained on ECs, which are known to upregulate their selectin expression upon stimulation with inflammatory cytokines such as TNF-α and IL-1β (26). HCMECs were treated with DS-IkL under stimulatory conditions prior to incubation with neutrophils. Neutrophils exhibited reduced adhesion to treated ECs as compared with vehicle controls ($p<0.01$, **Figure 3-3D**), to a similar extent as on selectin-coated microbeads. These results support our hypothesis that DS-IkL reduces selectin-mediated neutrophil capture at sites of inflammation.

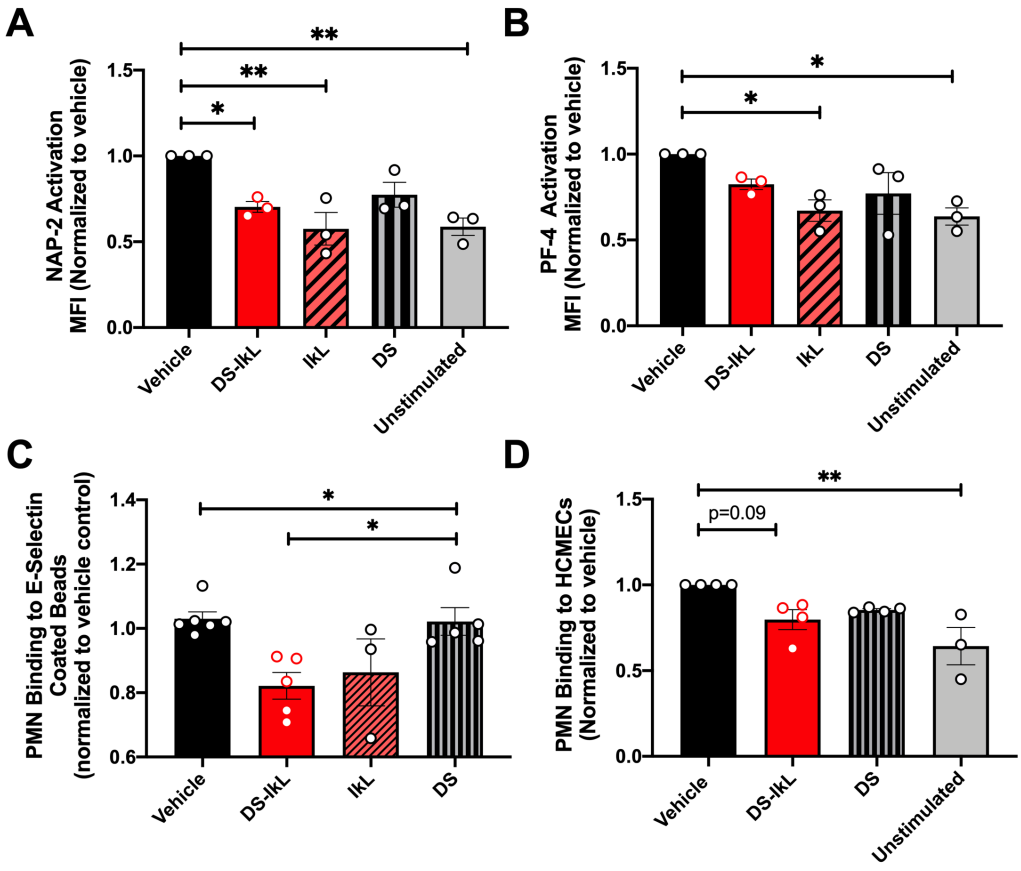

Figure 3-3 Treatment with DS-IkL reduced neutrophil binding and platelet activation. Platelet activation on stimulated HCMECs as assessed by **A)** NAP-2 and **B)** PF-4 was reduced after treatment with DS-IkL (30 µM) and/or IkL peptide (450 µM), but not DS (30 µM). **C)** E-selectin coated microspheres were treated with HBSS, DS-IkL, IkL peptide, or DS prior to incubation with isolated human neutrophils (PMN). Data represent PMN binding to microspheres as assessed by flow cytometry. **D)** DS-IkL reduced PMN binding to stimulated HCMECs toward the level of unstimulated controls (p=0.09). Data are represented as means ± SEM of n=3-4 biological replicates. * $p<0.05$, ** $p<0.01$, *** $p<0.001$ by one-way ANOVA with post-hoc Tukey test.

3.4.5 DS-IkL targeted to the heart after I/R

Since DS-IkL suppressed neutrophil adhesion *in vitro*, we investigated whether this would occur *in vivo* following a myocardial infarction, induced by 45 minutes of ischemia at the LAD with subsequent reperfusion. To verify proper occlusion of the LAD, we monitored ECG recordings during occlusion (**Supplementary Figure 3-2**). Only I/R mice with ST-segment elevations were included in the I/R group. Immediately after sham or LAD operation, we injected either 30 µM DS-IkL conjugated to a fluorophore

(CF594-DS-IkL) or saline with equal concentration of the fluorophore, and monitored *in vivo* fluorescent intensity at 1, 12, 24, and 36 hours after surgery. Representative images of all four groups are shown in **Figure 3-4A**. As evidenced by these images, fluorescence signals were primarily localized to the cardiac region only in the I/R group after the CF594-DS-IkL injection. We observed some targeting to throat regions that sustained damage during tracheotomy, as well as background fluorescence in the abdomen, likely from autofluorescent components of mouse chow (27). Quantitatively, signal intensity was significantly higher an hour after surgery in mice treated with DS-IkL after I/R, relative to mice treated with the fluorophore dissolved in saline ($p<0.001$, **Figure 3-4B**). There was no difference in fluorescent intensity in the cardiac region in saline sham mice vs saline I/R mice, suggesting that the molecule just circulated in the blood, but did not localize to the heart. In addition, fluorescent signal persisted for at least 24 hours in the cardiac region after I/R surgery in mice treated with DS-IkL. After a subsequent dosage at the 24-hour mark, no noticeable difference was observed in this group relative to the other groups at the 36-hour time point. Taken together, our *in vivo* imaging suggested that DS-IkL targeted to the heart, and the binding of DS-IkL lasted for at least 24 hours.

3.4.6 Mice treated with DS-IkL exhibited reduced infarct size and improved cardiac function after I/R

To examine the *in vivo* effects of DS-IkL on cardiac structure and function, we performed either sham or 45 mins I/R. To assess the short-term effects of DS-IkL on cardiac injury, we administered one injection of either saline or DS-IkL immediately after surgery and examined the degree of myocardial infarction and extent of cardiac injury after 24 hours of reperfusion. Representative sections stained with TTC are displayed in **Figure 3-5A**. As evident from the sections, I/R induced a more pronounced increase in damaged, non-viable cardiac regions, relative to DS-IkL treated mice. Sham-operated sections are displayed in **Supplementary Figure 3-4**. Quantification, percentage of infarcted region relative to left ventricular area, demonstrated a significant reduction in infarct size in DS-IkL hearts (**Figure 3-5B**).

Cardiac injury was assessed by measuring cardiac Troponin I. Although there was not a significant difference, there was a trend towards a reduction in injury at 24 hours post injury (**Figure 3-5C**).

To determine the long-term effects of DS-IkL, we performed the same procedure, but mice were subjected to 2 weeks of reperfusion. To ensure robust activity of DS-IkL, we administered an additional dose of DS-IkL 24 hours after surgery on top of the dose given immediately after surgery. Cardiac structure and function were assessed 2 weeks post-operation. Representative M-mode tracings at the parasternal short-axis are shown for all four groups and display the beat-to-beat changes in wall thickness and diameter of the left ventricle (**Figure 3-5D**). Recordings were performed in conscious mice; heart rate in all groups were therefore similar (**Figure 3-5E**). Structurally, I/R resulted in an increase in the left ventricular mass in groups treated with either saline or DS-IkL, relative to their respective sham-operated groups ($p<0.05$, **Figure 3-5F**). Similar to our echocardiography findings, I/R induced an increase in heart weight to tibial length ratio in mice treated with either saline or DS-IkL, relative to their sham-operated controls **Supplementary Figure 3-3)**. Even though I/R resulted in a reduction in fractional shortening (**Figure 3-5G**) and ejection fraction (**Supplementary Table 3-1**) in both groups, there was a significant improvement in fractional shortening in the DS-IkL treated mice compared to saline alone ($p<0.05$**, Figure 3-5G**). Furthermore, strain analysis revealed a significant reduction in global radial strain (**Figure 3-5H**) in both I/R groups relative to their respective sham groups. However, the decrease was significantly less in DS-IkL mice treated groups. Although the local radial strain was not significant (**Figure 3-5I**), the small improvement in all the different regions of the heart contributed to an overall and global increase in global radial strain in DS-IkL mice. Global circumferential strain was significantly reduced in saline treated mice relative to their control sham (**Figure 3-5J**). However, this was not observed in DS-IkL treated mice.

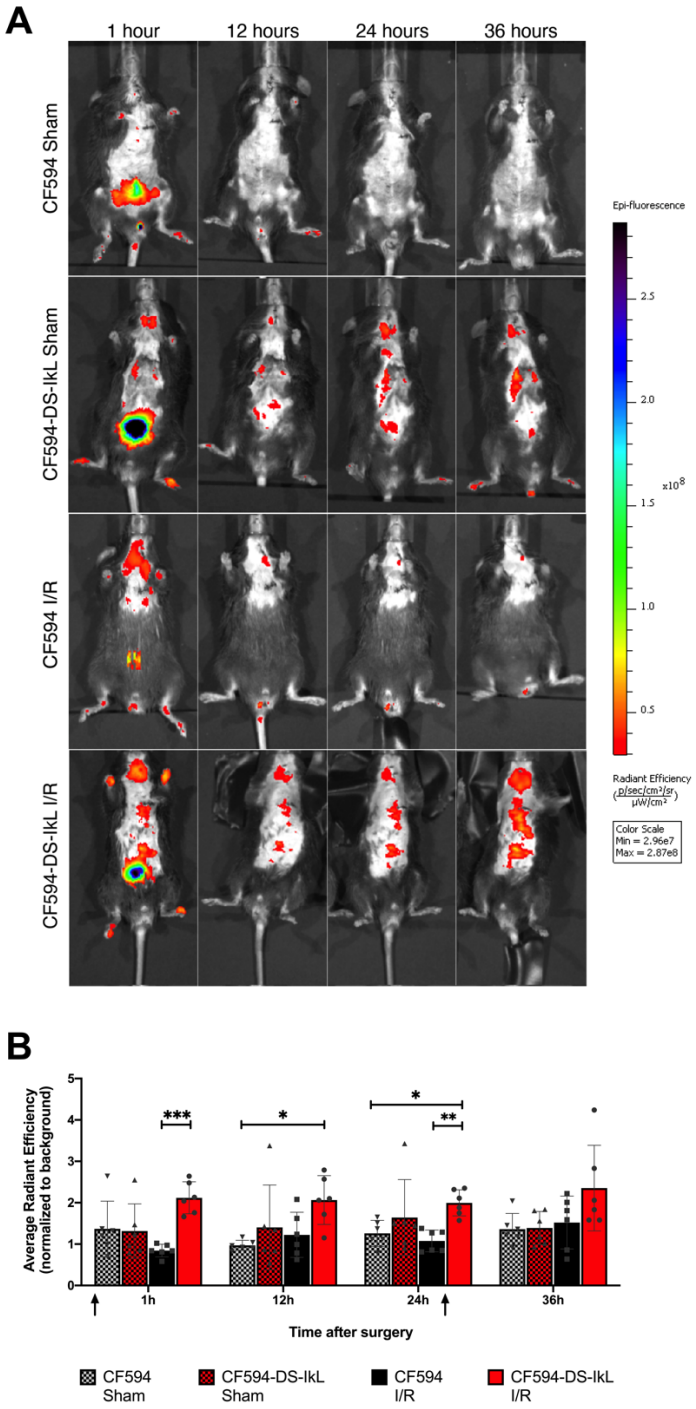

Figure 3-4 DS-IkL targeted to the heart after I/R. Animals were injected with either CF594 dissolved in saline or CF594-DS-IkL after surgery and 24 hours later. **A**) Representative images taken 1 hour after each injection, and every 12 hours after reperfusion until the 36-hour time point. **B)** Data summary of CF594 (black bars) and CF594-DS-IkL (red bars) targeting to heart at 1, 12, 24, and 36 hours after surgery. Black arrows depict injections. Data are represented as means ± SEM of n=6 mice per group. * $p<0.05$, ** $p<0.01$; *** $p<0.001$ by two-way ANOVA with post-hoc Tukey test.

Diastolic function was assessed using the blood flow velocity through the mitral valve during the cardiac cycle. Representative tracings using pulse-wave Doppler show two distinct waveforms, which correspond to left ventricular filling during early diastole (E wave) and left ventricular filling during late diastole (A wave, **Figure 3-5K**). The ratio of the two provides an indication of diastolic function(28). Mice treated with DS-IkL did not exhibit a change in diastolic function, as compared to their sham control; whereas, mice treated with saline showed a significant reduction in the E/A ratio, indicating an impairment in diastolic function (**Figure 3-5L**). Indeed, the E/A ratio of mice treated with DS-IkL was significantly higher than mice treated with saline, after I/R ($p<0.05$). Although the isovolumetric relaxation time (IVRT, **Figure 3-5M**) did not change significantly, the MV deceleration time was significantly elevated in the I/R group treated with saline, relative to the saline sham group ($p<0.05$, **Figure 3-5N**). This was not seen when the mice were treated with DS-IkL. Together, these data suggest that both systolic and diastolic function was significantly improved with the treatment with DS-IkL.

3.4.7 DS-IkL limited fibrosis after I/R

MI induces loss of cardiomyocytes with concomitant increase in fibrosis (29). Histological analyses of cardiac sections were performed 2 weeks after I/R. Representative whole heart images of all four groups, and short-axis sections stained with Masson's Trichrome (MT) and Picrosirius Red (PSR) are shown (**Figure 3-6A**). Percentages of fibrotic area relative to the total left ventricular area were quantified in a blinded fashion and were low and not significantly different in the sham-operated groups. In contrast, there was a significant elevation in collagen deposition in both I/R groups, relative to their respective sham-operated controls ($p<0.01$, **Figure 3-6B**). However, I/R mice treated with DS-IkL showed significantly less fibrosis than mice treated with saline (**Figure 3-6D-E**, $p<0.05$), consistent with TTC data observed 24 hours after I/R (**Figure 3-5A-B**). Together, the data show that DS-IkL limited fibrosis, which in part contributed to the improved cardiac function as assessed by echocardiography.

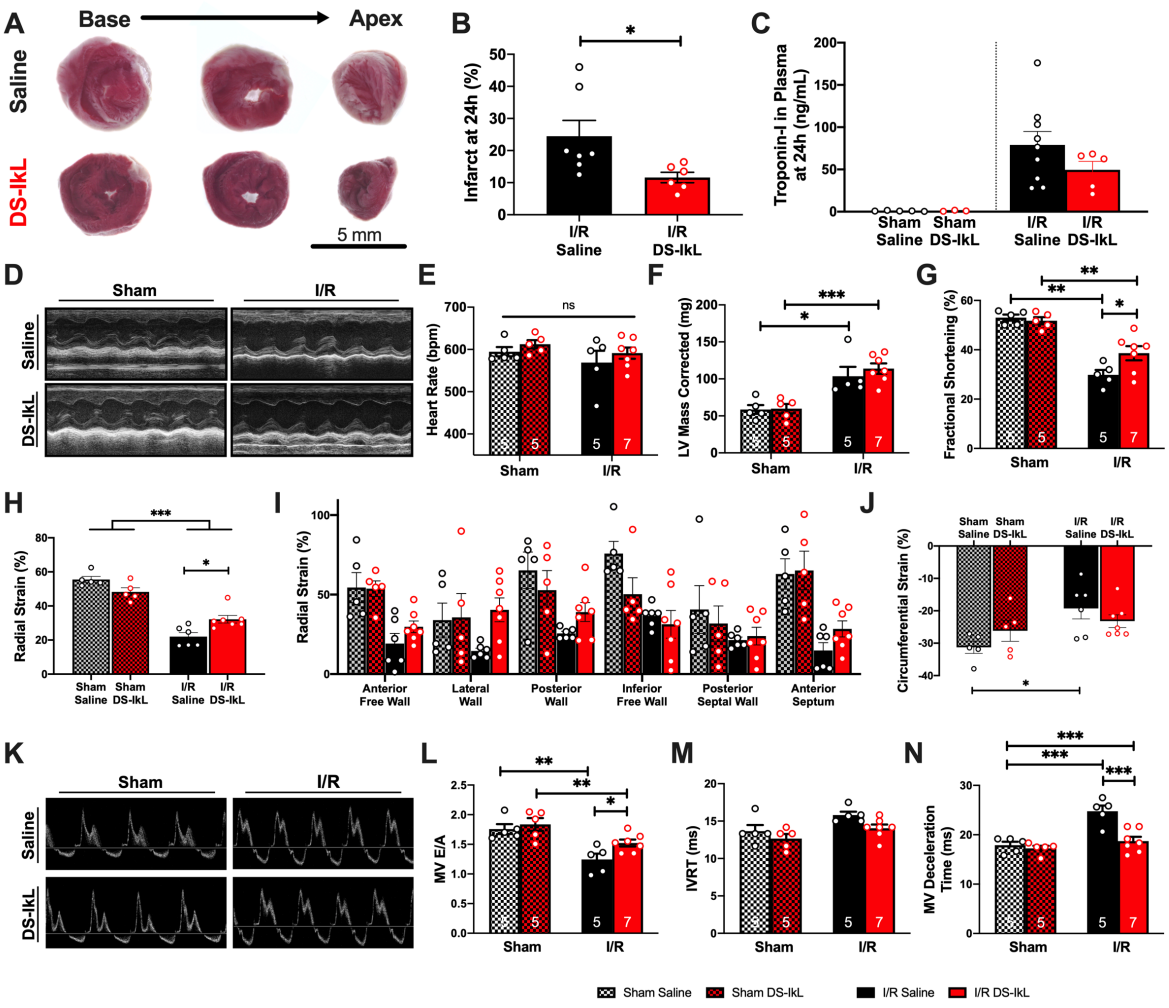

Figure 3-5 Mice treated with DS-IkL exhibited reduced infarct size and improved cardiac function after I/R. **A)** After 24 hours of reperfusion, we assessed size of myocardial infarction using TTC staining. Representative sections are shown. **B**) Quantification revealed an increase in infarct size with saline treated mice. **C**) Cardiac injury was also assessed using cardiac troponin I. After 2 weeks of reperfusion, mice were subjected to conscious echocardiography to examine the cardiac structure and function. **D**) Representative M-mode images at the parasternal short-axis for all four groups are depicted. **E**) Heart rate was not significantly different in these conscious mice. **F**) I/R induced an increase in left ventricular (LV) mass, and **G**) reduced fractional shortening and **H**) global radial strain. **I**) Summary data of region-specific radial strain and **J**) circumferential strain are displayed. **K**) Diastolic function was assessed by the blood flow velocity through the mitral valve, as shown in representative images in all four groups. **L**) The E/A ratio was significantly decreased in both groups but was more obvious in the saline I/R group. **M**) Although the isovolumetric relaxation time (IVRT) was not significantly different in all four groups, **N**) there was a difference in the mitral valve (MV) deceleration time in the saline I/R group vs the saline sham group. Data are represented as means ± SEM of n=5-7 mice per group. * $p<0.05$, ** $p<0.01$ by one-way ANOVA with post-hoc Tukey test.

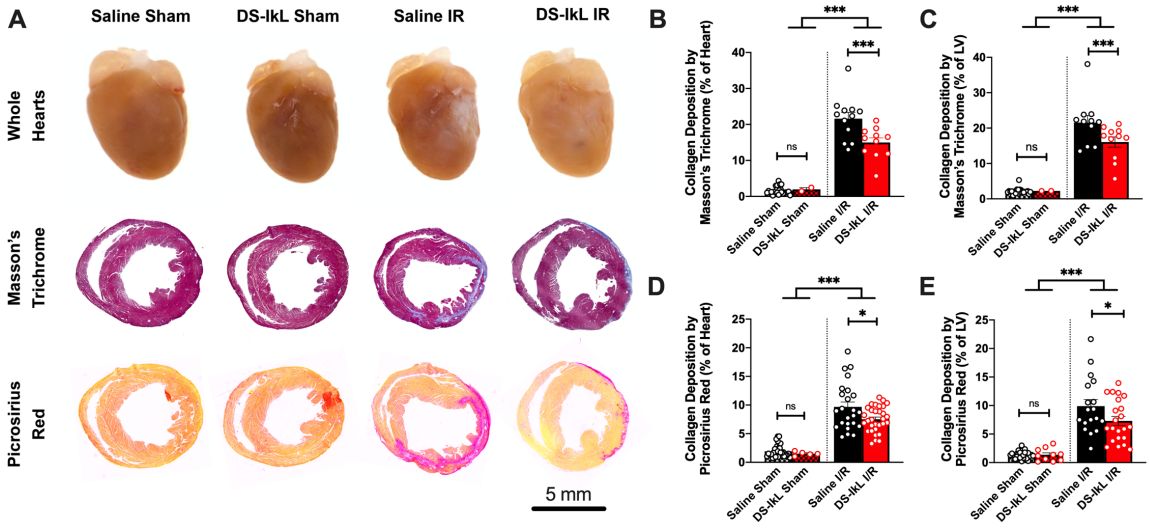

Figure 3-6 DS-IkL limited fibrosis after I/R. A) Representative images of whole hearts (top), Masson's Trichome (middle), and Picrosirius Red (bottom) stained sections. Collagen deposition by Masson's Trichrome (**B and C**) and Picrosirius Red (**D and E**) was significantly reduced in DS-IkL treated mice after I/R. Data are represented as means ± SEM of n=5-7 mice per group; 6 sections were analysed per mouse. * $p<0.05$, ** $p<0.01$, *** $p<0.001$ by one-way ANOVA with post-hoc Tukey test.

3.4.8 DS-IkL prevented neutrophil and macrophage aggregation, fibroblast proliferation, and endothelial cell proliferation after I/R

I/R causes cardiac endothelial cell dysfunction, leading to an amplified inflammatory state and an increase in vascular permeability (30). If not tightly regulated, immune cells recruited to the damaged regions accentuate damage and contribute to tissue fibrosis. To determine the effect of DS-IkL on neutrophil and fibroblast accumulation, we isolated non-myocyte cell populations from the hearts from all four groups 36 hours after sham or I/R surgeries. Flow cytometric analysis showed a significant increase in $CD11b^{+}/Ly6\text{-}C/G^{+}$ neutrophils in the saline treated I/R group compared to sham controls ($p<0.05$), but no significant increase in the DS-IkL treated I/R group **(Figure 3-7A-B)**, suggesting that treatment with DS-IkL limited neutrophil accumulation after I/R. Furthermore, there was a significant increase in both total ($CD31^{+}$) and proliferative ECs ($Ki67^{+}/CD31^{+}$) in the saline I/R group, but not in the DS-IkL treated I/R

groups (**Figure 3-7C-E**), suggesting a significant decrease in adverse vascular remodelling by DS-IkL. Moreover, the percentage of proliferative fibroblasts ($Thy1.2^{+}$) in the saline I/R group was significantly higher than in the DS-IkL treated I/R group (**Figure 3-7F-H**), consistent with the significant increase in collagen deposition observed 2 weeks after reperfusion.

Although the immune response is heightened shortly after MI, the effects can manifest long-term as the body tries to re-establish homeostasis. To determine the long-term effects of DS-IkL on neutrophil and macrophage accumulation, we performed immunohistochemistry on all four groups after 2 weeks of I/R. Representative images of IHC are shown in **Figure 3-7I**. Tissue sections were stained with α-actinin to stain for cardiomyocytes, F4/80 to stain for macrophages, and Ly6G to stain for neutrophils. DS-IkL treatment significantly reduced the number of macrophages per area (**Figure 3-7I and J**) and neutrophils per area (**Figure 3-7I** and **K**) at both 36 hours (**Figure 3-7**I) and 2 week (**Figure 3-7J** and **K**). Together, our data suggest that DS-IkL limited neutrophil and macrophage aggregation, as well as fibroblast and EC proliferation. Mechanistically, DS-IkL treatment prevented multiple aspects of the immune response by acting as a molecular bandage on the damaged endothelial surface, which ultimately resulted in less fibrosis and improved cardiac function **(Figure 3-7L**).

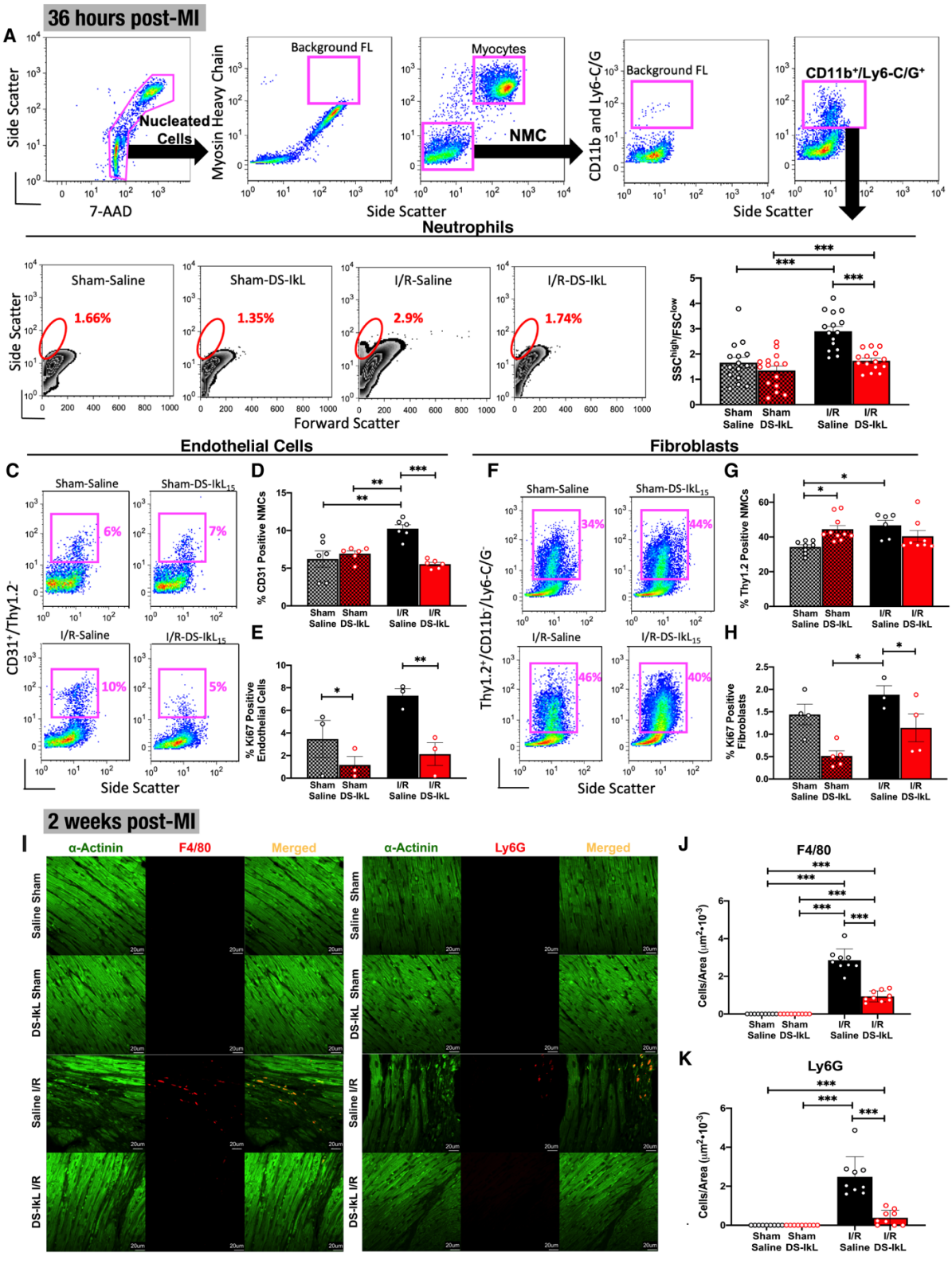

Figure 3-7 DS-IkL prevented neutrophil and macrophage aggregation, fibroblast proliferation, and endothelial cell proliferation after I/R. We investigated the short- and long-term effects of DS-IkL on the immune response. **A**) Flow cytometric analysis of isolated cardiac cells. Nucleated cells were selected from debris based on the incorporation

of 7-ADD and the separation of the myocytes from the non-myocyte cells (NMC) using a cardiac myosin heavy chain (MF20)-specific antibody. Neutrophils and monocytes were separated based on the presence of CD11b/Lys6-C/G from all four groups as depicted. Neutrophils were further distinguished by gating on the SSC-high and FSC-low cells from $CD11b^{+}/Ly6C/G^{+}$ population. **B**) Summary data shows that there was a significant reduction in neutrophils in the DS-IkL I/R group, compared to the saline I/R group. **C**) Flow cytometric analysis of $CD31^{+}/Thy1.2^{-}$ endothelial cells in all four groups. **D**) Summary data showing a significant increase in endothelial cells in saline I/R group relative to saline sham. DS-IkL prevented the increase. **E**) Assessment of proliferation using the Ki67 proliferative marker showed a similar trend. **F**) Fibroblasts ($Thy1.2^{+}/CD11b^{-}/Ly6^{-}C/G^{-}$) were detected using flow cytometric analysis. **G**) Summary data of Thy1.2 positive cells and **H**) proliferative Thy1.2 positive cells using Ki67 are shown. X and Y axes represent arbitrary units. **I**) We examined the accumulation of neutrophils (Ly6G) and macrophages (F4/80) after 2 weeks of I/R using IHC. Representative images are shown for all four groups. DS-IkL prevented accumulation of both **J**) macrophages and **K**) neutrophils. n=5 mice per group for flow cytometric analysis. n=3 mice per group for IHC. Data are represented as means ± SEM. * $p<0.05$, ** $p<0.01$, *** $p<0.001$ by one-way ANOVA with post-hoc Tukey test.

3.5 Discussion

Inflammatory responses significantly contribute to further injury after the initial insult of an MI. Ischemic coronary vessels undergo drastic alterations to their microstructure and homeostasis upon reperfusion, conducive to immune cell infiltration. Ion imbalance disrupts cell-cell junction integrity along the endothelium (31), creating migration points for neutrophils and macrophages that are recruited to these cytokine-rich environments (30). Furthermore, ECs exhibit signs of endothelial cell dysfunction, namely enhanced cell contractility, upregulated cell adhesion molecules such as E- and P-selectin, and the loss of the glycocalyx (10, 30). The dysfunctional EC phenotype facilitates neutrophil recruitment and extravasation. Neutrophils that have been recruited to these sites activate and secrete a milieu of pro-inflammatory cytokines that in turn recruit additional leukocytes (32), shifting the inflammatory process from restorative to destructive. Therapeutics that limit the initial binding and activation of circulating immune cells could tip the balance back to a restorative state.

3.5.1 Design of the novel DS-IkL

We previously described a molecule termed “EC-SEAL” composed of oxidized dermatan sulphate (DS), to which known selectin-binding peptides were conjugated via a heterobifunctional crosslinker (20).

Although EC-SEAL mitigated the immune response *in vitro*, it is not an acceptable drug candidate for the clinic. The chemistry used to functionalize the DS uses glycol splitting by periodate oxidation, a mechanism which cleaves carbohydrate rings at vicinal diols to create a reactive intermediate (33). This chemistry renders the molecule unstable; thus, it cannot be stored long-term. Furthermore, the chain conformation changes dramatically, resulting in a chain coiled polymer chain rather than an extended linear structure seen with natural glycosaminoglycans.

In this study, we designed an improved molecule termed DS-IkL. We demonstrated that DS could be modified with peptides without cleaving the ring structure and still maintain the ability to bind to the selectin receptors to interfere with platelet and neutrophil binding. Importantly, this new chemistry, which better maintains DS structure, eliminates the reactive intermediates that reduced the stability of EC-SEAL. Additionally, the selectin binding sequence in EC-SEAL consisted solely of L-amino acids, which are readily degraded by proteolytic enzymes present at sites of inflammation. Though not directly addressed here, we believe that the incorporation of D-amino acids within the selectin binding sequence delays DS-IkL's degradation and clearance, supporting its presence on ECs for at least 24 hours.

To design DS-IkL, we first created a combinatorial peptide library containing unnatural amino acids, biased toward the E-selectin binding sequence of EC-SEAL (19, 20). We chose to use the one-bead-one-compound combinatorial library method, which allows for the unrestricted incorporation of natural and unnatural amino acids (21), to discover the sequence I-k-L-L-p-Hyp-R. Our preliminary efforts focused on the ability of IkL peptide and our DS-IkL glycoconjugate to bind selectins (**Figure 3-2**) and interfere with neutrophil binding to E-selectin coated microspheres (**Figure 3-3A**). Selectins mediate the initial capture of leukocytes to the vascular surface(15), and are therefore a promising target for modulating leukocyte recruitment. We hypothesized that selectins blanketed with our glycoconjugate would be masked from circulating leukocytes, therefore limiting their capture. In line with this hypothesis, we observed significant reductions in neutrophil binding to both selectin coated microspheres and stimulated ECs upon treatment with DS-IkL_{15}, suggesting DS-IkL_{15} interacted with upregulated selectins on the cell surface.

3.5.2 DS-IkL reduced platelet activation on endothelial cells

Given the destructive role platelets play in myocardial I/R injury (16, 34), we were interested in DS-IkL's effect on the activation state of platelets incubated on stimulated ECs. Interestingly, we saw significant reductions in NAP-2 levels and a trend toward reduction in PF-4 in cultures that had been pre-treated with DS-IkL as compared to HBSS treated controls, suggesting ECs treated with DS-IkL presented fewer available platelet activating ligands such as endothelial P-selectin. Though we did not observe significant reductions in PF-4, a chemokine which induces firm adhesion of neutrophils in the presence of TNF-α (24, 35), we believe our modest results may be an artefact of the experiment. PF-4 has an affinity for GAGs (35) and therefore may have been sequestered by DS-IkL or heparin on the cell surface or within the media.

In addition to direct damage caused by activated platelets, these bioactive blood components have been shown to play a pivotal role in neutrophil capture along inflamed endothelium, offering an anchor point via platelet P-selectin and facilitating endothelial transmigration (23, 34). Although E- and P-selectin are very similar molecules, both in structure and function, we observed slight differences in binding to E- and P-selectin coated surfaces (**Figure 3-2**), with DS-IkL exhibiting more consistent binding to E-selectin at higher concentrations. Our results suggest that IkL peptide plays a more influential role in E- and P-selectin binding when DS-IkL is administered at higher concentrations, whereas at lower concentrations, selectin binding may be influenced more by DS. By interacting with both P- and E-selectin, DS-IkL may simultaneously protect from neutrophil interactions, platelet aggregation, and the formation of platelet-neutrophil complexes. Therefore, DS-IkL presents a two-fold cardioprotective potential by limiting damage from both activated platelets and neutrophils.

3.5.3 DS-IkL improved cardiac function by disrupting components of the immune response

Since one of the hallmarks of reperfusion injury is overactivation of the immune system due to leukocyte accumulation and platelet activation, we assessed the potential therapeutic benefits of DS-IkL in

a clinically relevant murine model of I/R. Our data show that DS-IkL localized to the damaged cardiac region (**Figure 3-4**) and limited neutrophil and fibroblast accumulation after I/R, which resulted in less tissue fibrosis (**Figure 3-6**), reduced myocardial infarction, and improved cardiac function (**Figure 3-5**). Interestingly, DS-IkL treated I/R mice did not exhibit the increase in total and proliferative ECs that was observed in the saline I/R group. In some cases, a heightened presence of proliferative ECs may indicate tissue regeneration (36); however, the saline treated I/R group exhibited poor cardiac function and enhanced fibrosis. Our results therefore suggest that rather than regeneration, early remodelling and myocardial hypertrophy was beginning to occur, necessitating an increase in cardiac angiogenesis (37).

3.5.4 Proposed Mechanism of DS-IkL

Other attempts have been made to limit I/R induced injury after MI(38), including ischemic pre- and postconditioning, pharmacologic interventions targeting metabolic pathways that contribute to RI(39, 40), and the use of monoclonal antibodies to limit platelet and neutrophil adhesion(38). In particular, antibody therapy to P-selectin (41, 42) and ICAM-1 have been investigated as cardioprotective therapies against neutrophil and platelet mediated RI (43). However, as evidenced by the SELECT-ACS trial evaluating the effect of Inclacumab (44), a recombinant monoclonal antibody against P-selectin, a major drawback of antibody therapy is the need for high doses for therapeutic effect(45), lending to high production costs(46). It is worth noting that monoclonal P-selectin antibody crizanluzumab (47) (awarded Breakthrough Therapy designation) and the pan-selectin inhibitor Rivipansel (48) (failed at Phase 3) have shown promise in vaso-occlusive crises in sickle cell disease. However, neither of these have been tested in RI.

Our strategy is unique from antibody therapeutics. DS-IkL is generally smaller than antibody therapeutics (~62 kDa) and has been designed to interrupt multiple parts of the immune pathway simultaneously by masking adhesion molecules on the endothelial surface. We designed a *molecular bandage* that targets DS – a native component of the glycocalyx – to inflamed endothelium. By blanketing

DS over the dysfunctional endothelial surface, we aimed to directly reduce selectin availability while indirectly interfering with immune cell interactions with other adhesion molecules on the endothelial surface. We demonstrated that DS-IkL binds to E- and P-selectin, limited neutrophil and platelet adhesion to inflamed ECs, reduced neutrophil, macrophage, and fibroblast accumulation after MI (**Figure 3-7**), and improved cardiac function after MI. We conducted our current study at a treatment concentration of 30 uM. **Figure 3-2** suggests DS-IkL may have a greater therapeutic benefit at higher concentrations; therefore, future studies will be required to determine the concentration of DS-IkL that produces the optimum therapeutic effect, as well as to further elucidate the mechanism by which DS-IkL works.

3.6 Conclusions

We created DS-IkL using the one-bead-one-peptide synthesis approach. *In vitro*, DS-IkL bound to both P- and E-selectin coated surfaces and prevented neutrophil binding and platelet activation. *In vivo,* DS-IkL localized to the cardiac region in mice after MI and limited neutrophil and fibroblast accumulation. Mice treated with DS-IkL exhibited improved cardiac function and less fibrosis. Taken together, our data suggest that our recently developed, novel DS-IkL molecule reduced the inflammatory response induced by MI, which resulted in cardioprotection.

3.7 Acknowledgements

This work was supported by a Predoctoral Fellowship from Tobacco-Related Disease Research Program (TRDRP) T29DT0237 (TD), Postdoctoral Fellowships from NIH T32 Training Grant in Basic & Translational Cardiovascular Science HL86350 and NIH F32 HL149288 (PNT), NIH R01 HL085727, HL085844, HL137228, and S10 RR033106, Research Award from the Rosenfeld Foundation, VA Merit Review Grant I01 BX000576 and I01 CX001490 (NC). NC is the holder of the Roger Tatarian Endowed

Professorship in Cardiovascular Medicine and a part-time staff physician at VA Northern California Health Care System, Mather, CA. The authors would like to thank the Combinatorial Chemistry and Chemical Biology Shared Resource at University of California Davis for assistance of synthesis and sequence decoding of OBOC peptide library. Utilization of this Shared Resource was supported by the UC Davis Comprehensive Cancer Center Support Grant awarded by the National Cancer Institute (NCI P30CA093373).

3.8 Authors' Contributions

TD and PNT designed the research study, conducted experiments, acquired data, analysed data, and wrote the manuscript. HS, LR, and PS conducted experiments, acquired data, analysed data. CN and VT conducted experiments. JLO analysed data. XL and KL helped conceptualize and design the peptide library. NC and AP designed the research study, provided monetary support, and wrote the manuscript.

3.9 Conflict of Interest

The authors claim no conflict of interest.

3.10 Supplementary Methods

3.10.1 Peptide Library

1 g of resin was swollen in dimethylformamide (DMF) overnight and divided in half. Half of the resin was coupled to the first amino acid in the known sequence; the other half was split equally into 30 polypropylene columns, each containing a different amino acid (10 equivalents in DMF). Ten equivalents of N-N'-diisopropylcarbodiimide (DIC) and hydroxybenzotriazole (HOBt) were added. Complete coupling was confirmed by a colorless Kaiser test. The resin was then combined into a single column and deprotected with 20-25% piperidine. The process was repeated for the next amino acid in the known sequence.

3.10.2 Library Screening for E-Selectin Binding Peptide

Peptide-conjugated Tentagel S resin was immobilized with 90% DMF to form a confluent monolayer on a 12-well polystyrene plate. Resin was blocked with 5% bovine serum albumin (BSA) in phosphate buffered saline (PBS) then pre-screened for binding to the HRP-anti-His secondary antibody (1:400 in PBS, 1 hour at room temperature with rocking). Resin which stained positive was removed prior to screening. Resin was then blocked with a human FC fragment (1mg/ml in 1% BSA) for 1 hour at room temperature with rocking. FC-chimera human recombinant E-selectin with a 6-histidine tag (R&D Systems) was added to each well and incubated overnight at 4°C with rocking, washed 3x with PBS, then treated with HRP-anti-His for 1 hour at room temperature. Resin was washed and visualized using a 3,3' diaminobenzidine (DAB) solution. Resin which stained positive for E-selectin binding was removed and sequenced. This procedure was repeated until 30 unique sequences were identified. Sequences were compared for homology and multiple selected for further analysis. Sequences were remade on Tentagel S resin and binding to E-selectin compared.

3.10.3 DS-IkL inhibiting selectin and ICAM binding to neutrophils

Isolated neutrophils were resuspended in HBSS+/+ with 0.4% HSA and added at 165k cells per tube. DS-IkL was dissolved in HBSS+/+ at 120 uM, sterile filtered through a 0.2 um filter, and serially diluted to 60 uM, 30 uM, and 10 uM. Fifty microlitres of DS-IkL was added to a 1.5 mL Eppendorf tube containing 40 uL of the neutrophil suspension, followed by 10 uL of 100 ug/mL recombinant human ICAM, P-selectin, or E-selectin. This yielded final DS-IkL concentrations of 60 uM, 30 uM, 15 uM, and 5 uM and 10 ug/mL selectin. For stimulated groups, TNF-□ was added to samples at a final concentration of 5 ng/mL. Tubes were gently mixed then incubated on ice with rotation (120 RPM). After 30 minutes samples were washed twice with HBSS+/+ then blocked with 5% BSA in HBSS+/+ + 5mM HEPES for 60 minutes. Samples were stained with PE anti-human CD62E, PE anti-human CD62P, or PE anti-human CD54 antibodies (BioLegend, San Diego, CA) for 30 minutes (4 uL antibody per 100 uL solution), washed twice, then immediately ran on an Attune NxT Flow Cytometer. Data was analysed in FlowJo by plotting SSC-A versus FSC-A and selecting the granulocyte population, excluding doublets by plotting FSC-A versus FSC-H, then gating for PE+ populations compared to unstained controls.

3.10.4 Troponin I Measurements

Mice were injected with heparin before they were sacrificed. After removal of hearts, blood was collected into EDTA-coated blood tubes and spun down at 2000xg for 30 mins. Separated plasma was transferred into a new tube and flash frozen. Troponin I (CNTI) was measured using a commercial kit (Life Diagnostics). Plasma was thawed then centrifuged at 2000xg for 20 minutes at 7°C. Supernatant was diluted 1:4 in plasma diluent, then further diluted in standard diluent as needed (final dilution 1:8 or 1:12). Standards were prepared by serially diluting a CNTI stock solution to 10, 5, 2.5, 1.25, 0.625, 0.313, and 0.156 ng/mL. HRP conjugate (100 µL) was added to anti-CTNI coated wells followed by 100 µL of standards or diluted plasma, each ran in duplicate. Wells were incubated on an orbital micro-plate shaker at 150 rpm and room temperature for one hour. Wells were emptied and washed 6x with 1x wash solution.

TMB chromogen (100 µL) was added and incubated for 15 minutes at 150 rpm and room temperature. Stop solution (100 µL) was added to each well and absorbance measured immediately at 450 nm. Sample concentrations were extrapolated from a standard curve generated in GraphPad Prism (San Diego, CA) using 4-parameter logistic regression. Sample concentrations were multiplied by their respective dilution factors to obtain final concentration values.

3.10.5 Cell Isolation

Mice were injected with 0.1 ml heparin (1000 units/ml) 10 mins prior to heart extraction. Mice were anesthetized with ketamine/xylazine (80 mg/kg / 5 mg/kg). Hearts were removed and placed in Tyrode's solution containing in mM: 140 NaCl, 5.4 KCl, 1.2 $MgCl_2$, 5 N-2-hydroxyethylpiperazine-N'-2-ethanesulphonic acid (HEPES), and 5 glucose at a pH 7.4. The aorta was cannulated, mounted on a Langendorff setup, and retrogradely perfused with Tyrode's solution containing O_2 at 37°C for 3 mins at a flow rate of approximately 3 ml/min. The perfusion pressure was monitored, and the flow rate was adjusted to maintain perfusion pressure at ~80 mmHg. The solution was then switched to Tyrode's solution containing collagenase type 2 (1 mg/ml, 330 units/mg, Worthington Biochemical Corporation). After about 12 mins of enzyme perfusion, hearts were removed from the perfusion apparatus and gently separated in high K^+ solution containing in mM: 120 potassium glutamate, 20 KCl, 1 $MgCl_2$, 0.3 EGTA, 10 glucose, and 10 HEPES, pH 7.4 with KOH. All chemicals were acquired from Sigma Chemicals (St. Louis, MO) unless stated otherwise.

3.11 Supplementary Figures

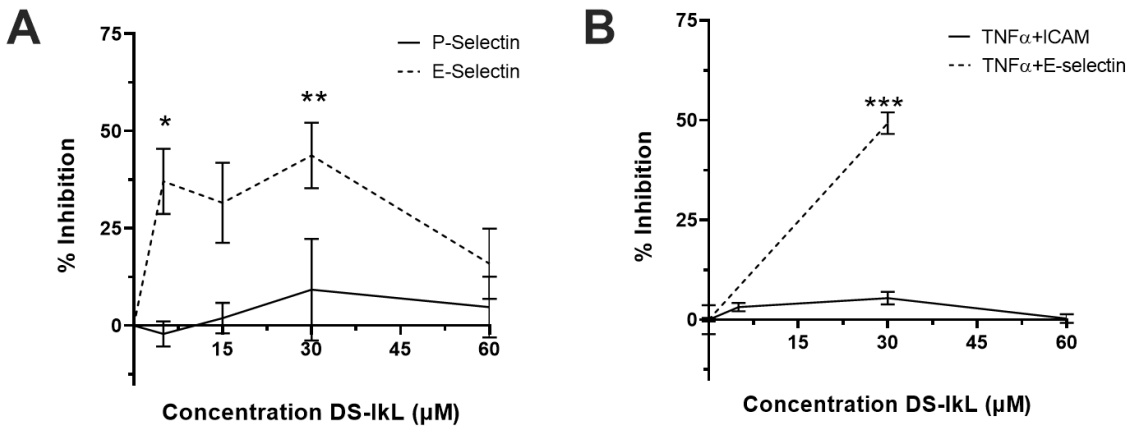

Supplementary Figure 3-1 A) Neutrophils bound less E-selectin, but not P-selectin, in the presence of 5, 15, and 30 uM DS-IkL. **B)** Under stimulatory conditions (5ng/mL TNF-α), 30 uM of DS-IkL had no effect on neutrophil binding to ICAM. Data are represented as means ± SEM of 3 biological replicates. * $p<0.05$, ** $p<0.01$, *** $p<0.001$ by one-way ANOVA with post-hoc Tukey test.

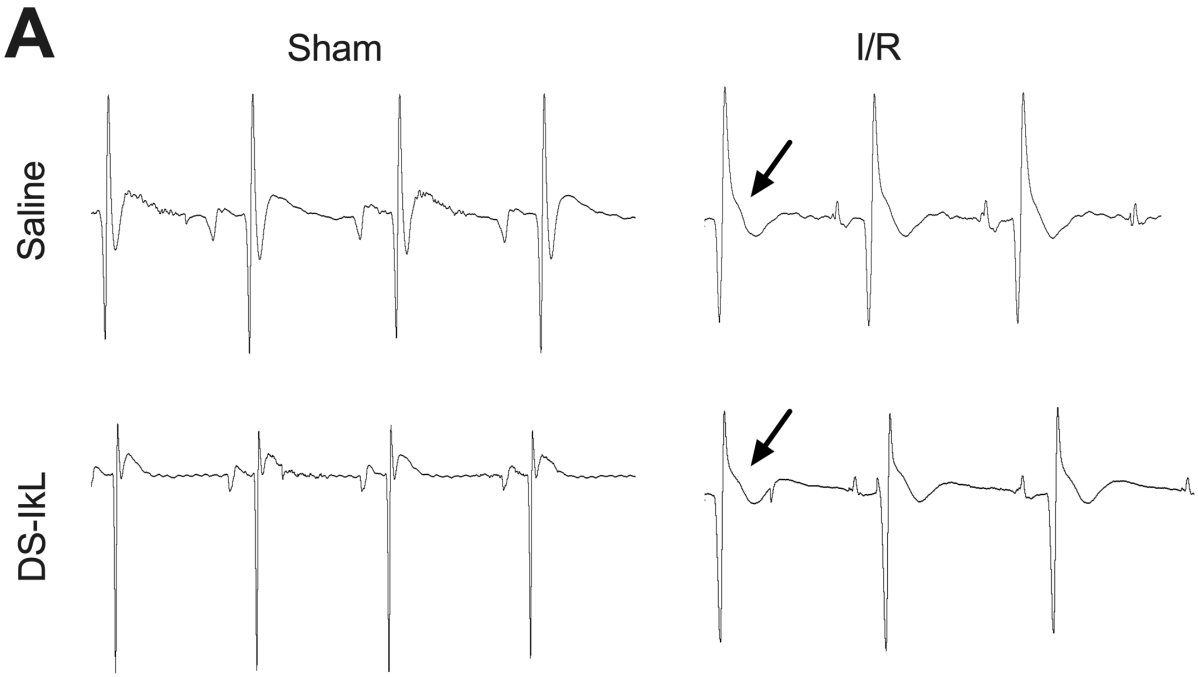

Supplementary Figure 3-2 Representative ECG recordings during surgical procedure. For I/R mice, confirmation of LAD ligation was done visually (blanching of the heart) and also by the presence of ST-elevation.

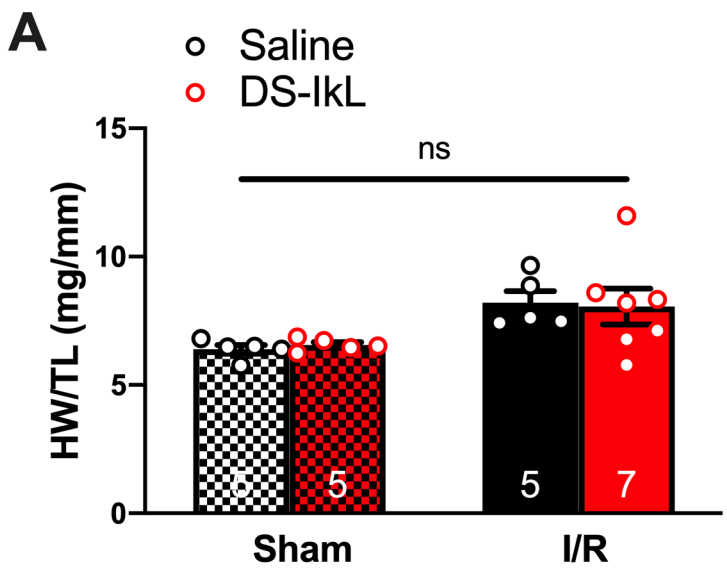

Supplementary Figure 3-3 Heart weight normalized to tibial length of all four groups. n=5-7 mice per group.

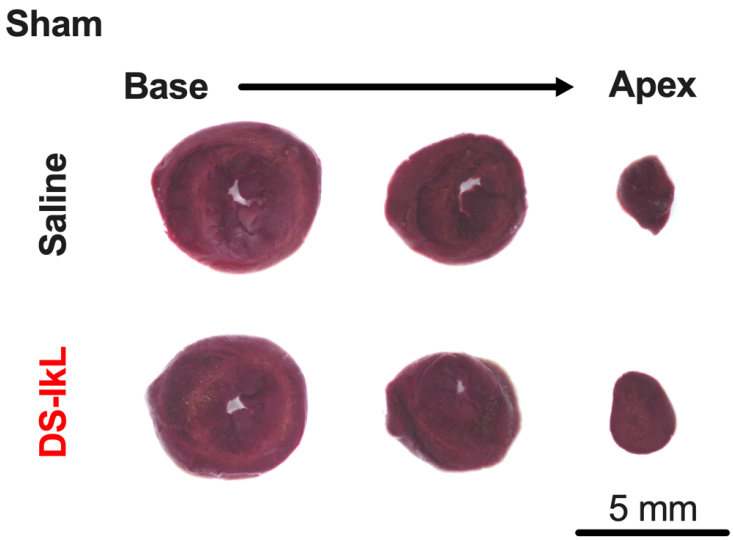

Supplementary Figure 3-4 Representative heart sections from sham-operated mice after TTC staining. Sections were taken from base to apex. n=5 mice per group.

Supplementary Table 3-1 Echocardiography Table

	Saline Sham (n=5)	DS-IkL Sham (n=5)	Saline I/R (n=6)	DS-IkL I/R (n=7)	p-value: Saline I/R vs DS-IkL I/R
Heart Rate (bpm)	580±3	612±10	569±28	591±13	NS
LV Mass Corr (mg)	58.6±6.0	59.8±6.4	103.6±12.6	113.9±7.1	NS
LVAW;d (mm)	0.77±0.02	0.78±0.07	0.90±0.06	0.86±0.02	NS
LVAW;s (mm)	1.43±0.05	1.44±0.09	1.39±0.10	1.54±0.04	NS
LVID;d (mm)	3.12±0.07	3.17±0.13	3.91±0.28	3.85±0.20	NS
LVID;s (mm)	1.41±0.05	1.53±0.09	2.76±0.24	2.41±0.25	NS
LVPW;d (mm)	0.76±0.04	0.78±0.05	0.85±0.06	0.87±0.04	NS
LVPW;s (mm)	1.38±0.08	1.45±0.11	1.21±0.11	1.48±0.09	NS
CO (ml/min)	20.1±1.1	20.1±2.3	22.1±4.4	25.4±1.8	NS
Ejection Fraction (%)	86.5±1.1	83.5±1.4	57.4±3.1	68.2±4.4	<0.05
Fractional Shortening (%)	54.8±1.3	51.8±1.4	29.8±2.0	38.1±3.2	<0.05
LV Vol;d (µl)	38.7±1.9	40.5±4.3	68.6±12.7	65.5±8.5	NS
LV Vol;s (µl)	5.8±0.4	6.5±0.9	29.9±6.6	22.8±6.4	NS
Stroke Volume (µl)	34.3±1.8	32.7±3.4	38.4±6.7	42.9±2.9	NS
Radial Strain (%)	55.5±1.83	48.25±2.4	22.0±2.4	32.19±2.2	<0.05
Circumferential Strain (%)	-31.3±1.9	-26.2±3.2	-19.3±3.2	-23.2±2.0	NS
IVRT	13.67±0.8	12.7±0.6	15.8±0.5	14.1±0.5	NS
MV E/A	1.77±0.08	1.84±0.1	1.24±0.1	1.52±0.06	<0.05
MV Deceleration Time (s)	17.89±0.7	17.2±1.2	24.8±1.6	18.7±0.9	<0.001

Supplementary Table 3-2 Commercial Reagent List

Reagent/Antibody	Vendor	Location	Catalog Number
PE anti-human CD62E antibody, clone HCD62E	BioLegend	San Diego, CA, USA	322606
PE anti-human CD62P antibody, clone AK4	BioLegend	San Diego, CA, USA	304906
Dermatan Sulfate	Celsus Labs	Cincinnati, OH, USA	
Recombinant human E-selectin-FC chimera protein	R&D Systems	Minneapolis, MN, USA	724-ES-100
Recombinant human P-selectin-FC chimera protein	R&D Systems	Minneapolis, MN, USA	137-PS-050
EasySep™ Direct Human Neutrophil Isolation Kit	StemCell Technologies	Cambridge, MA, USA	19666
PE anti-human CD54 antibody, close HA58	BioLegend	San Diego, CA, USA	353106
Human Cardiac Microvascular Endothelial Cells	PromoCell	Heidelberg Germany	C-12285
Endothelial growth medium MV	PromoCell	Heidelberg Germany	C-22120
Calcein-AM	BioLegend	San Diego, CA, USA	425201
Human Serum Albumin Solution – 25%	Gemini Bio		800-120
AF488 anti-human CD11a/CD18, clone m24	BioLegend	San Diego, CA, USA	363404
PE anti-human CD15, clone HI98	BioLegend	San Diego, CA, USA	301906
CF594 Dye Hydrazide	Biotium	Fremont, CA, USA	92158
Prostaglandin E1	Enzo Life Sciences	Farmingdale, NY, USA	BML-PG006-0010
Solid state peptide synthesis products	CEM and AAPPTec		Various
4-(4,6-Dimethoxy-1,3,5-triazin-2-yl)-4-methylmorpholinium chloride	Sigma-Aldrich	St. Louis, MO, USA	74104-1G-F
Human CXCL7/NAP-2 Antibody	R&D Systems	Minneapolis, MN, USA	MAB393
Human CXCL7/NAP-2 Biotinylated Antibody	R&D Systems	Minneapolis, MN, USA	BAF393
Human CXCL4/PF4 Antibody	R&D Systems	Minneapolis, MN, USA	AF795
Human CXCL4/PF4 Biotinylated Antibody	R&D Systems	Minneapolis, MN, USA	BAF795
EDTA Solution	Promega	Madison, WI, USA	V4231
Theophylline	Sigma-Aldrich	St. Louis, MO, USA	T1633-100G
PolyLink Protein Coupling Kit	PolySciences, Inc.	Warrington, PA, USA	24350-1
Fluoresbrite® 641 Carboxylate Microspheres 1.75µm	PolySciences, Inc.	Warrington, PA, USA	17797

Pierce™ Recombinant Protein A/G	ThermoFisher	Waltham, Massachusetts, USA	21186
BS3 (bis(sulfosuccinimidyl)suberate)	ThermoFisher	Waltham, Massachusetts, USA	21580
Thy1.2-PE antibody	e-Bioscience	San Diego, CA, UCSA	12-0902-81
Rat Anti-Mouse CD11b antibody	BD Bioscience	Franklin Lakes, NJ, USA	557397
Rat Anti-Mouse Ly-6C/G antibody	BD Bioscience	Franklin Lakes, NJ, USA	553128
MyHC antibody	Developmental Studies Hybridoma Bank	Iowa City, IA, USA	
Rat Anti-Mouse CD31 antibody	BD Bioscience	Franklin Lakes, NJ, USA	558737
Rat Anti-Mouse Ki-67 antibody	BD Bioscience	Franklin Lakes, NJ, USA	558615
Mouse Cardiac Troponin-I ELISA	Life Technologies	West Chester, PA, USA	CTNI-1 HSP

3.12 References

1. Fryar CD, Chen TC, Li X. Prevalence of uncontrolled risk factors for cardiovascular disease: United States, 1999-2010. NCHS Data Brief. 2012(103):1-8.
2. Myerburg RJ, Junttila MJ. Sudden cardiac death caused by coronary heart disease. Circulation. 2012;125(8):1043-52.
3. Kalogeris T, Baines CP, Krenz M, Korthuis RJ. Cell biology of ischemia/reperfusion injury. Int Rev Cell Mol Biol. 2012;298:229-317.
4. Hausenloy DJ, Yellon DM. Myocardial ischemia-reperfusion injury: a neglected therapeutic target. J Clin Invest. 2013;123(1):92-100.
5. Rusinkevich V, Huang Y, Chen Z-y, Qiang W, Wang Y-g, Shi Y-f, et al. Temporal dynamics of immune response following prolonged myocardial ischemia/reperfusion with and without cyclosporine A. Acta Pharmacologica Sinica. 2019;40(9):1168-83.
6. Frangogiannis NG. The inflammatory response in myocardial injury, repair, and remodelling. Nat Rev Cardiol. 2014;11(5):255-65.
7. Hausenloy DJ, Chilian W, Crea F, Davidson SM, Ferdinandy P, Garcia-Dorado D, et al. The coronary circulation in acute myocardial ischaemia/reperfusion injury: a target for cardioprotection. Cardiovasc Res. 2019;115(7):1143-55.
8. Chappell D, Hofmann-Kiefer K, Jacob M, Rehm M, Briegel J, Welsch U, et al. TNF-alpha induced shedding of the endothelial glycocalyx is prevented by hydrocortisone and antithrombin. Basic Res Cardiol. 2009;104(1):78-89.
9. Mulivor AW, Lipowsky HH. Inflammation- and ischemia-induced shedding of venular glycocalyx. American Journal of Physiology-Heart and Circulatory Physiology. 2004;286(5):H1672-H80.
10. McDonald KK, Cooper S, Danielzak L, Leask RL. Glycocalyx Degradation Induces a Proinflammatory Phenotype and Increased Leukocyte Adhesion in Cultured Endothelial Cells under Flow. PLoS One. 2016;11(12):e0167576.
11. van Haaren PM, VanBavel E, Vink H, Spaan JA. Localization of the permeability barrier to solutes in isolated arteries by confocal microscopy. Am J Physiol Heart Circ Physiol. 2003;285(6):H2848-56.
12. Sieve I, Munster-Kuhnel AK, Hilfiker-Kleiner D. Regulation and function of endothelial glycocalyx layer in vascular diseases. Vascul Pharmacol. 2018;100:26-33.
13. Rehm M, Bruegger D, Christ F, Conzen P, Thiel M, Jacob M, et al. Shedding of the endothelial glycocalyx in patients undergoing major vascular surgery with global and regional ischemia. Circulation. 2007;116(17):1896-906.
14. Potter DR, Jiang J, Damiano ER. The recovery time course of the endothelial cell glycocalyx in vivo and its implications in vitro. Circ Res. 2009;104(11):1318-25.
15. McEver RP. Selectins: initiators of leucocyte adhesion and signalling at the vascular wall. Cardiovasc Res. 2015;107(3):331-9.
16. Palazzo AJ, Jones SP, Anderson DC, Granger DN, Lefer DJ. Coronary endothelial P-selectin in pathogenesis of myocardial ischemia-reperfusion injury. Am J Physiol. 1998;275(5):H1865-72.
17. Manchanda K, Kolarova H, Kerkenpaß C, Mollenhauer M, Vitecek J, Rudolph V, et al. MPO (myeloperoxidase) reduces endothelial glycocalyx thickness dependent on its cationic charge. Arteriosclerosis, Thrombosis, and Vascular Biology. 2018;38(8):1859-67.
18. Timofeyev V, Myers RE, Kim HJ, Woltz RL, Sirish P, Heiserman JP, et al. Adenylyl cyclase subtype-specific compartmentalization: differential regulation of L-type Ca2+ current in ventricular myocytes. Circ Res. 2013;112(12):1567-76.
19. Wodicka JR, Morikis VA, Dehghani T, Simon SI, Panitch A. Selectin-Targeting Peptide-Glycosaminoglycan Conjugates Modulate Neutrophil-Endothelial Interactions. Cell Mol Bioeng. 2019;12(1):121-30.
20. Wodicka JR, Chambers AM, Sangha GS, Goergen CJ, Panitch A. Development of a Glycosaminoglycan Derived, Selectin Targeting Anti-Adhesive Coating to Treat Endothelial Cell Dysfunction. Pharmaceuticals (Basel). 2017;10(2).
21. Lam KS, Lehman AL, Song A, Doan N, Enstrom AM, Maxwell J, et al. Synthesis and screening of "one-bead one-compound" combinatorial peptide libraries. Methods Enzymol. 2003;369:298-322.
22. Kawashima H, Hirose M, Hirose J, Nagakubo D, Plaas AH, Miyasaka M. Binding of a large chondroitin sulfate/dermatan sulfate proteoglycan, versican, to L-selectin, P-selectin, and CD44. J Biol Chem. 2000;275(45):35448-56.

23. Lisman T. Platelet-neutrophil interactions as drivers of inflammatory and thrombotic disease. Cell Tissue Res. 2018;371(3):567-76.
24. Pitchford S, Pan D, Welch HC. Platelets in neutrophil recruitment to sites of inflammation. Curr Opin Hematol. 2017;24(1):23-31.
25. Wang J. Neutrophils in tissue injury and repair. Cell Tissue Res. 2018;371(3):531-9.
26. Kuldo JM, Westra J, Asgeirsdottir SA, Kok RJ, Oosterhuis K, Rots MG, et al. Differential effects of NF-{kappa}B and p38 MAPK inhibitors and combinations thereof on TNF-{alpha}- and IL-1{beta}-induced proinflammatory status of endothelial cells in vitro. Am J Physiol Cell Physiol. 2005;289(5):C1229-39.
27. Bhaumik S, DePuy J, Klimash J. Strategies to minimize background autofluorescence in live mice during noninvasive fluorescence optical imaging. Lab Animal. 2007;36(8):40-3.
28. Gao S, Ho D, Vatner DE, Vatner SF. Echocardiography in Mice. Curr Protoc Mouse Biol. 2011;1:71-83.
29. Talman V, Ruskoaho H. Cardiac fibrosis in myocardial infarction-from repair and remodeling to regeneration. Cell Tissue Res. 2016;365(3):563-81.
30. Yang Q, He GW, Underwood MJ, Yu CM. Cellular and molecular mechanisms of endothelial ischemia/reperfusion injury: perspectives and implications for postischemic myocardial protection. Am J Transl Res. 2016;8(2):765-77.
31. Li W, Wang W. Structural alteration of the endothelial glycocalyx: contribution of the actin cytoskeleton. Biomechanics and modeling in mechanobiology. 2018;17(1):147-58.
32. Ley K, Laudanna C, Cybulsky MI, Nourshargh S. Getting to the site of inflammation: the leukocyte adhesion cascade updated. Nat Rev Immunol. 2007;7(9):678-89.
33. Perlin AS. Glycol-cleavage oxidation. Adv Carbohydr Chem Biochem. 2006;60:183-250.
34. Xu Y, Huo Y, Toufektsian MC, Ramos SI, Ma Y, Tejani AD, et al. Activated platelets contribute importantly to myocardial reperfusion injury. Am J Physiol Heart Circ Physiol. 2006;290(2):H692-9.
35. von Hundelshausen P, Weber C. Platelets as immune cells: bridging inflammation and cardiovascular disease. Circ Res. 2007;100(1):27-40.
36. Herrler T, Wang H, Tischer A, Schupp N, Lehner S, Meyer A, et al. Decompression of inflammatory edema along with endothelial cell therapy expedites regeneration after renal ischemia-reperfusion injury. Cell Transplant. 2013;22(11):2091-103.
37. Gogiraju R, Bochenek ML, Schafer K. Angiogenic Endothelial Cell Signaling in Cardiac Hypertrophy and Heart Failure. Front Cardiovasc Med. 2019;6:20.
38. Nigam A, Kopecky SL. Therapeutic Potential of Monoclonal Antibodies in Myocardial Reperfusion Injury. American Journal of Cardiovascular Drugs. 2002;2(6):367-76.
39. Yellon DM, Hausenloy DJ. Myocardial Reperfusion Injury. New England Journal of Medicine. 2007;357(11):1121-35.
40. Davidson SM, Ferdinandy P, Andreadou I, Bøtker HE, Heusch G, Ibáñez B, et al. Multitarget Strategies to Reduce Myocardial Ischemia/Reperfusion Injury. Journal of the American College of Cardiology. 2019;73(1):89-99.
41. Weyrich AS, Ma XY, Lefer DJ, Albertine KH, Lefer AM. In vivo neutralization of P-selectin protects feline heart and endothelium in myocardial ischemia and reperfusion injury. J Clin Invest. 1993;91(6):2620-9.
42. Schmitt C, Abt M, Ciorciaro C, Kling D, Jamois C, Schick E, et al. First-in-Man Study With Inclacumab, a Human Monoclonal Antibody Against P-selectin. Journal of cardiovascular pharmacology. 2015;65(6):611-9.
43. Fukushima S. A Novel Strategy for Myocardial Protection by Combined Antibody Therapy Inhibiting Both P-Selectin and Intercellular Adhesion Molecule-1 Via Retrograde Intracoronary Route. Circulation. 2006;114(1_suppl):I-251-I-6.
44. Tardif JC, Tanguay JF, Wright SR, Duchatelle V, Petroni T, Gregoire JC, et al. Effects of the P-selectin antagonist inclacumab on myocardial damage after percutaneous coronary intervention for non-ST-segment elevation myocardial infarction: results of the SELECT-ACS trial. J Am Coll Cardiol. 2013;61(20):2048-55.
45. Niwa R, Satoh M. The Current Status and Prospects of Antibody Engineering for Therapeutic Use: Focus on Glycoengineering Technology. Journal of Pharmaceutical Sciences. 2015;104(3):930-41.
46. Chames P, Van Regenmortel M, Weiss E, Baty D. Therapeutic antibodies: successes, limitations and hopes for the future. Br J Pharmacol. 2009;157(2):220-33.
47. Riley TR, Riley TT. Profile of crizanlizumab and its potential in the prevention of pain crises in sickle cell disease: evidence to date. J Blood Med. 2019;10:307-11.
48. Telen MJ, Wun T, McCavit TL, De Castro LM, Krishnamurti L, Lanzkron S, et al. Randomized phase 2 study of GMI-1070 in SCD: reduction in time to resolution of vaso-occlusive events and decreased opioid use. Blood. 2015;125(17):2656-64.

CHAPTER 4: USE OF DS-IKL AS AN ANTAGONIST TO PLATELET-NEUTROPHIL AND PLATELET-NEUTROPHIL-ENDOTHELIAL INTERACTIONS

4.1 Abstract

Neutrophils, platelets, and endothelial cells each play a significant role in inflammatory disease. Interactions among these cell types further complicate the inflammatory environment, leading to increased thrombosis, vascular dysfunction, and organ damage. Here, we investigate the efficacy of DS-IkL, a selectin-targeting peptide-glycosaminoglycan conjugate that we recently reported on, on platelet-neutrophil-endothelial interactions. DS-IkL was shown to interact with endothelial E-selectin and, to a lesser extent, P-selectin, leading to reductions in neutrophil binding to inflamed endothelium. Platelet P-selectin engagement by neutrophil PSGL-1 is a pivotal component of platelet-neutrophil interactions. We were therefore interested in exploring whether DS-IkL has an effect on platelet-neutrophil complexing, cytokine secretion, and neutrophil extracellular trap (NET) formation in the presence of activated platelets. DS-IkL reduced platelet-neutrophil complexes (PNCs) but did not significantly affect cytokine secretion. When endothelial cells were added to the system, cytokine secretion increased considerably. Platelet activation and PNC formation did not elicit NET release, even in inflammatory endothelial cell environment. These data suggest that, though DS-IkL may help reduce PNC formation, selectin-independent mechanisms may have a greater impact on PNC-endothelial interactions in the systems described herein.

4.2 Introduction

During acute sterile inflammation, the vasculature undergoes a phenotypic shift that facilitates pro-coagulant functions, immune cell adhesion, and vascular leakage. In particular, endothelial cells lining the afflicted blood vessels exhibit endothelial dysfunction, a complex phenotype that is characterized in part by the loss of the glycosaminoglycan- and proteoglycan-rich glycocalyx (1-3) and upregulation of immune cell adhesion molecules E- and P-selectin. Upregulated selectins on the luminal surface of endothelial cells aid in the capture of circulating leukocytes (e.g., neutrophils) and platelets (4), which are recruited though signals secreted by damaged cells (5). While these first responders are vital to the resolution of inflammation, too robust of a response can be detrimental to the vasculature and the surrounding tissue, perpetuating vascular damage and promoting fibrotic remodeling.

This story becomes increasingly complicated when neutrophil-platelet and neutrophil-platelet-endothelial cell interactions are considered. In a recent review (6), we described the complex and dynamic relationship among neutrophils, platelets, and endothelial cells in inflammatory disease. Tethered platelets and platelet thrombi facilitate leukocyte tethering *via* platelet P-selectin—neutrophil P-selectin glycoprotein ligand-1 (PSGL-1) and platelet glycoprotein Ibα (GPIbα)—neutrophil Mac-1 (7, 8). These interactions have been further correlated with elevated neutrophil extracellular trap (NET) formation and thrombus formation (9), though the mechanisms behind these events remain unclear and are likely context dependent.

Platelet-neutrophil complexes (PNCs) have been observed both in circulation and along inflamed vessel walls. Discrete mechanisms become even more obscured in the latter scenario, as endothelial adhesion molecules and secreted soluble factors further promote neutrophil and platelet engagement (6). Furthermore, as the number of cell types involved increases, so does the body's capacity to compensate for interactions inhibited by small molecule or antibodies therapeutics, further blurring the mechanistic lines.

Rather than target an individual component of these interactions, we propose that multifunctional therapeutics may have greater efficacy in these complex environments.

We have recently reported on a selectin-targeting glycosaminoglycan-peptide conjugate, DS-IkL, that reduced neutrophil-endothelial interactions, platelet activation on cytokine-stimulated endothelial cells, and cardiac fibrotic remodeling after acute myocardial infarction (10). In our previous work, our investigations were limited to neutrophil-endothelial and platelet-endothelial interactions after endothelial stimulation or damage. However, others have shown that PNCs play a nontrivial role in disorders such as ischemia reperfusion injury (11). We have shown previously that DS-IkL has a slight affinity for P-selectin (10), potentially mediated in part by the DS backbone (12, 13). Given the prominent role P-selectin engagement plays in PNC formation, DS-IkL could be an interesting therapeutic for disrupting platelet-neutrophil-endothelial cell interactions.

In the present work, we investigate the interaction between platelets, neutrophils, and endothelial cells in the presence of several inflammatory mediators. The experiments described herein focus on platelet activation as an initiator of neutrophil and endothelial inflammation. Adenosine di-phosphate (ADP) and fibrillar collagen type-1 were used as soluble inflammatory mediators to activate resting platelets in platelet-rich plasma. DS-IkL interfered with PNC formation but did not significantly reduce cytokine secretion by PNC-endothelial cell mixtures. Stimulated PNC suspensions did not elicit NET release, even in high cytokine environments. Additional work is needed to elucidate the central mechanisms behind these results.

4.3 Methods

4.3.1 Neutrophil and platelet rich plasma isolation

Blood was collected into EDTA or sodium citrate BD Vacutainer Venous Blood Collection Tubes (BD Biosciences) for neutrophil or platelet isolation, respectively, in accordance with approved protocols

of the Institutional Review Board Administration at UC Davis, which conform to the principles outlined in the Declaration of Helsinki. Polymorphonuclear neutrophils (PMN) were isolated using an EasyStep neutrophil isolation kit (StemCell) according to the manufacturer's instructions. For platelet studies, citrate tubes were centrifuged at 200 x g for 25 minutes with no brake. The top two-thirds of the clear platelet rich plasma (PRP) layer was collected into a sterile 5 mL polypropylene test tube for later use. If layers did not sufficiently separate, tubes were spun an additional 5 minutes. Cell suspensions were kept at room temperature with light rotation until use.

4.3.2 Molecule synthesis

Molecules were synthesized as previously described (10). Briefly, C-terminus hydrazide-functionalized peptides (ROpLLkIsGRG-N2H3) were conjugated to dermatan sulfate (DS, 41816 Da, Celsus Labs) at a 15:1 molar ratio using 4-(4,6-dimethoxy-1,3,5-triazin-2-yl)-4-methylmorpholinium chloride (DMTMM, Sigma-Aldrich) as a coupling regent at a 1:45 molar ratio. Samples were reacted for 48 h with end-over-end rotation before quenching with ultrapure water and purifying against ultrapure water using tangential flow filtration with a 10 kDa cutoff (Spectrum Labs). Samples were frozen and lyophilized, and the average number of peptides per DS backbone determined using a standard curve of free peptide absorbance at 205 nm on a NanoDrop Spectrophotometer (ThermoFisher). For unmodified DS, fresh buffer was added instead of dissolved peptide and the reaction protocol was carried out as described.

4.3.3 Platelet-neutrophil complex formation

20 µL of PRP was added to 0.5 mL microcentrifuge tubes and diluted with 25 µL of buffer [Hank's Balanced Salt Solution (HBSS) with calcium and magnesium, 0.3% human serum albumin (HSA), 20 mM HEPES)]. 50 µL treatments were added before addition of 5 µL stimulation buffer [400 µM ADP (final concentration 20 uM) or 60 µg/mL fibrillar collagen type 1 (final concentration 3 ug/ml)]. Treatment groups included buffer (vehicle), DS (4 or 40µM), DS-IkL (4 or 40 µM), IkL peptide (600 µM) and anti-P-selectin [5 µL purified anti-P-selectin (Biolegend) + 45 µL buffer]. Samples were gently mixed and incubated at

room temperature (RT) with orbital rotation (120 RPM). After 10 minutes, 150,000 neutrophils (100 µL of a 1.5 million cells/mL suspension) were gently mixed into each tube and incubated for 20 minutes with rotation. Cell populations were stained for CD45 (leukocytes), CD15 (neutrophils), and CD41 (platelets) (Biolegend) for 10 minutes at RT. In tubes with cell clotting, clots were carefully removed using a 1 mL pipette tip to prevent clogging. Samples were then run on an Attune NxT flow cytometer (ThermoFisher) (**Table 4-1**, **Table 4-2**). All data were normalized to vehicle control for each experiment's respective donor.

Table 4-1 Attune NxT Antibody Information and Laser Settings

Target	Clone	Fluorophore	Laser Line	Voltage
CD41	HIP8	PE	YL1	350
CD45	HI30	APC	RL1	385
CD15	HI98	FITC	BL1	270
CD11a/CD18	m24	AF488	BL1	300
CD62P	AK4	PE	YL1	340

Table 4-2 Flow cytometer settings

PARAMETER	SETTING
FSC	Voltage: 350
SSC	Voltage: 350
Flow rate (fast)	200 µL/min
Flow rate (slow)	25 µL/min
Draw volume (high)	500 µL
Draw volume (low)	200 µL
# Events max	25,000 or off

4.3.4 Cell clotting during PNC formation

To quantify cell clotting, we measured the number of cells remaining after clot removal from each tube. Draw volumes (100-500 µL) were allowed to run in full (no event maximum). Draw volumes and run speeds were adjusted for each sample as needed to maintain 50-150 events/s (**Table 4-2**). Data were extrapolated to total tube volume by multiplying by the corresponding dilution factor (total volume divided by draw volume). Treatment groups included vehicle, anti-P-selectin (5 µL stock), DS (40 µM), and DS-IkL (40 µM).

4.3.5 Activated partial thromboplastin time coagulation testing

Activated partial thromboplastin time (aPTT) was used to test the anticoagulative properties of DS and DS-IkL. Plasma from healthy donors or a control plasma (Pacific Biosciences) was used for coagulation testing. For data from healthy donors, whole blood was collected into sodium citrate tubes and centrifuged at 1500 x g for 15 minutes with no brake. The top cell-free plasma layer was collected into a polypropylene test tube. All reagents were kept at 37°C throughout the duration of the experiment. FibroTube cups (0.3 mL, Thomas Scientific) were placed into the warming wells of a BBL Fibrometer Precision Coagulation Timer (Beckton, Dickinson and Company). Plasma (100 µL) and treatment (50 µL) were added and incubated for 1 minute before adding 100 µl APTT-XL solution (Pacific Biosciences). Heparin (Bioiberica) was used as a positive control. After incubating for 3 minutes, 50 µl of 0.04 M $CaCl_2$ solution was added forcefully and the fibrometer started. Time to coagulation was recorded for each sample.

4.3.6 Endothelial activation by platelet-neutrophil complexes

CellBind 96-well plates (ThermoFisher) were coated with 50 µg/mL of rat tail collagen type-I (Corning) in 20 mM acetic acid for 1 hour at RT then rinsed 3x with Dulbecco's Phosphate Buffered Saline (DPBS). Human umbilical cord endothelial cells, pooled donor (HUVEC, PromoCell) passage 2-5 were

seeded at 20,000-30,000 cells/cm^2. Media was changed every other day until cells were confluent. Confluent cells were rinsed 1x with pre-warmed DPBS before use.

Twenty microliters of platelet rich plasma were added to wells of a polypropylene 96-well plate containing 25 µl buffer (HBSS$^{+/+}$ + 0.3% HSA + 20 mM HEPES), 50 µl treatments, and 5 µl stimulation buffer [400 µM ADP (final concentration 20 µM) or 60 µg/mL fibrillar collagen type 1 (final concentration 3 µg/mL)]. Plates were incubated for 10 minutes at RT with rotation (120 RPM). After 10 minutes, 100 µL of a neutrophil suspension (1.5 x 10^6 cells/mL) was added to each well and gently mixed. The entire PRP-PMN suspension was transferred to the HUVEC plate. Cells were incubated for 4 h at 37°C with rotation (120 RPM).

After 4 hours, supernatant was collected from all wells and transferred into a polypropylene 96-well plate. Plates were centrifuged at 900 x g for 10 minutes with no brake to pellet cells. Supernatants were collected immediately into a new polypropylene 96-well plate and frozen at -80°C until use.

4.3.7 Quantification of cytokine expression after PNC incubation

A custom U-Plex Biomarker Group 1 Assay (Mesoscale Discovery) for human IFN-γ, IL-1β, IL-6, IL-8, IL-10, and TNF-α was performed according to the manufacturer's instructions. U-Plex plates were coated with analyte-coupled linkers for 1 hour at RT with shaking (750 RPM). Plates were washed 3x with PBS-Tween (PBST), then samples (30 µl sample + 20 µl diluent) or serially diluted standards (25 µl standard + 25 µl diluent) were added. Plates were incubated for 1 hour at RT with shaking. Plates were washed 3x with PBST before adding secondary antibody cocktail for 1 hour at RT with shaking. After 3x washes, 1x read buffer was added and the plates read on an MSD QuickPlex SQ 120 (Mesoscale Discovery). Concentrations were determined within the Discovery Workbench software using a standard curve, then dilution corrected in Excel.

4.3.8 Neutrophil extracellular trap detection

Neutrophil extracellular trap (NET) experiments were repeated 1 time for an n = 2. Isolated neutrophils (50 µl of a 1.5 x 10^6 cells/mL suspension) were added to a black clear bottomed 96-well plate (Corning) and incubated for 10 minutes. Platelet-rich plasma (20 µL), treatments or buffer (50 µL), and stimulation buffer (5 µL) were gently mixed in. Diluted Sytox green (25 µL, ThermoFisher) was then added to a final concentration of 2.5 µM. Plates were immediately transferred into a SpectraMax M5 Microplate Reader (Molecular Devices) pre-warmed to 37°C. Fluorescence kinetics was monitored by reading fluorescence values at 488/540 nm (ex/em) every 5 minutes for 4 hours, with a 2 second shake between reads. After 4 hours, DNAse I (New England Biolabs) was added to a final concentration of 2 U/mL and fluorescence read every 10 minutes for 60 minutes. Two fluorescence images per well were acquired using a Keyence BZ-X700 All-In-one Fluorescence Microscope (Keyence).

In some experiments, HUVECs (passage 2-5) were seeded at 20,000-30,000 cells/cm^2 and grown to confluence before use. Neutrophils were added into HUVEC-coated wells and the experiment conducted as described. In experiments without HUVECs, bottom reads were taken every hour in addition to the described data collection. Fluorescence data were normalized to each group's respective initial value.

4.3.9 Statistics

Experiments were conducted at least three independent times for an n≥3 unless otherwise stated. For each experiment, data is summarized as the average of 2-4 technical replicates. At least 3 different blood donors were used in experiments requiring blood components. Data are represented as mean +/- standard deviation (SD). In experiments with 2 groups, an unpaired two-tailed student's t-test was used. In experiments with more than 2 groups, a one- or two-way analysis of variance (ANOVA) with post-hoc Tukey test was used to assess statistical differences. A p-value < 0.05 was considered statistically significant.

4.4 Results

4.4.1 Platelet-neutrophil complex formation

In addition to their independent responses to inflammatory injury, platelets and neutrophils can complex with one another to form inflammatory aggregates (14). Platelet-neutrophil complexes (PNCs) have been associated with exacerbation of chronic disease (14, 15); therefore, reducing their formation could aid in slowing disease progression. To test if DS-IkL affects the formation of PNCs, PRP was pre-activated with ADP or fibrillar collagen type-1 in the presence of buffer, DS (40 μM), DS-IkL (40 μM), IkL peptide (600 μM), or an antibody to P-selectin. Neutrophils were then added to the suspension and the resulting aggregates analyzed using flow cytometry.

In ADP-stimulated suspensions, treatment with 40 μM of DS resulted in a significant decrease in PNC formation, as assessed by $CD45^+/CD15^+/CD41^+$ (neutrophils positive for platelets) populations (**Figure 4-1**). Low concentrations of DS and DS-IkL had no effect on PNC formation, and 40 μM DS-IkL caused only a small (~25%) reduction in PNC formation. It is worth noting that large donor-to-donor variability was observed in these experiments (**Figure 4-2**).

We were next interested in assessing if treatment with DS or DS-IkL would affect the proportion of $CD41^+/CD45^+/CD15^+$ aggregates, or platelets positive for neutrophil markers (**Figure 4-1**). No effect was observed with this gating. However, in collagen-stimulated samples, treatment with both DS and DS-IkL was associated with a significant decrease in platelets positive for neutrophil markers (**Figure 4-3B**), but not neutrophils positive for platelet markers (**Figure 4-3A**).

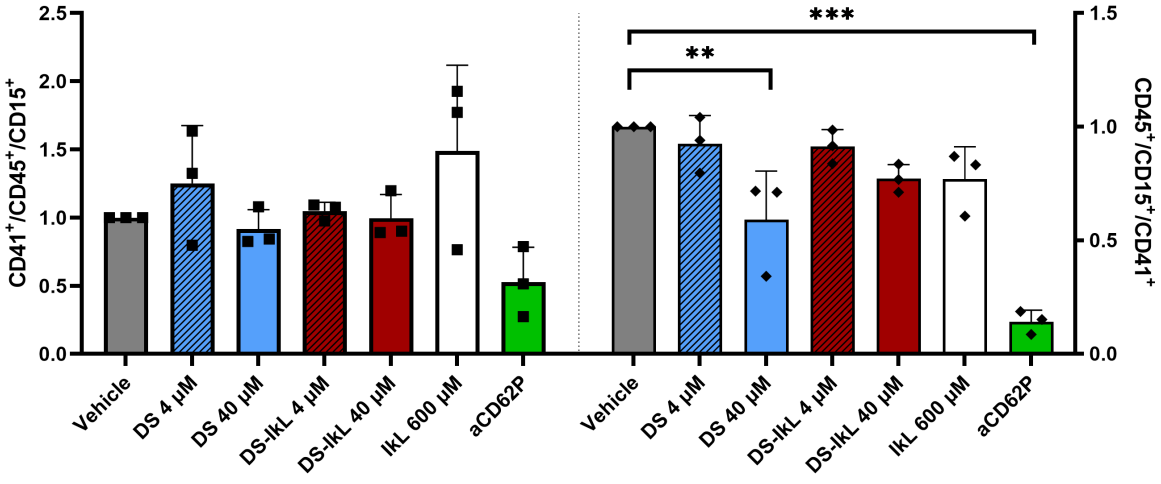

Figure 4-1 Effect of treatments on ADP-induced PNC formation. Treatment with DS and aCD62P lead to significant reductions in PNC formation. While treatments had no effect on platelet populations positive for neutrophils (left), they did affect neutrophil populations positive for platelets (right). Data represent mean ± SD of 2 technical replicates from 3 independent experiments (n=3). In panel B, * $p < 0.05$, ** $p < 0.01$, **** $p < 0.001$.

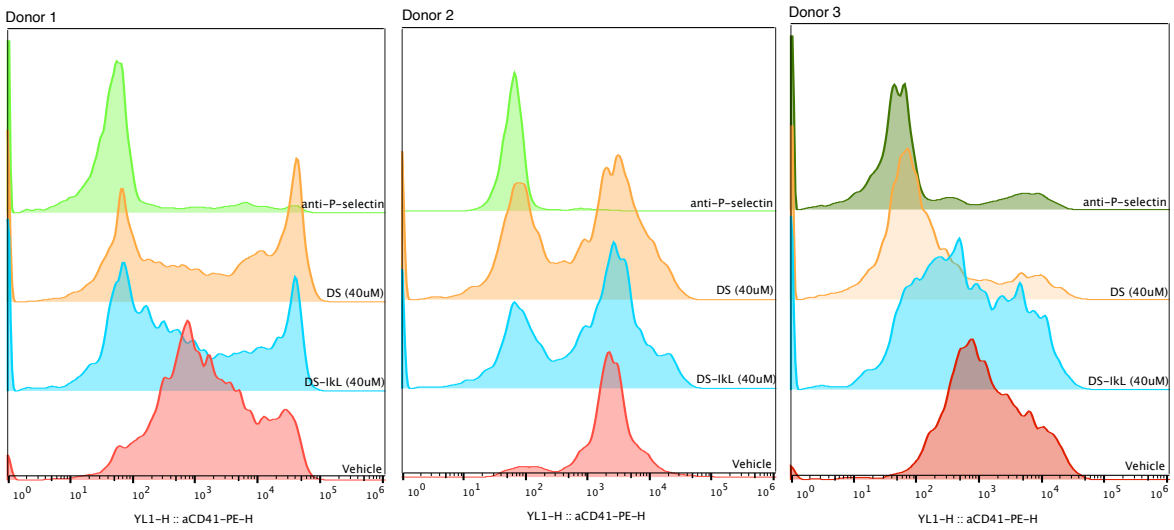

Figure 4-2 Donor-to-donor variability. In three separate experiments, healthy donors elicited differing responses to treatments. Variable shifts in $CD45^+CD15^+CD41^+$ cell populations are shown.

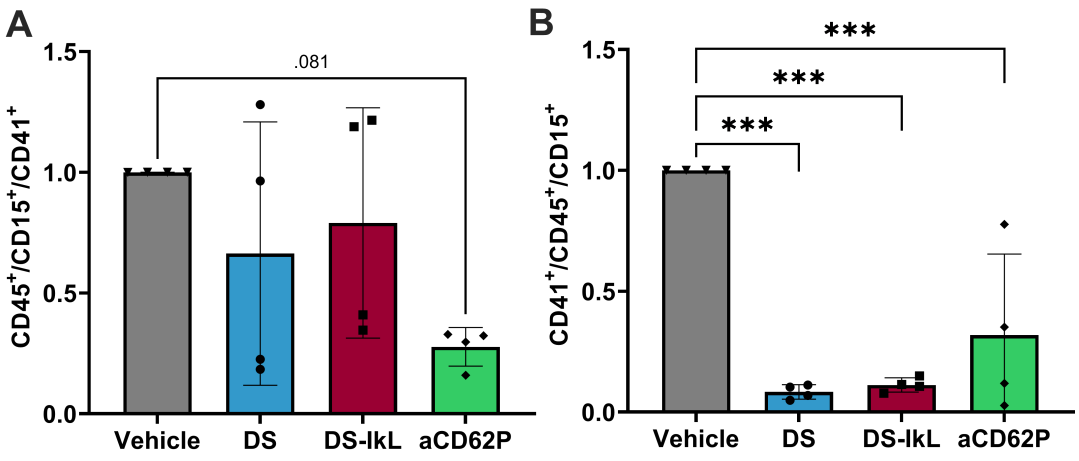

Figure 4-3 Effect of treatments on collagen-stimulated suspensions. DS, DS-IkL, and aCD62P groups exhibited reductions in neutrophils positive for platelet CD41 (**A**), but not to a significant level. However, all three treatments were associated with significantly reduced levels of platelets positive for neutrophil CD45/CD15 (**B**). Data points represent mean ± SD of 2 technical replicates from 3-4 independent experiments. n = 3-4; *** $p < 0.001$.

4.4.2 Cell clotting and coagulation testing

During PNC experiments, we noticed small fibrin clots formed at the bottom of the microcentrifuge tube in vehicle, aCD62P, antibody controls, isotype controls, and even unstimulated vehicle control samples within the first 10-15 minutes of coincubation. Clots were not observed in DS or DS-IkL treated samples. To examine how clotting affected total and differential cell counts available for flow cytometry in collagen-stimulated samples, draw volumes were allowed to run in full rather than setting an event maximum. **Figure 4-4A** shows that vehicle and anti-P-selectin treated groups had an almost 100-fold reduction in cells remaining, suggesting a large proportion of cells are lost in the clot. When cells were further gated to analyze neutrophil and platelet populations individually, only platelet populations were significantly reduced in vehicle and P-selectin groups compared to DS and DS-IkL treated samples, with neutrophil populations exhibiting smaller differences (10-fold).

Cell suspensions were further analyzed to determine what percent of the total cell population neutrophils and platelets made up. In vehicle and anti-P-selectin groups, platelets comprised a slightly lower

percent of the total cell population compared to DS and DS-IkL treated samples (**Figure 4-4B**). This trend was reversed for neutrophils, wherein neutrophils made up a larger percent of total cell population in vehicle and anti-P-selectin groups.

To further investigate the anticoagulative properties of DS and DS-IkL, we tested coagulation using aPTT (**Figure 4-5**). Heparin was tested at a maximum concentration of 7 µg/mL; plasma was unable to clot at higher concentrations. Plasma coagulated when treated with up to 750 µg/mL DS, and up to 2000 µg/mL of DS-IkL (maximum concentration tested). Coagulation ability began to differ between DS and DS-IkL at concentrations as low at 100 µg/mL, suggesting DS-IkL is minimally anticoagulative compared to both DS and heparin.

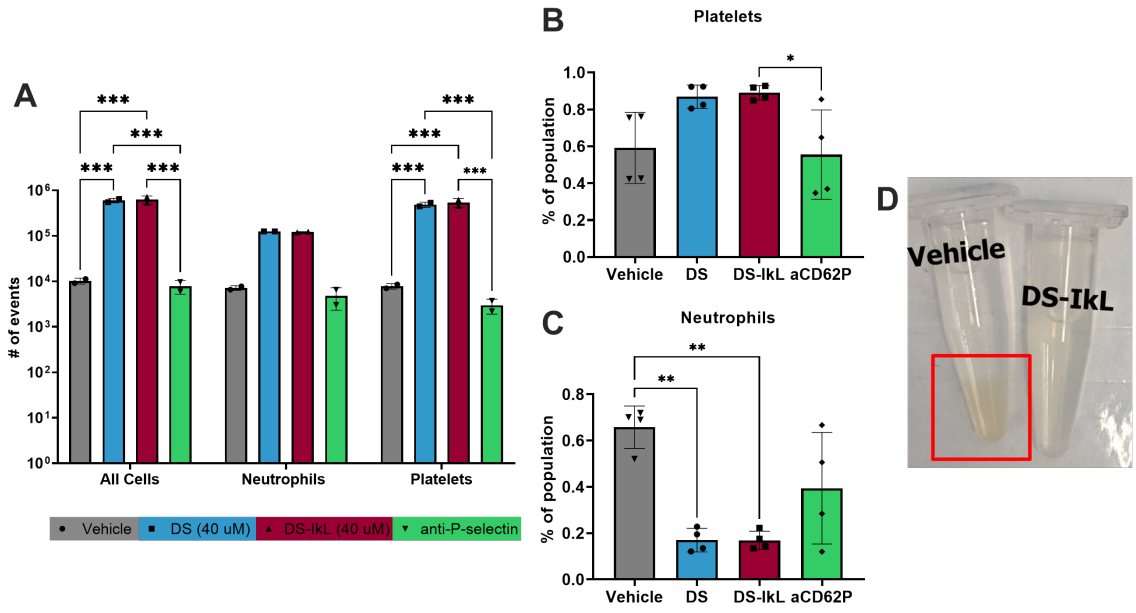

Figure 4-4 Quantification of cell clotting in collagen-stimulated groups. Total number of events was significantly reduced in vehicle and anti-P-selectin treated groups compared to DS and DS-IkL-treated groups (**A**). After further breakdown of these populations, a trend toward a decreased proportion of platelets (**B**) and increased proportion of neutrophils (**C**) was observed in vehicle-treated groups compared to DS and DS-IkL. (**D**) Representative image of cell clotting in Vehicle (left) versus DS-IkL (right) treated samples. Data represents mean ± SD of 2 technical replicates from 2-4 independent experiments (n = 2-4). * $p < 0.05$, ** $p < 0.01$, *** $p < 0.001$.

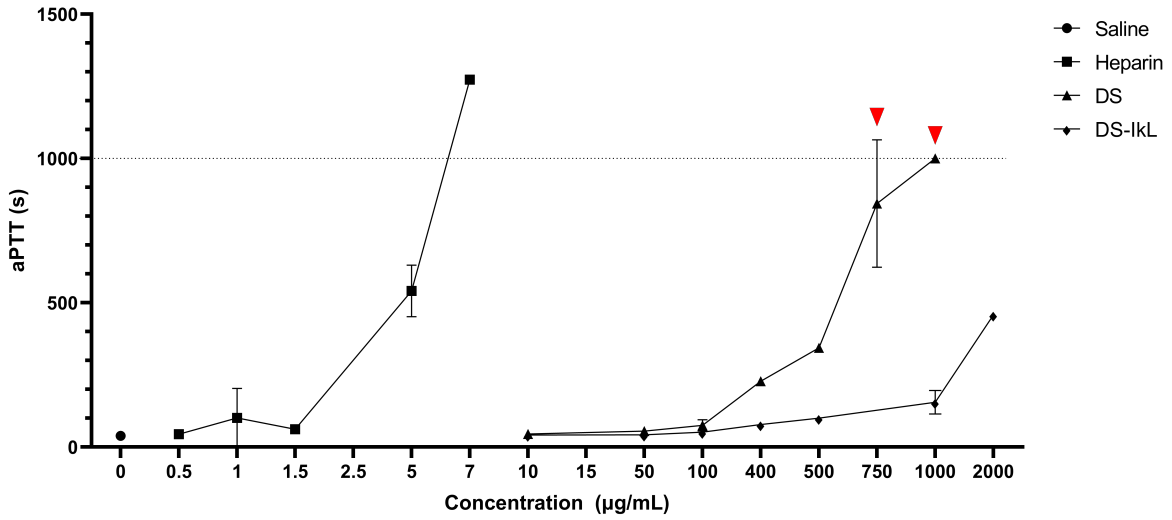

Figure 4-5 Activated partial thromboplastin time. Plasma was briefly pre-treated with increasing concentrations of heparin, DS, or DS-IkL before coagulation testing. DS-IkL exhibited minimal anti-coagulative properties compared to DS. Data represents mean ± SD of 2 technical replicates from 3 independent experiments. Red triangles denote samples that were stopped after 1000 s.

4.4.3 Endothelial activation by platelet-neutrophil complexes

Given the differences in PNC formation, we were interested in probing how this translated to cytokine secretion. Levels of proinflammatory cytokines IFN-γ, IL-1β, IL-6, IL-8, IL-10, TNF-α in supernatants of ADP or collagen-stimulated cell suspensions were analyzed (**Figure 4-6**). Interestingly, neutrophil-platelet suspensions did not secrete significant levels of proinflammatory cytokines when stimulated with collagen (**Figure 4-6A**) or ADP (**Figure 4-6B**). However, when HUVECs were added to the system, cytokine expression increased by up to 30-fold in ADP-stimulated groups and 40-fold in collagen-stimulated groups (**Figure 4-7**).

Despite seeing reductions in PNC formation in DS- and DS-IkL-treated suspensions, cytokine levels were similarly elevated in all PNC-HUVEC treatment groups (**Figure 4-8**). Collagen stimulation led to a slight increase in cytokine expression compared to ADP-stimulated groups, particularly for IL-10 and IL-8. In ADP-stimulated suspensions, treatment with DS led to slight reductions in all cytokines except

TNF-α (**Figure 4-8A**). DS-IkL treatment did not significantly reduce the relative expression of most analytes and was associated with slight increases in TNF-α expression.

In collagen-stimulated suspensions, IL-8 expression was significantly reduced in DS-treated groups; a trend toward reduced IFN-γ, IL-1β, IL-6, and IL-10 was also observed (**Figure 4-8B**). Treatment with DS-IkL did not cause a significant reduction in cytokine expression; however, a trend toward reduction was observed for IFN-γ, IL-10, IL-1β, and IL-8. Similar to ADP-stimulated mixtures, TNF-α expression was slightly elevated in DS-IkL-treated samples.

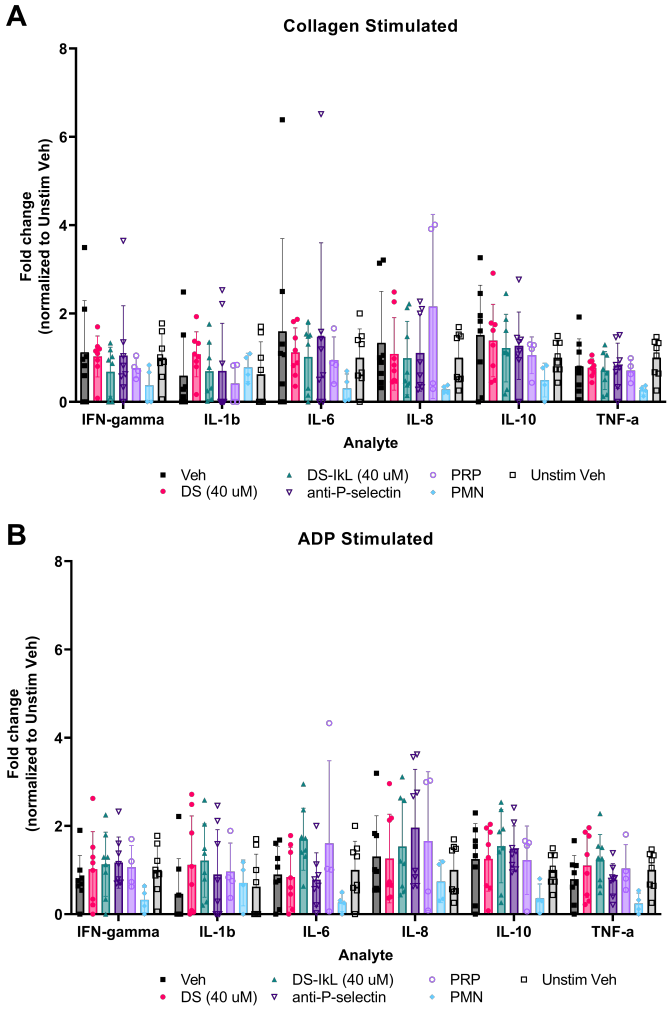

Figure 4-6 Cytokine secretion by PNC suspensions. Cytokine secretion by collagen-stimulated PNCs (**A**) and ADP-stimulated PNCs (**B**) was similarly low in all treatment groups. Data represents means ± SD for all technical replicates of 4 independent experiments.

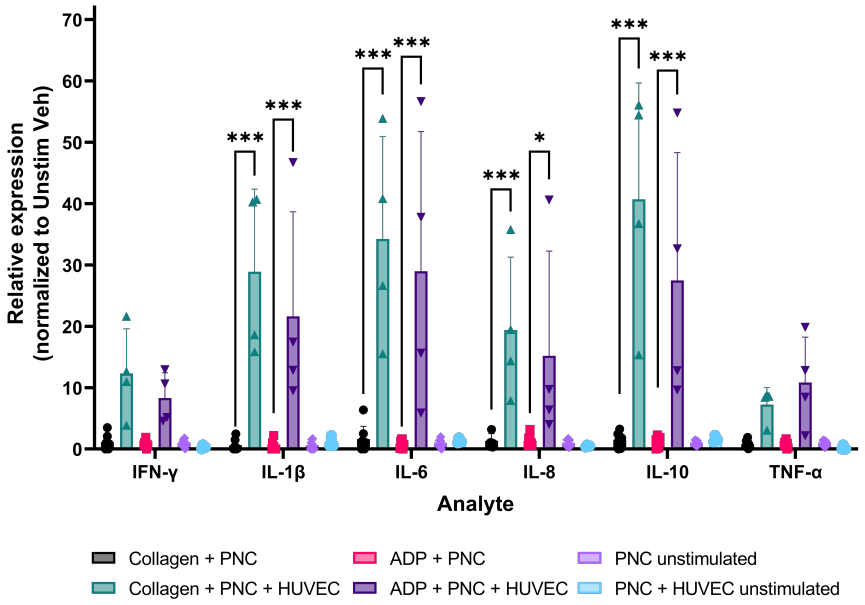

Figure 4-7 Proinflammatory cytokine secretion increased in the presence of HUVECs. Cytokine secretion was significantly increased in PNC-HUVEC suspensions compared to PNCs alone. Data represents means ± SD of 2 technical replicates from 4 independent experiments (n = 4). * $p < 0.05$, *** $p < 0.001$.

4.4.4 Neutrophil NET formation in the presence of activated PRP

To determine if PRP activation and PNC formation induces NET production, we next monitored the presence of extracellular DNA in PNC suspensions over a 4-hour incubation time using Sytox Green. Neutrophils incubated with 100 nM PMA served as a positive control. In these experiments, activation *via* fibrillar collagen or ADP did not elicit significant neutrophil NET production (**Figure 4-9**). PMA-stimulated PNC suspensions exhibited an approximately 50-fold increase in DNA content after 3 hours; however, ADP- and collagen-stimulated groups exhibited a less than 2-fold increase compared to initial values, regardless of treatments (**Figure 4-9D-E**). Incorporations of HUVECs into this system did not lead to increased NET production in ADP and collagen-stimulated groups (**Figure 4-10**). Again, only PMA stimulation elicited NET production in both neutrophil-only samples and PNC suspensions.

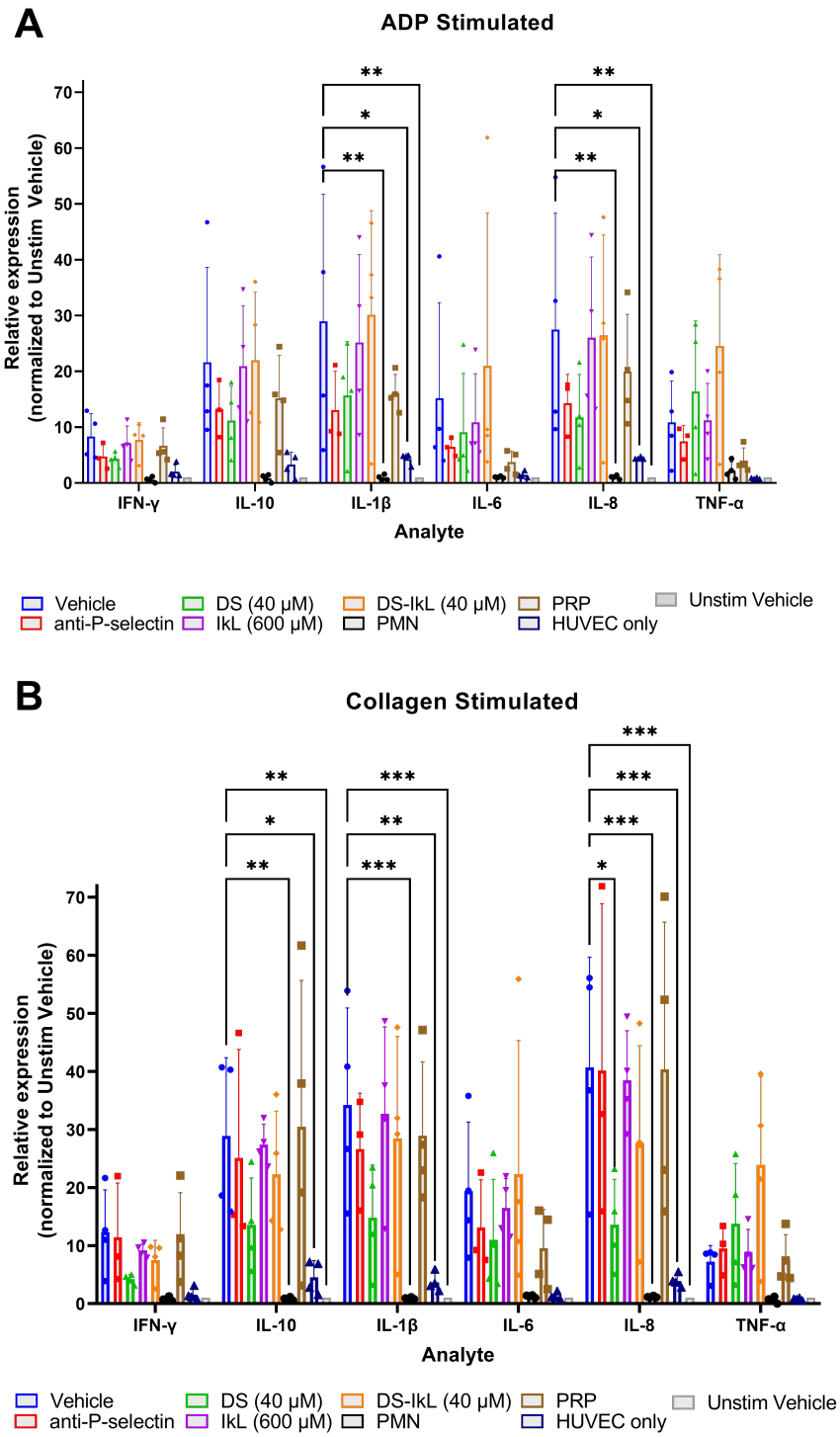

Figure 4-8 Cytokine expression from PNC-HUVEC mixtures. Similar trends in cytokine expression between ADP (**A**) and collagen (**B**) stimulated groups was observed. While DS-treated groups saw some reduction in cytokine expression, DS-IkL had minimal effects in both stimulants. Data represents means ± SD of 2 technical replicates from 2 independent experiments. * $p < 0.05$, ** $p < 0.01$, *** $p < 0.001$.

4.5 Discussion

Platelets, neutrophils, and platelet-neutrophil complexes have been implicated in many inflammatory disease mechanisms (15-20). Platelet-neutrophil complexing is facilitated primarily through platelet P-selectin–neutrophil PSGL-1 or platelet GPIbα-neutrophil Mac-1 (17), with P-selectin—PSGL-1 engagement playing a greater role in initial tethering and intracellular signaling cascades. In the current work, we investigated the effect of DS-IkL on several aspects of neutrophil and platelet activation, including platelet-neutrophil complexing, fibrin clot formation, NET release, and plasma coagulation.

4.5.1 DS-IkL reduced PNC formation without being anticoagulative

Due to the multivalent, multifunctional nature of DS-IkL, we hypothesized that the molecule would interfere with PNC formation, endothelial cell engagement, and subsequent proinflammatory cytokine secretion. To test this, PRP was activated with ADP or fibrillar collagen type-1 in the presence of DS, DS-IkL, IkL peptide, or an antibody to P-selectin (aCD62P) prior to coincubation with isolated human neutrophils. Interestingly, flow cytometry data from these studies suggest that the mechanisms behind PNC formation in response to these stimulants differs slightly. In ADP-treated groups, DS-IkL did not have a significant effect on PNC formation as assessed by $CD41^{+}CD45^{+}CD15^{+}$ (platelets positive for neutrophils) or $CD45^{+}CD15^{+}CD41^{+}$ (neutrophils positive for platelets) (**Figure 4-1**). However, donor-to-donor variability plots in **Figure 4-2** suggest that there is a slight shift toward aCD62P control values in DS and DS-IkL treated groups.

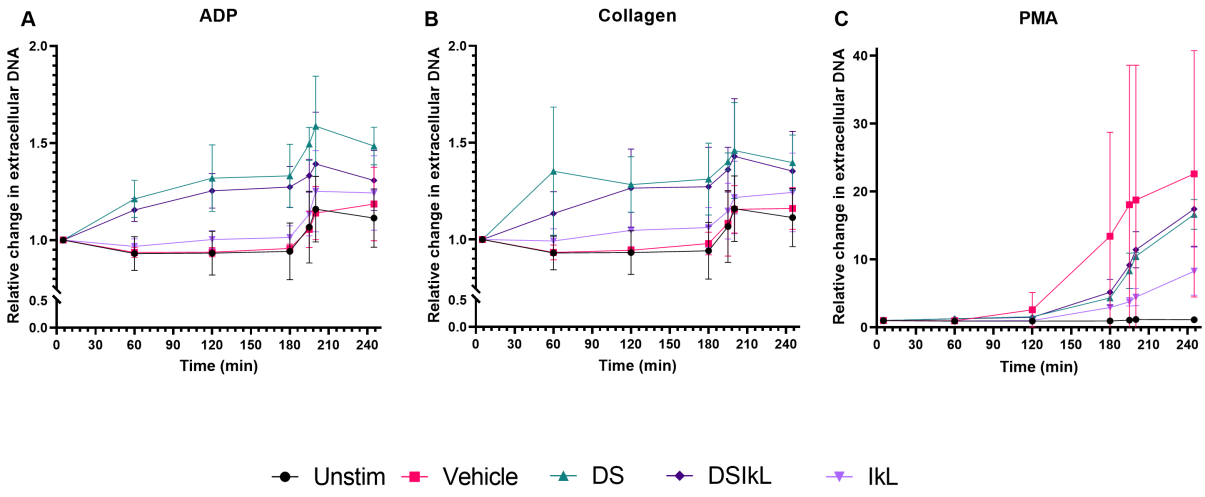

Figure 4-9 NET release in PNC-only suspensions. NET formation was detected using Sytox Green and monitored over a 3-hour incubation time. Though NET formation in ADP-stimulated (**A**) and collagen-stimulated (**B**) suspensions was increased compared to initial values, relative changes over the 3-hour incubation were minimal. Only PMA-stimulated groups showed significant increases in NET release (**C**). Data are normalized to the first reading of respective group in panels **A-C**. Fluorescence intensity after 3.5 hours was compared to each group's respective initial value (**D and E**) to determine changes in NET release over time. Data represented as mean ± SD from 2 replicates.

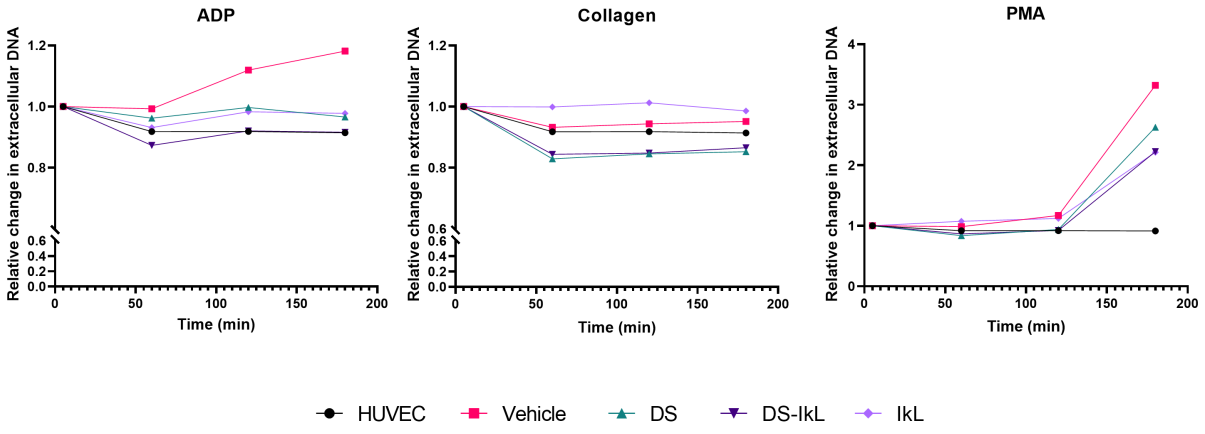

Figure 4-10 NET formation in PNC-HUVEC mixtures. NET formation was monitored in PNC-HUVEC mixtures over a 4-hour incubation period by staining for extracellular DNA using Sytox Green. Like PNC-only groups, NET formation was minimal in ADP (left) and collagen (center) stimulated groups compared to PMA-treated groups (right). Only PMA incubation resulted in an increase in NET formation. Data are normalized to the first reading of each respective group.

In collagen treated samples, we saw a significant decrease in $CD41^{+}CD45^{+}CD15^{+}$ populations after treatment with DS or DS-IkL (**Figure 4-3**), as well as a slight reduction in $CD45^{+}CD15^{+}CD41^{+}$ populations, albeit with a high degree of variability. Data from collagen-stimulated groups was further complicated by the formation of fibrin clots within vehicle and aCD62P sample tubes. Flow cytometer settings had to be adjusted to account for significant cell loss to clot removal (**Figure 4-4**, **Table 4-2**), wherein greater draw volumes were required to collect enough events from samples with clots for analysis. This loss was further quantified in **Figure 4-4 B-C**, which show the breakdown of cell counts as well as the relative contribution neutrophils and platelets made to the total cell. Clots were occasionally observed in ADP-stimulated samples, but to a lesser extent; therefore, cell counts were only quantified in collagen-stimulated suspensions. In groups in which clots were removed, neutrophils made up a higher proportion of the cell population in vehicle-treated groups compared to DS and DS-IkL; however, significant differences were only observed in vehicle-treated groups. These results suggest that, since platelet losses were proportionally higher in vehicle and aCD62P treated groups compared to DS and DS-IkL, platelets were likely the primary population within cell clots.

To further investigate the absence of clot formation in DS and DS-IkL treated groups, we tested the anticoagulant properties of these molecules using activated partial thromboplastin time (aPTT). DS is the primary anticoagulant and antithrombotic glycosaminoglycan along vessel walls (12, 21, 22). In designing DS-IkL, we aimed to create a targeted anti-inflammatory molecule that has minimal effect on blood coagulation, thereby addressing one of the major drawbacks of heparin as a treatment for inflammatory disease (23). aPTT testing showed that coagulation time remained relatively stable even at the highest concentrations tested (**Figure 4-5**), whereas coagulation time of DS-treated samples was significantly elevated compared to DS-IkL-treated samples at 100 μg/mL and 400 μg/mL concentrations.

These results were promising, given only approximately 15% of the available -COOH groups on the DS polymer are modified with the IkL peptide when synthesizing DS-IkL, suggesting anticoagulative properties may be another tunable parameter for this molecule. 400 μg/mL was chosen as the upper limit

for coagulation studies because it was the approximate serum concentration used in previous *in vivo* work (10, 24). PNC experiments were conducted at 40 μM in 200 μl suspensions, making the working concentration of molecule approximately 2.4 mg/mL. Therefore, additional studies are needed to determine both the efficacy of DS-IkL at lower concentrations *in vitro,* as well as the anticoagulative properties of DS-IkL at higher concentrations.

4.5.2 Endothelial cells bolster cytokine secretion regardless of treatment

To further investigate the downstream effects of PNC formation, we probed for proinflammatory cytokine levels in the supernatants of PNC suspensions. Neither ADP nor collagen stimulation of PNC suspensions elicited a robust inflammatory response, as measured by IFN-γ, IL-1β, IL-6, IL-8, IL-10, TNF-α (**Figure 4-6**). Once HUVECs were introduced into the system, cytokine expression increased significantly with both collagen and ADP stimulated PNC suspensions (**Figure 4-7** and **Figure 4-8**), particularly IL-1β, IL-6, IL-8, IL-10. However, very large variations were observed in experiments involving HUVECs, making it difficult to extrapolate the effect of DS or DS-IkL on cytokine expression. The large variation in cytokine expression was not surprising, given a different blood donor was used for each experiment and HUVECs were sourced from a donor pool. Donor populations were diversified intentionally to create a more clinically relevant *in vitro* system; however, this strategy will require a larger sample size to power the results. Currently, in our preliminary system it appears modifying the DS backbone with the IkL peptide may negatively affect the capacity of DS as an anti-inflammatory.

4.5.3 Activated PRP induces marginal NET formation

Finally, we monitored the kinetics of DNA release over a 4-hour period to examine if activated PRP and PNC-stimulated endothelial cells elicit NET release, and if treatment with DS or DS-IkL affects this. Others have shown that activated platelets and PRP can elicit NET release *in vitro* (25, 26). However, in our hands, activated PRP alone did not lead to significant NET release compared to unstimulated controls (**Figure 4-9 A-B**), and only marginal increases were observed when fluorescence values at the 3 hour

timepoint were compared to initial values (**Figure 4-9 A-C**). However, within these small increases, it appears groups treated with DS-IkL and IkL peptide exhibited slight reductions in NET formation, suggesting these treatments may be interfering with platelet-neutrophil complex formation and neutrophil activation. Similarly, in the presence of HUVECs, NET formation remained relatively constant over time (**Figure 4-10**); an appreciable increase in extracellular DNA content was only observed in PMA-treated groups. Further work is needed to understand the interplay between platelets, neutrophils, and endothelial cells in this system.

Of note, clotting was once again detected in NET experiments for all groups except those treated with DS and DS-IkL. It is possible that NETs were sequestered within the fibrin clot and DNA from secreted NETs therefore inaccessible to the Sytox dye. Further studies are necessary to determine if NETs are detectible when fibrin clotting mechanisms are inhibited or clots are digested prior to DNA staining. In addition, preliminary studies showed neutrophil activation (measured by CD11a/CD18 upregulation) was increased in PNC suspensions compared to neutrophil-only controls (data not shown). Activated neutrophils have been shown to express tissue factor (25), an initiator of blood coagulation. Quantifying levels of tissue factor in the supernatants of PNC suspensions may give insight into coagulation mechanisms at play in this system; however, these are outside of the scope of the current work.

4.6 Conclusions

Neutrophils, platelets, and endothelial cells play dynamic roles in acute and chronic inflammatory environments. Unregulated interactions among these three key players can drive the progression of disease. In this work, we further characterize DS-IkL as a therapeutic for inflammatory disease. We first characterize the anti-coagulant properties of DS and DS-IkL compared to a clinical gold-standard, heparin. DS-IkL was significantly less anticoagulative than DS at concentrations that showed efficacy in previous *in vivo* work. We next showed DS and DS-IkL interfere with platelet-neutrophil complex formation in the presence of

platelet stimuli, but this reduction did not translate to reduced cytokine expression in a PRP-PMN-HUVEC system. Finally, PNC formation in the presence of platelet activation factors ADP and fibrillar collagen did not prompt appreciable NET formation by resident neutrophils. Further work is necessary to characterize the effect DS-IkL has on neutrophil, platelet, and endothelial cell mediated inflammation.

4.7 References

1. Drenjancevic I, Jukic I, Stupin A, Cosic A, Stupin M, Selthofer-Relatic K. The Markers of Endothelial Activation. Endothelial Dysfunction - Old Concepts and New Challenges2018.
2. Park KH, Park WJ. Endothelial dysfunction: Clinical implications in cardiovascular disease and therapeutic approaches. Journal of Korean Medical Science. 2015;30:1213-25.
3. Delgadillo LF, Lomakina EB, Kuebel J, Waugh RE. Changes in endothelial glycocalyx layer protective ability after inflammatory stimulus. Am J Physiol Cell Physiol. 2021;320(2):C216-C24.
4. Ley K, Laudanna C, Cybulsky MI, Nourshargh S. Getting to the site of inflammation: the leukocyte adhesion cascade updated. Nature Reviews Immunology. 2007;7(9):678-.
5. Chen GY, Nuñez G. Sterile inflammation: sensing and reacting to damage. Nature Reviews Immunology. 2010;10(12):826-37.
6. Dehghani T, Panitch A. Endothelial cells, neutrophils and platelets: getting to the bottom of an inflammatory triangle. Open Biol. 2020;10(10):200161.
7. Zuchtriegel G, Uhl B, Puhr-Westerheide D, Pörnbacher M, Lauber K, Krombach F, et al. Platelets Guide Leukocytes to Their Sites of Extravasation. 2016;14(5):e1002459.
8. Ghasemzadeh M, Kaplan ZS, Alwis I, Schoenwaelder SM, Ashworth KJ, Westein E, et al. The CXCR1/2 ligand NAP-2 promotes directed intravascular leukocyte migration through platelet thrombi. Blood. 2013;121(22):4555-66.
9. Stakos DA, Kambas K, Konstantinidis T, Mitroulis I, Apostolidou E, Arelaki S, et al. Expression of functional tissue factor by neutrophil extracellular traps in culprit artery of acute myocardial infarction. Eur Heart J. 2015;36(22):1405-14.
10. Dehghani T, Thai PN, Sodhi H, Ren L, Sirish P, Nader CE, et al. Selectin-Targeting Glycosaminoglycan-Peptide Conjugate Limits Neutrophil Mediated Cardiac Reperfusion Injury. Cardiovasc Res. 2020.
11. Singbartl K, Forlow SB, Ley K. Platelet, but not endothelial, P-selectin is critical for neutrophil-mediated acute postischemic renal failure. FASEB J. 2001;15(13):2337-44.
12. Tovar AMF, de Mattos DA, Stelling MP, Sarcinelli-Luz BSL, Nazareth RA, Mourão PAS. Dermatan sulfate is the predominant antithrombotic glycosaminoglycan in vessel walls: Implications for a possible physiological function of heparin cofactor II. Biochimica et Biophysica Acta (BBA) - Molecular Basis of Disease. 2005;1740(1):45-53.
13. Kawashima H, Hirose M, Hirose J, Nagakubo D, Plaas AHK, Miyasaka M. Binding of a large chondroitin sulfate/dermatan sulfate proteoglycan, versican, to L-selectin, P-selectin, and CD44. Journal of Biological Chemistry. 2000;275(45):35448-56.
14. Mauler M, Seyfert J, Haenel D, Seeba H, Guenther J, Stallmann D, et al. Platelet-neutrophil complex formation-a detailed in vitro analysis of murine and human blood samples. J Leukoc Biol. 2016;99(5):781-9.
15. Morris G, Bortolasci CC, Puri BK, Olive L, Marx W, O'Neil A, et al. The pathophysiology of SARS-CoV-2: A suggested model and therapeutic approach. Life sciences. 2020;258:118166-.
16. Totani L, Piccoli A, Dell'Elba G, Concetta A, Di Santo A, Martelli N, et al. Phosphodiesterase type 4 blockade prevents platelet-mediated neutrophil recruitment at the site of vascular injury. Arterioscler Thromb Vasc Biol. 2014;34(8):1689-96.
17. Lisman T. Platelet-neutrophil interactions as drivers of inflammatory and thrombotic disease. Cell and tissue research. 2018;371(3):567-76.
18. Ramirez GA, Manfredi AA, Maugeri N. Misunderstandings Between Platelets and Neutrophils Build in Chronic Inflammation. Frontiers in immunology. 2019;10:2491-.
19. Zarbock A, Singbartl K, Ley K. Complete reversal of acid-induced acute lung injury by blocking of platelet-neutrophil aggregation. The Journal of Clinical Investigation. 2006;116(12):3211-9.
20. Kornerup KN, Salmon GP, Pitchford SC, Liu WL, Page CP. Circulating platelet-neutrophil complexes are important for subsequent neutrophil activation and migration. Journal of Applied Physiology. 2010;109(3):758-67.
21. Buchanan MR, Liao P, Smith LJ, Ofosu FA. Prevention of thrombus formation and growth by antithrombin III and heparin cofactor II-dependent thrombin inhibitors: importance of heparin cofactor II. Thromb Res. 1994;74(5):463-75.
22. Trowbridge JM, Gallo RL. Dermatan sulfate: new functions from an old glycosaminoglycan. Glycobiology. 2002;12(9):117R-25R.
23. Oduah EI, Linhardt RJ, Sharfstein ST. Heparin: Past, Present, and Future. Pharmaceuticals (Basel, Switzerland). 2016;9(3):38.

24. Wodicka JR, Morikis VA, Dehghani T, Simon SI, Panitch A. Selectin-Targeting Peptide-Glycosaminoglycan Conjugates Modulate Neutrophil-Endothelial Interactions. Cell Mol Bioeng. 2019;12(1):121-30.
25. Maugeri N, Campana L, Gavina M, Covino C, De Metrio M, Panciroli C, et al. Activated platelets present high mobility group box 1 to neutrophils, inducing autophagy and promoting the extrusion of neutrophil extracellular traps. Journal of Thrombosis and Haemostasis. 2014;12(12):2074-88.
26. Caudrillier A, Kessenbrock K, Gilliss BM, Nguyen JX, Marques MB, Monestier M, et al. Platelets induce neutrophil extracellular traps in transfusion-related acute lung injury. The Journal of clinical investigation. 2012;122(7):2661-71.

CHAPTER 5: CONCLUSIONS AND FUTURE OUTLOOKS

5.1 Conclusions

Endothelial dysfunction is a complex phenomenon that can simultaneously cause, result from, and perpetuate disease. Adverse changes in endothelial phenotype, including reduced nitric oxide production, actin stress fiber formation, glycocalyx shedding, and upregulation of immune cell adhesion molecules such as selectins (1-4), are shared among most organ systems, providing a platform for disease agnostic drug discovery. Through the chapters of this dissertation, we introduce a novel selectin-binding glycosaminoglycan-peptide conjugate (DS-IkL) as a therapeutic addressing multiple elements of endothelial dysfunction, including selectin upregulation, glycocalyx shedding, and aberrant immune cell adhesion and influx (1, 5).

Chapter 2 detailed the design and synthesis of a one-bead-one-compound combinatorial peptide library (6, 7) weighted toward a known E-selectin binding sequence. Use of this method enabled the simple incorporation of D- and unnatural amino acids into the library, rendering improved enzymatic stability to the lead E-selectin binding sequence, IkLLpOR. By having many copies of a unique peptide sequence on each resin bead and using an on-bead screening format, we were able to circumvent the low affinity E-selectin has for monovalent binding ligands by imitating a multivalent system (8). This worked in our favor, as it also recapitulated the multivalent molecule we planned to synthesize using the lead sequence. We went on to validate that our lead sequence could be conjugated to a dermatan sulfate backbone in a tunable manner. This was pivotal for later examination of the effect our molecule, DS-IkL, had on immune cell-endothelial interactions in future chapters.

In Chapters 3 and 4, we began to establish the therapeutic efficacy of our glycan therapeutic, DS-IkL. Chapter 3 detailed inhibitory effects DS-IkL had on neutrophil binding to recombinant human selectin and inflamed endothelial cells. Neutrophil interactions with upregulated selectins have been associated with

acute organ dysfunction (9-12), chronic inflammation (13-16), and fibrotic remodeling (10, 17) in several organ systems, including the heart (16, 18, 19), lungs (20-22), and kidneys (23). Circulating neutrophils are recruited to sites of sterile injury by damage activated molecular patterns (DAMPs) released by damaged or disrupted cells (24). Endothelial selectins facilitate the initial tethering and rolling of circulating neutrophils along the inflamed endothelial surface (25). Neutrophil engagement of endothelial selectin stimulates the transition of neutrophil lymphocyte function-associated antigen 1 (LFA-1) to an intermediate affinity conformation, facilitating firm adhesion and arrest through engagement with endothelial intercellular adhesion molecule 1 (ICAM-1) (26). In most organ systems, these steps are critical for downstream neutrophil adhesion and transmigration into the underlying tissue, where myofibroblast activation and fibrotic remodeling can occur (13, 27).

In a model of cardiac ischemia reperfusion injury (IRI) by acute myocardial infarction, DS-IkL protected against neutrophil and macrophage infiltration into infarcted tissues. Animals treated with DS-IkL after the reperfusion phase exhibited early reductions in infarct size, reduced fibrosis, and improved cardiac function compared to those treated with saline. Live *in vivo* imaging confirmed that DS-IkL targeted to inflamed regions after surgery, suggesting the E-selectin binding peptide on the dermatan sulfate (DS) backbone aids in DS homing to inflamed vasculature. Additional studies are needed to confirm this localization would not be achieved and/or sustained with unmodified DS, and that the individual molecule components (DS and IkL peptide) are not sufficiently cardioprotective on their own. However, given DS interacts with the endothelium transiently (28) and monovalent binding ligands typically bind selectins with low affinity (8, 29), we do not anticipate the individual components would have equivalent efficacy.

In Chapter 4, we began to address the benefits of modifying the DS backbone. Though DS itself has been shown to have inherent anti-platelet and anti-neutrophil properties, the heterogeneity of natural and even commercially available DS make the extent of these properties unpredictable (28). In addition, DS is known to interact with heparin cofactor II and thereby acts as an anticoagulant (30), increasing the likelihood of systemic side effects when used as a therapeutic. In Chapter 4 we showed that, though DS-

IkL may retain some anticoagulative properties, they are minimal compared to DS and heparin. Anticoagulants have therapeutic value in some indications, but in many cases anticoagulation, or "blood thinning," is an undesirable systemic side effect of drugs such as heparin (31). Finally, Chapter 4 discussed the ability of DS-IkL to interfere with platelet-neutrophil complex (PNC) formation and endothelial cell activation in the presence of activated PNCs, perhaps by interfering with interactions between platelet P-selectin and neutrophil P-selectin glycoprotein ligand 1 (PSGL-1). PNCs have been implicated in many diseases, including sepsis, thrombotic disease, and the recent SARS-COV-2 epidemic (32-37).

The work presented here suggests a molecule such as DS-IkL, which can regionally limit endothelial-neutrophil interactions and platelet-neutrophil interactions without greatly affecting blood coagulation, could have therapeutic value in numerous disease indications. Many otherwise seemingly disparate diseases, including cancer, deep vein thrombosis, and chronic obstructive pulmonary disease, share inflammatory mechanisms that could be addressed by our glycan therapeutic. By focusing on inflammatory disease from the vascular side, we hope that this work can broadly impact disease progression.

5.2 Future outlooks

The current work serves as a foundation for many interesting studies into disease mechanisms mediated by leukocyte, platelet, and endothelial cell interactions. In part 2 of the Appendix, we began to establish a model of renal ischemia reperfusion injury with warm ischemia time, a phenomenon that occurs during organ transplant (38-40). As the number of viable donor kidneys remains in a severe shortage, there is an urgent need to develop strategies and/or therapies that help preserve high-risk kidneys, facilitate graft success, and improve patient survival. Kidney IRI, delayed graft function, and acute kidney injury have all been shown to be driven in part by neutrophil influx and activation (23, 41) and platelet-driven

inflammation (41). A molecule such as DS-IkL could aid in regulating inflammatory processes and immune cell interactions, thereby improving transplant outcomes.

Further work on our preliminary model is necessary to investigate the efficacy of DS-IkL in renal indications. This will include assessing the optimal warm ischemia time to elicit endothelial dysfunction and neutrophil influx, reperfusion time, and dosing parameters (e.g., timing and concentration) for maximal therapeutic effect. Thus far, our results indicate that immediate dosing with DS-IkL after 21 minutes of warm ischemia time with contralateral nephrectomy does not affect kidney damage as assessed by serum creatinine, lactate, glucose, and blood urea nitrogen at post-op day 3. However, pulmonary and peripheral edema appear to be less severe in DS-IkL treated animals at this time point. Additional studies into the renal-pulmonary axis (42, 43) may shed light onto these results.

Future investigations into the effect of DS-IkL on the inflammatory triangle formed by endothelial cells, neutrophils, and platelets may be worth consideration. This triad is implicated in many diseases, with the relative contributions of each cell type to inflammation shifting in response to a given environment (13). The initial work described in Chapter 4 suggests DS-IkL may have protective characteristics in an inflammatory environment driven by these three cell types, and it would be worth investigating the mechanisms behind this interaction. It is possible that DS-IkL's mechanism of action is similarly fluid, shifting from DS-mediated, to peptide-mediated, depending on the physiological environment.

DS-IkL was designed as a disease-agnostic molecule, offering a treatment modality that can be applied to numerous inflammatory disease indications. The molecule functions primarily by 1) occupying upregulated selectins on the endothelial (and potentially platelet) surface, and 2) creating a steric, band-aid-like barrier between inflamed endothelial cells and circulating blood components (e.g., immune cells). Given the dynamic role both selectins and the glycocalyx play in vascular homeostasis, it is possible DS-IkL has additional effects not explored in this dissertation, including adverse effects. These may include endothelial stimulation by selectin engagement, immune cell activation by the increase in circulating

glycosaminoglycans, and regional sequestering of chemokines, etc. once bound to the endothelium. These and other safety factors should be considered when designing future experiments.

5.3 References

1. Harding IC, Mitra R, Mensah SA, Nersesyan A, Bal NN, Ebong EE. Endothelial barrier reinforcement relies on flow-regulated glycocalyx, a potential therapeutic target. Biorheology. 2019;56(2-3):131-49.
2. Park KH, Park WJ. Endothelial dysfunction: Clinical implications in cardiovascular disease and therapeutic approaches. Journal of Korean Medical Science. 2015;30:1213-25.
3. Tousoulis D, Kampoli A-M, Tentolouris C, Papageorgiou N, Stefanadis C. The role of nitric oxide on endothelial function. Current vascular pharmacology. 2012;10(1):4-18.
4. Yang Q, He GW, Underwood MJ, Yu CM. Cellular and molecular mechanisms of endothelial ischemia/reperfusion injury: perspectives and implications for postischemic myocardial protection. Am J Transl Res. 2016;8(2):765-77.
5. Bar A, Targosz-Korecka M, Suraj J, Proniewski B, Jasztal A, Marczyk B, et al. Degradation of Glycocalyx and Multiple Manifestations of Endothelial Dysfunction Coincide in the Early Phase of Endothelial Dysfunction Before Atherosclerotic Plaque Development in Apolipoprotein E/Low-Density Lipoprotein Receptor-Deficient Mice. J Am Heart Assoc. 2019;8(6):e011171.
6. Lam KS, Lake D, Salmon SE, Smith J, Chen ML, Wade S, et al. A One-Bead One-Peptide Combinatorial Library Method for B-Cell Epitope Mapping. Methods. 1996;9(3):482-93.
7. Lam KS, Salmon SE, Hersh EM, Hruby VJ, Kazmierski WM, Knapp RJ. A new type of synthetic peptide library for identifying ligand-binding activity. Nature. 1991;354(6348):82-4.
8. Kaila N, Thomas Iv BE. Design and synthesis of sialyl Lewisx mimics as E- and P-selectin inhibitors. Medicinal Research Reviews. 2002;22(6):566-601.
9. Narasaraju T, Tang B, Herrmann M, Muller S, Chow VTK, Radic M. Neutrophilia and NETopathy as Key Pathologic Drivers of Progressive Lung Impairment in Patients with COVID-19. OSF Preprints. 2020.
10. Calvente CJ, Tameda M, Johnson CD, del Pilar H, Lin YC, Adronikou N, et al. Neutrophils contribute to spontaneous resolution of liver inflammation and fibrosis via microRNA-223. The Journal of Clinical Investigation. 2019;129(10):4091-109.
11. Sokolowska M, Quesniaux VFJ, Akdis CA, Chung KF, Ryffel B, Togbe D. Acute Respiratory Barrier Disruption by Ozone Exposure in Mice. Frontiers in Immunology. 2019;10(2169).
12. Vinten-Johansen J. Involvement of neutrophils in the pathogenesis of lethal myocardial reperfusion injury. 2004. p. 481-97.
13. Dehghani T, Panitch A. Endothelial cells, neutrophils and platelets: getting to the bottom of an inflammatory triangle. Open Biol. 2020;10(10):200161.
14. Barnes PJ. Inflammatory mechanisms in patients with chronic obstructive pulmonary disease. Journal of Allergy and Clinical Immunology. 2016;138(1):16-27.
15. Tanguay J-F, Hammoud T, Geoffroy P, Merhi Y. Chronic Platelet and Neutrophil Adhesion: A Causal Role for Neointimal Hyperplasia in In-Stent Restenosis. Journal of Endovascular Therapy. 2003;10(5):968-77.
16. Jones SP, Trocha SD, Strange MB, Granger DN, Kevil CG, Bullard DC, et al. Leukocyte and endothelial cell adhesion molecules in a chronic murine model of myocardial reperfusion injury. American Journal of Physiology - Heart and Circulatory Physiology. 2000;279(5 48-5).
17. Maugeri N, Rovere-Querini P, Baldini M, Baldissera E, Sabbadini MG, Bianchi ME, et al. Oxidative Stress Elicits Platelet/Leukocyte Inflammatory Interactions via HMGB1: A Candidate for Microvessel Injury in Sytemic Sclerosis. Antioxidants & Redox Signaling. 2013;20(7):1060-74.
18. Dehghani T, Thai PN, Sodhi H, Ren L, Sirish P, Nader CE, et al. Selectin-Targeting Glycosaminoglycan-Peptide Conjugate Limits Neutrophil Mediated Cardiac Reperfusion Injury. Cardiovasc Res. 2020.
19. Briaud SA, Ding ZM, Michael LH, Entman ML, Daniel S, Ballantyne CM. Leukocyte trafficking and myocardial reperfusion injury in ICAM-1/p-selectin-knockout mice. American Journal of Physiology - Heart and Circulatory Physiology. 2001;280(1 49-1).
20. Li H, Pan P, Su X, Liu S, Zhang L, Wu D, et al. Neutrophil Extracellular Traps Are Pathogenic in Ventilator-Induced Lung Injury and Partially Dependent on TLR4. BioMed research international. 2017;2017:8272504-.
21. Barnes BJ, Adrover JM, Baxter-Stoltzfus A, Borczuk A, Cools-Lartigue J, Crawford JM, et al. Targeting potential drivers of COVID-19: Neutrophil extracellular traps. J Exp Med. 2020;217(6):e20200652.
22. Zarbock A, Singbartl K, Ley K. Complete reversal of acid-induced acute lung injury by blocking of platelet-neutrophil aggregation. The Journal of Clinical Investigation. 2006;116(12):3211-9.

23. Turunen AJ, Lindgren L, Salmela KT, Kyllönen LE, Mäkisalo H, Siitonen SM, et al. Association of graft neutrophil sequestration with delayed graft function in clinical renal transplantation. Transplantation. 2004;77(12):1821-6.
24. Chen GY, Nuñez G. Sterile inflammation: sensing and reacting to damage. Nature Reviews Immunology. 2010;10(12):826-37.
25. Ley K, Laudanna C, Cybulsky MI, Nourshargh S. Getting to the site of inflammation: the leukocyte adhesion cascade updated. Nature Reviews Immunology. 2007;7(9):678-.
26. Morikis VA, Chase S, Wun T, Chaikof EL, Magnani JL, Simon SI. Selectin catch-bonds mechanotransduce integrin activation and neutrophil arrest on inflamed endothelium under shear flow. Blood. 2017;130(19):2101-10.
27. Wynn TA. Cellular and molecular mechanisms of fibrosis. The Journal of pathology. 2008;214(2):199-210.
28. Trowbridge JM, Gallo RL. Dermatan sulfate: new functions from an old glycosaminoglycan. Glycobiology. 2002;12(9):117R-25R.
29. Fukuda MN, Ohyama C, Lowitz K, Matsuo O, Pasqualini R, Ruoslahti E, et al. A Peptide Mimic of E-Selectin Ligand Inhibits Sialyl Lewis X-dependent Lung Colonization of Tumor Cells. Cancer Research. 2000;60(2):450 LP-6.
30. Tykesson E, Maccarana M, Thorsson H, Liu J, Malmström A, Ellervik U, et al. Recombinant dermatan sulfate is a potent activator of heparin cofactor II-dependent inhibition of thrombin. Glycobiology. 2019;29(6):446-51.
31. Alquwaizani M, Buckley L, Adams C, Fanikos J. Anticoagulants: A Review of the Pharmacology, Dosing, and Complications. Curr Emerg Hosp Med Rep. 2013;1(2):83-97.
32. Asaduzzaman M, Lavasani S, Rahman M, Zhang S, Braun OÖ, Jeppsson B, et al. Platelets support pulmonary recruitment of neutrophils in abdominal sepsis*. Critical Care Medicine. 2009;37(4):1389-96.
33. Darbousset R, Thomas GM, Mezouar S, Frère C, Bonier R, Mackman N, et al. Tissue factor–positive neutrophils bind to injured endothelial wall and initiate thrombus formation. Blood. 2012;120(10):2133-43.
34. Etulain J, Martinod K, Wong SL, Cifuni SM, Schattner M, Wagner DD. P-selectin promotes neutrophil extracellular trap formation in mice. Blood. 2015;126(2):242-6.
35. Gros A, Ollivier V, Ho-Tin-Noe B. Platelets in inflammation: regulation of leukocyte activities and vascular repair. Front Immunol. 2014;5(678):678.
36. Lisman T. Platelet-neutrophil interactions as drivers of inflammatory and thrombotic disease. Cell and tissue research. 2018;371(3):567-76.
37. Le Joncour A, Biard L, Vautier M, Bugaut H, Mekinian A, Maalouf G, et al. Neutrophil-Platelet and Monocyte-Platelet Aggregates in COVID-19 Patients. Thrombosis and haemostasis. 2020;120(12):1733-5.
38. Au - Hesketh EE, Au - Czopek A, Au - Clay M, Au - Borthwick G, Au - Ferenbach D, Au - Kluth D, et al. Renal Ischaemia Reperfusion Injury: A Mouse Model of Injury and Regeneration. JoVE. 2014(88):e51816.
39. Salvadori M, Rosso G, Bertoni E. Update on ischemia-reperfusion injury in kidney transplantation: Pathogenesis and treatment. World J Transplant. 2015;5(2):52-67.
40. Tennankore KK, Kim SJ, Alwayn IP, Kiberd BA. Prolonged warm ischemia time is associated with graft failure and mortality after kidney transplantation. Kidney Int. 2016;89(3):648-58.
41. Jansen MPB, Florquin S, Roelofs JJTH. The role of platelets in acute kidney injury. Nature Reviews Nephrology. 2018;14(7):457-71.
42. Faubel S. Pulmonary complications after acute kidney injury. Adv Chronic Kidney Dis. 2008;15(3):284-96.
43. Faubel S, Edelstein CL. Mechanisms and mediators of lung injury after acute kidney injury. Nature Reviews Nephrology. 2016;12(1):48-60

– APPENDICES –

A: EFFECT OF DS-IKL ON PULMONARY INFLAMMATION

A.1 Introduction

With nearly 6 million deaths per year worldwide and more than 480,000 deaths per year in the United States, smoking is the leading cause of preventable death (1). Tobacco smoke is a key factor in the onset of Chronic Obstructive Pulmonary Disease (COPD), the third leading cause of death in the United States (2). COPD patients are highly susceptible to acute exacerbations, short-lived event characterized by worsening of respiratory symptom. Acute exacerbations are the primary cause of COPD patient hospitalization, and overall account for approximately 50% of the cost of the disease. Exacerbations tend to come in clusters over approximately two-month periods and their onset is often predictable by patients, lending a method for predicting timely dosing of medicines to reduce the occurrence and severity of exacerbations, and by proxy the downstream complications and tissue destruction (3).

There is currently no effective treatment for COPD; instead, common approaches to treating COPD include smoking cessation and oxygen therapy (4). However, though cigarette smoking is the primary cause of COPD, smoking cessation is unable to relieve symptoms (5) or ease pulmonary inflammation (6). Persistency of pulmonary inflammation seen in COPD patients after quitting smoking indicates permanent changes to pulmonary immune responses; however, detailed pathways and mechanisms remain elusive. Treatment strategies employing deletion of a single cytokine, such as TNF-α, have proved ineffective given inflammatory cytokine levels in lung tissue and peripheral blood are persistently elevated in COPD patients (7)

Exacerbations are associated with detrimental changes in lung function, including endothelial dysfunction (8). Endothelial dysfunction is characterized by the loss of the glycocalyx, a thin glycosaminoglycan-rich layer on the endothelial cell (EC) surface, which provides a protective interface that regulates immune cell adhesion. Data indicate increased infiltration of neutrophils into the lung tissue

as a result of endothelial insult and inflammation (9). In the lung, neutrophil emigration occurs in both the capillaries surrounding alveoli as well as the post-capillary venules of the airways, creating multiple regions of therapeutic interest.

We have recently discovered a glycosaminoglycan derived, selectin targeting anti-adhesive coating (termed DS-IkL) consisting of a dermatan sulfate backbone and multiple selectin-binding peptides. We've shown that DS-IkL profoundly diminished the ability of neutrophils to attach to interact with endothelium (10, 11). With respect to its ability to control cell adhesions at the vascular interface, DS-IkL is a promising therapeutic for pulmonary inflammation and inflammation-induced acute exacerbations seen in COPD. In the following work, we use cigarette smoke exposed media *in vitro* (12) and inhaled ozone *in vivo* (13) as models of pulmonary inflammation in order to test the efficacy of DS-IkL as a pulmonary therapeutic.

A.2 Methods

A.2.1 Cigarette smoke exposed media

Endothelial growth medium MV (ECGM MV, PromoCell) was exposed to cigarette smoke at the UC Davis Center for Health and the Environment as described previously ((12, 14)). Medium was exposed to 106 +/- 13 mg/m^3 total suspended particulate matter (TSP) for 4 hours. Average carbon monoxide in the chamber was 250 ppm. Cigarette smoke exposed (CSE) medium was filtered through a 0.45 μM syringe filter, aliquoted, and frozen until use.

A.2.2 Cell culture

Human pulmonary microvascular endothelial cells (HPMEC, PromoCell) were expanded to passage 3-6 in tissue culture treated T75 flasks. ECGM MV was changed every other day until cells were 70-85% confluent. TrypLE was used for all dissociation steps (passaging and cell seeding). Cells were rinsed 1x with 5 mL prewarmed DPBS the incubated with 3 mL TrypLE for 3-5 minutes at room

temperature (RT). After gentle agitation, 4 mL ECGM MV was added. The suspension was collected and centrifuged for 5 minutes at 200 x g. Supernatant was aspirated and the cell pellet resuspended in ECGM MV, counted, and diluted to indicated concentrations.

A.2.3 E- and P-selectin expression and molecule binding after CSE exposure

HPMECs were seeded at 10,000 cells/cm^2 into a tissue culture treated T25 flask and grown to 90% confluence. Flasks were stimulated with 0%, 3%, or 5% CSE medium or 10 ng/mL TNF-α in ECGM MV for 6 hours in a cell culture incubator (37°C, 5% CO_2). After 6 h, cells were dissociated from the flask as described and resuspended at 1.95 x 10^6 cells/mL in buffer [Hank's buffered salt solution with calcium and magnesium ($HBSS^{+/+}$) supplemented with 0.3% human serum albumin (HSA)]. Suspensions were aliquoted into individual 1.5 mL microcentrifuge tubes (100 µL into 2-3 tubes for each treatment) and stained with 3 µL PE anti-human CD62E antibody (BioLegend) or PE anti-human CD62P antibody (BioLegend) for 30 minutes on ice in the dark. Cells were washed 3x with buffer, resuspended in 1 mL, and run on an Attune NxT flow cytometer (ThermoFisher). In some experiments, cells were fixed for 10 minutes in 3% PFA in PBS, centrifuged, and resuspended in DPBS before flow cytometry.

To test molecule binding, tissue culture treated 96-well plates (Thermo) were coated with 50 µg/ml rat tail collagen type-1 solution in DPBS. Plates were incubated at 37°C for 1 hour then washed 3x with Dulbecco's phosphate buffered saline (DPBS). HPMECs were seeded at 40,000 cells/cm^2 and used after reaching at least 90% confluence. Confluent cells were treated with 30 µM CF633-DS or CF633-DS-IkL (11) in 200 µL stimulation media (10% CSE or 10 ng/ml TNF-α). After 6 hours, wells were rinsed 3x with DPBS and fluorescence measured using a SpectraMax M5 Microplate Reader (ex/em 630/650, Molecular Devices).

A.2.4 Cell viability after CSE exposure

Tissue culture treated 96-well plates (Thermo) were coated with 50 μg/ml rat tail collagen type-1 solution in DPBS. HPMECs seeded at 40,000 cells/cm^2 and grown overnight before use. CSE was serially diluted in fresh medium to 50%, 30%, 20%, 15%, 10%, 5%, and 2.5%. CSE medium that was not diluted was considered as 100%. HPMECs were rinsed 1x with pre-warmed DPBS, then 150 μL of pre-warmed CSE medium (2.5-100%) was added. For longer studies, medium was replaced every other day.

Cell proliferation was quantified at day 0, 1, 3, and 5 using a CyQUANT NF Cell Proliferation Assay (ThermoFisher). HPMECs were rinsed 2x with pre-warmed DPBS before adding 100 μL CyQuant solution (5 μL solution A, 1 μL solution B into 2.5 mL HBSS). Plates were incubated for 60 minutes then read on a SpectraMax M5 Microplate Reader (Molecular Devices) at ex/em 485/530 nm. Additional readings were taken at the 2 h and 3 h time points.

Cell metabolism was quantified using an MTS assay kit. Cells were rinsed 1x with pre-warmed sterile DPBS then incubated with MTS (100 μL HBSS$^{+/+}$ + 0.3% HSA, 20 μL MTS solution) for up to 4 hours. Absorbance readings (490 nm) were taken at the 2 h, 3 h, and 4 h time points.

For both assays, readings were normalized to day 0, 0% CSE baseline readings. Four technical replicates were averaged for each group. The experiment was conducted 2 independent times for an n=2.

A.2.5 Ozone exposure

Male BALB/c mice were obtained from the Jackson Laboratories (Bar Harbor, ME). All experiments were performed on 10-12-week-old mice. All animal handling and laboratory procedures were performed in accordance with the approved protocols of the Institutional Animal Care and Use Committee of the University of California, Davis, which conforms to the Guide for the Care and Use of Laboratory Animals published by the US National Institutes of Health (8th Edition, 2011). Mice were injected intravenously via the tail vein with 100 μL of 30 μM DS-IkL or saline before and after exposures. Mice

were placed in mire mesh cages without food or water in an exposure chamber before being exposed to 3 ppm ozone or ambient air for 2 h, then placed back into normal cages for overnight housing. Animals were euthanized and necropsies performed 12 hours after O_3 exposure.

A.2.6 Bronchoalveolar lavage fluid collection

Tracheas were cannulated and lungs were gently lavaged using a total of 1 mL sterile DPBS (two 0.5 mL lavages). The total amount of liquid retained after bronchoalveolar lavage (BAL) was greater than 0.5 mL. Total cell counts obtained in BAL were performed using a Countess Automated Cell Counter, and differential cell counts were determined using cytospin preparations (Cytospin 3; Thermo Scientific) stained with Kwik-Diff (Thermo Scientific). Differential cell counting was performed at 40X magnification under a light microscope. Immune and inflammatory cell morphology appeared normal in the BAL samples and macrophages displayed inflammatory alterations in response to ozone as expected.

A.3 Results

A.3.1 Cell viability after CSE exposure

To test the toxicity of CSE media to HPMECs, cells were incubated with increasing concentrations of CSE over a 5-day period. Cell viability was assessed by metabolism (MTS) and proliferation (CyQuant NF) (**Figure A-1**). Cells tolerated CSE up to 10%, with concentrations at or above 20% leading to reductions in cell metabolism and proliferation over the 5-day incubation period. Within the tolerable range, cell viability as assessed by proliferation decreased with increasing CSE concentration (**Figure A-1B**) as expected. Interestingly, cell metabolism increased after 1-5% CSE treatment even out to day 5, despite reductions in proliferation.

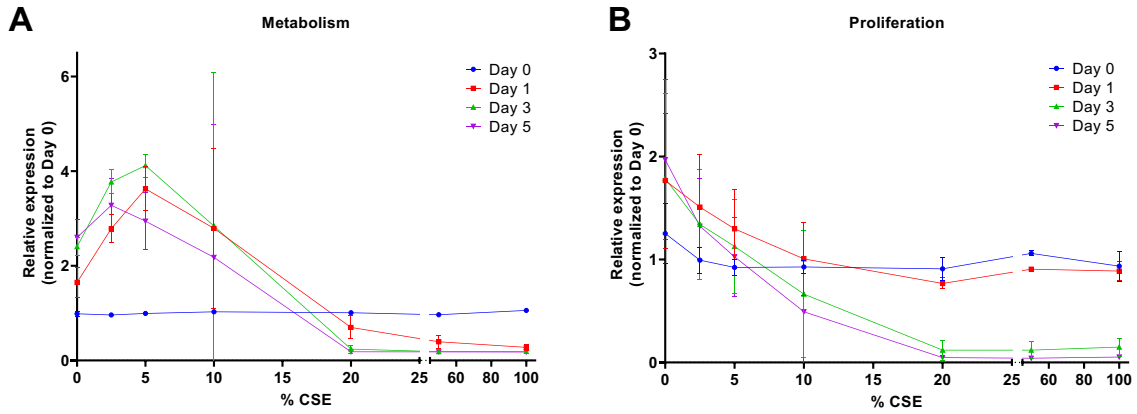

Figure A-1 CSE viability measurements over 5 days of exposure. HPMECs were treated with increasing concentrations of CSE media for up to 5 days. Metabolism (A) and proliferation (B) were used as measures of cell viability.

A.3.2 E- and P-selectin expression and molecule binding

Cigarette smoke is a known irritant of lung epithelial cells, translating into inflammation within the pulmonary vasculature (15-17). To investigate the effect of acute cigarette smoke exposure on endothelial selectin expression, HPMECs were stimulated with increasing concentrations of CSE or 10 ng/ml TNF-α for 4-6 hours. TNF-α is known to stimulate endothelial cells and promote endothelial P-selectin mobilization (18) and E-selectin synthesis (19), and was therefore used as a positive control. E- and P-selectin expression were probed using flow cytometry (**Figure A-2**). P-selectin expression was maximized after 4 hours of 5% CSE stimulation (Figure 2A); however, we observed only slight increases in both E- and P-selectin expression regardless of stimulant.

We were next interesting in whether DS-IkL would bind to CSE stimulated HPMECs. Cells were incubated in 10% CSE or 10 ng/ml TNF-alpha for 6 hours, then treated with CF633-tagged DS or DS-IkL. DS-IkL bound to stimulated HPMECs to a greater extent than DS regardless of stimulant (**Figure A-2B**).

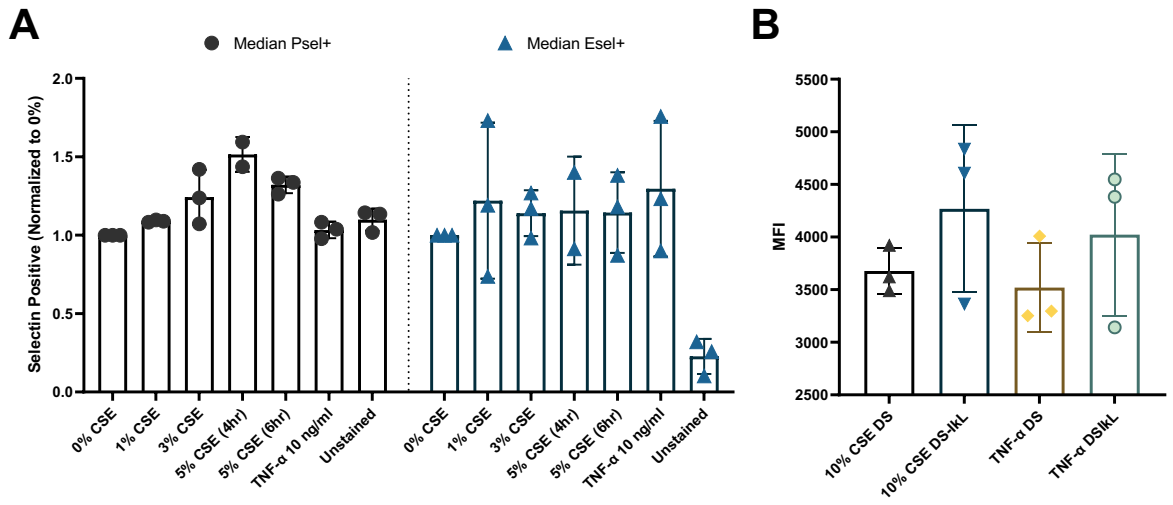

Figure A-2 Selectin expression and molecule binding. HPMECs were stimulated with CSE or TNF-α for up to 6 hours. P- and E-selectin expression were quantified using flow cytometry (**A**). To assess molecule binding, stimulated cells were incubated with fluorescently tagged DS or DS-IkL. Greater levels of binding were seen with DS-IkL compared to DS in both CSE and TNF-α stimulated HPMECs (**B**).

A.3.3 Effect of DS-IkL on immune cell influx after acute ozone exposure

After confirming that DS-IkL bound inflamed pulmonary endothelial cells, we next tested the *in vivo* efficacy of our molecule in a murine model of acute pulmonary inflammation by acute ozone exposure, an established model of pulmonary inflammation (13, 20) that has been shown to promote pulmonary vascular endothelial dysfunction (21, 22) and cause a sharp immune cell influx. Animals were treated with saline or 30 μM DS-IkL before and after ozone exposure to maximize potential effects of the molecule. Total and differential cell counts in BAL were similar in saline and DS-IkL treated mice 12 hours after exposure (**Figure A-3**), suggesting DS-IkL does not affect immune cell infiltration caused by ozone-induced pulmonary injury.

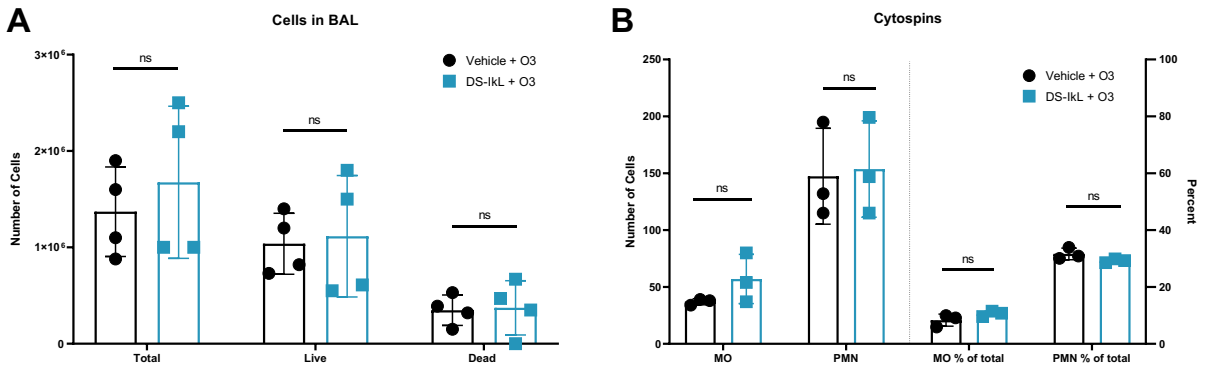

Figure A-3 *In vivo* effect of DS-IkL on ozone-induced immune cell influx. Mice were treated with DS-IkL or saline before and after ozone exposure. Total cells in BAL (**A**) and immune cells in cytospins (**B**) did not differ between groups 12 hours after exposure. MO: Macrophages; PMN: Neutrophils. ns: not significant.

A.4 Discussion

COPD and other cigarette smoking related pulmonary diseases present a huge health care and economic burden worldwide. Disease exacerbations are accompanied by heightened inflammatory events, including vascular barrier and endothelial dysfunction, epithelial damage, and immune cell influx via exposed immune cell adhesion molecules (23-26). Activated and adherent neutrophils release proteases and other products that degrade the endothelial glycocalyx, exposing additional immune cell adhesion molecules and amplifying the inflammatory cascade. Upregulated adhesion molecules (e.g., selectins) are therefore a promising target for anti-inflammatory therapeutics.

DS-IkL is a glycan therapeutic that targets dermatan sulfate, a glycocalyx component, to upregulated selectins on inflamed endothelium. We have shown DS-IkL reduces neutrophil interactions with inflamed endothelial cells *in vitro*, and is cardioprotective against ischemia reperfusion injury after acute myocardial infarction *in vivo* (11). In the present work, we aimed to test the efficacy of our glycosaminoglycan-peptide therapeutic DS-IkL against pulmonary inflammation. *In vitro*, we used cigarette smoke exposed media as a model of soluble cigarette smoke-induced vasculature inflammation.

In vivo, mice were challenged with inhaled ozone, a known pulmonary epithelial and endothelial irritant (13, 21, 22, 27).

We first wanted to determine the toxicity of cigarette smoke exposed media on pulmonary endothelial cells. HPMECs were challenged with 0-100% CSE media for up to 5 days. We were surprised to see that cells exhibited an increase in metabolism when treated with up to 5% CSE, perhaps due to metabolic stimulation by nicotine in the media, while total relative cell count simultaneously decreased (**Figure A-1**), (28). Unsurprisingly, cell viability as measured by CyQuant NF reduced with increasing concentrations of CSE. From these studies, we chose to move forward with 5% CSE as a non-lethal concentration for selectin expression studies.

Treatment with 5% CSE resulted in a slight upregulation of endothelial E- and P-selectin **Figure A-2A**, in some cases to a greater extent than TNF-α stimulation. However, relative expression changes were lower than expected. Several experimental parameters may have contributed to low expression levels. It is possible that too few cells were used, CSE concentration was not sufficient to initiate selectin expression, proteins were cleaved or endocytosed after TrypLE incubation, insufficient E/P-selectin antibody was used, or flow cytometer settings were not appropriately optimized. Further work is necessary to parse out the subtleties of these results.

For molecule binding studies, we chose to challenge cells with 10% CSE rather than 5% CSE to create a more acute inflammatory environment, in part due to the lower selectin expression levels observed with 5% CSE. Cells were stimulated with 10% CSE or 10 ng/ml TNF-α for 6 hours in the presence of fluorescently tagged DS or DS-IkL. **Figure A-2** shows DS-IkL exhibited greater binding to both CSE and TNF-α stimulated HPMECs compared to DS controls, suggesting the molecule may have targeting potential in an *in vivo* system.

Next, a pilot study of acute pulmonary inflammation by ozone exposure was conducted. Mice were treated with saline or DS-IkL before and after exposure to either ambient air or 3 ppm ozone for 2 hours.

Immune cell infiltration into the lungs was assessed by analyzing BAL collected 12 hours after exposure. No changes in total cell count or differential immune cell counts were observed in DS-IkL treated mice compared to saline treated mice (**Figure A-3**). Further studies are needed to better understand the outcomes of this pilot study. We speculate that inhaled ozone exposure may cause too severe of an epithelial injury, leading to a robust immune cell influx that is not mediated by endothelial mechanisms under these conditions. Additionally, it is possible that selectins do not mediate neutrophil trafficking in the pulmonary capillaries, particularly alveolar capillaries (29), making acute ozone exposure an incompatible model for testing the efficacy of DS-IkL. Alternative models such as ventilator induced injury (30, 31) should be explored further.

A.5 Conclusions

Smoking remains a leading cause of preventable death in the United States (1). In addition to epithelial damage, acute and chronic cigarette smoke exposure has been shown to promote endothelial dysfunction and pulmonary vascular dysfunction. In this work, we explored the effect cigarette smoke exposed media had on HPMEC viability and selectin expression *in vitro*. Up to 5% CSE was well tolerated by cells and caused a slight upregulation of endothelial selectins. DS-IkL bound to CSE-stimulated HPMECs, suggesting it may have potential as a pulmonary endothelial cell therapeutic. *In vivo* efficacy was tested using inhaled ozone as a model of acute pulmonary inflammation. In these preliminary studies, DS-IkL was not protective against immune cell influx into the lungs. Future work should explore the relative contribution selectins have in immune cell trafficking in this model, as well as alternative models of pulmonary vascular injury.

B: EFFICACY OF DS-IKL AS A TREATMENT FOR ACUTE KIDNEY INJURY

B.1 Introduction

Organ shortage (32), delayed graft function (33), prolonged cold or warm ischemia time (34), and ischemia reperfusion injury (35) continue to pose major clinical challenges for renal transplant efforts. Several preventative methods have been considered to expand the viable donor pool, including donor-targeted therapies (36) and *ex vivo* organ perfusion (32).

Ischemia reperfusion injury (IRI) is an unavoidable complication during renal transplant and can have a lasting impact on organ morbidity and transplant success. The complex physiology of kidney perfusion intensifies tissue damage caused by IRI compared to other organ systems (37). Regional changes in blood flow during an ischemic event exacerbates renal injury caused by the reperfusion phase, causing enhanced endothelial injury, vascular dysfunction, and a heightened inflammatory response. Pro-inflammatory mediators recruit circulating leukocytes to the injured regions, facilitating leukocyte extravasation into the kidney (37). If this cycle perpetuates, inflammatory IRI can progress to chronic kidney disease.

Therapeutics that protect the vasculature from immune cell infiltration could be pivotal in preventing the long-term effects of IRI. We have recently reported on a selectin-targeted glycosaminoglycan-peptide conjugate termed DS-IkL that reduced IRI-induced leukocyte infiltration and cardiac fibrosis after acute myocardial infarction (11). We have shown DS-IkL inhibits neutrophil binding to E-selectin *in* vitro and targets to damaged vasculature *in vivo*.

In this work, we aimed to establish a murine model of acute kidney injury through prolonged warm ischemia time and subsequent IRI (38). A pilot study was performed wherein left kidneys were subjected to 18, 21, or 23 minutes of ischemia with contralateral nephrectomy and treatment with DS-IkL or saline. Changes in serum biomarkers of kidney injury (creatinine, lactate, and glucose) were assessed over a 3-day

reperfusion time. Blood urea nitrogen and pulmonary edema were assessed after three days of reperfusion. Preliminary data suggests DS-IkL is not protective against acute injury under the parameters described.

B.2 Methods

B.2.1 AKI surgery protocol

Male and female 8-11-week-old C57BL6/J mice were purchased from the Jackson Laboratory and acclimated for at least one week before use. Mice were anesthetized using 5% inhaled isoflurane and blood collected via the retroorbital sinus for baseline point of care (POC) measurements. The abdomen was shaved and sanitized with an ethanol-iodine-ethanol wash sequence. Anesthesia was maintained at 1-2% isoflurane for the duration of the surgery. Body temperature was monitored and maintained at 36-38°C.

Abdomens were transected at the midline in two layers and the intestines externalized to expose the renal pedicle. Fat surrounding the pedicles was gently dissected. A nondestructive vascular clamp was placed onto the left renal pedicle for 18, 21, or 23 minutes. Meanwhile, the right renal pedicle and ureter were ligated, and the right kidney removed and placed in formalin for later analysis. In some studies, mice were injected with 50-75 µl of DS-IkL (60 µL), DS (60 µL), or saline i.v. via the inferior vena cava (IVC) 2 minutes before the vascular clamp was removed. A 35-gauge needle atop a 100 µL NonoFil low volume syringe (World Precision Instruments) was used for all IVC injections. After injection, gentle pressure was applied to the IVC until bleeding stopped, approximately 30 s. Intestines were replaced, and 1 mL of sterile pre-warmed saline was injected into the abdominal cavity. Animals were sutured in two layers and monitored until ambulatory. After surgery, mice were recovered under a heat lamp for 1 hour before being placed back into social housing.

At the study endpoints, mice were anesthetized and exsanguinated then perfused through the left ventricle with saline for 2 minutes at 2 mL/min. Perfused kidneys were dissected and fixed in formalin cups. In some experiments, lungs were grossly dissected for edema measurements.

B.2.2 Point of care measurements for serum biomarkers of kidney injury

Point of care measurements and animal weights were taken every 24 hours. Blood was collected from the retroorbital sinus using a heparinized capillary tube. Using a micropipette, blood droplets were placed onto creatinine (mg/dL), lactate (mmol/L), or glucose (mg/dL) test strips and read on Nova Biomedical StatSensor, StatStrip Xpress, and StatStrip Meter Systems, respectively. After each blood draw, mice were injected subcutaneously with 0.5 mL sterile saline. In some cases, creatinine levels were below the detection limit of the point of care device. When this occurred, creatinine was recorded at the lower detection limit, 0.3 mg/dL.

B.2.3 Pulmonary edema

Dissected lungs were placed into pre-weighed glass scintillation vials. Lungs were weighed immediately after dissection (wet weight) and after 3 days in a 200°C oven (dry weight). The ratio of wet:dry weight was taken as a measure of pulmonary edema.

B.2.4 Urine collection

In some experiments, mice were recovered for up to 12 h in social housing before being placed into individual metabolic cages (wire mesh cages with fluid capture trays) for urine collection before surgery and at post-op nights 1 and 2. Urine was collected into conical tubes overnight and frozen for later analysis.

B.2.5 Blood urea nitrogen

Blood was collected from the retroorbital sinus using a heparinized capillary tube into microcentrifuge tube and spun down at 1000 x g for 10 minutes to collect serum. Serum was stored at -

80°C until use. Blood urea nitrogen (BUN) levels were tested using a commercially assay kit (QuantiChrom™ Urea Assay Kit, BioAssay Systems). Samples were thawed then diluted 1:2, 1:10, or 1:30 in ultrapure water. Five microliters of standard or diluted sample were added to a clear flat bottomed 96-well plate in duplicate, followed by 200 µl of working reagent. Wells were gently mixed and incubated for 20 minutes at room temperature before reading optical density at 520 nm on a SpectraMax M5 Microplate Reader (Molecular Devices). Urea concentration was calculated as [Urea] = $OD_{sample} - OD_{blank}$ / $OD_{Standard} - OD_{blank}$ x dilution factor x [STD] (mg/dL). The conversion BUN (mg/dL) = [Urea] / 2.14 was used to calculate BUN concentration.

B.3 Results

B.3.1 Determining warm ischemia time (WIT)

To determine the duration of ischemia time required to elicit kidney injury, the left kidney was subjected to 18, 21, or 23 minutes of warm ischemia time. A nephrectomy was performed on the right kidney within 5 minutes of the start of left kidney ischemia. To remain consistent with later study protocols, mice were injected with 50 ul of sterile saline *via* the IVC immediately after reperfusion. Serum levels of creatinine, glucose, and lactate were measured every 24 hours to assess kidney damage. Mice that received 18 minutes of warm ischemia showed a slight increase in creatinine (**Figure B-1**) after 24 h, but returned to baseline levels after 48 h. However, mice subjected to 21 and 23 minutes of warm ischemia showed spikes in creatinine after 24h (**Figure B-1**), with 21 min WIT trending back down toward baseline after 48 h and 23 min WIT remaining elevated.

Glucose levels remained stable over the 48-h period in mice that received 18 min of WIT, but decreased in the 21-min and 23-min groups (**Figure B-1**). Lactate levels dropped in all groups (**Figure**

B-1). Due to high mortality rates in the 23 min group (data not shown), we decided to move forward with 21 minutes WIT in subsequent studies.

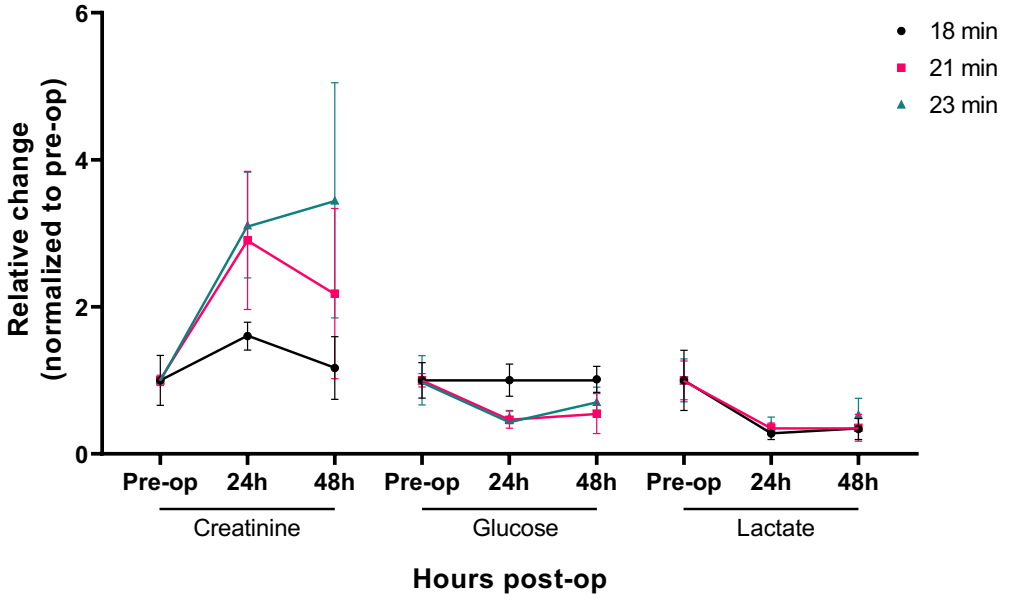

Figure B-1 Point of care readings after 18-, 21-, and 23-min WIT. Creatinine, glucose, and lactate levels were measured in saline treated mice over 2 days post-op. 21 minutes of WIT was chosen for the remainder of the study.

B.3.2 Serum markers of renal damage unaffected by treatment with DS-IkL

Creatinine, lactate, and glucose levels were measured from the blood every 24 hours to detect changes in renal damage. In some cases, serum biomarkers were below the meter system's limit of detection. Therefore, relative changes reported here may not accurately depict absolute changes in serum biomarker levels. As is, levels of all three soluble biomarkers remained statistically similar in all groups over the course of recovery (**Figure B-2 A-C**). DS-IkL treated mice exhibited trends toward increased creatinine levels at POD1 and POD2 compared to saline controls, suggesting that DS-IkL may not protect against fluctuations in creatinine, lactate, or glucose levels in serum after renal ischemia.

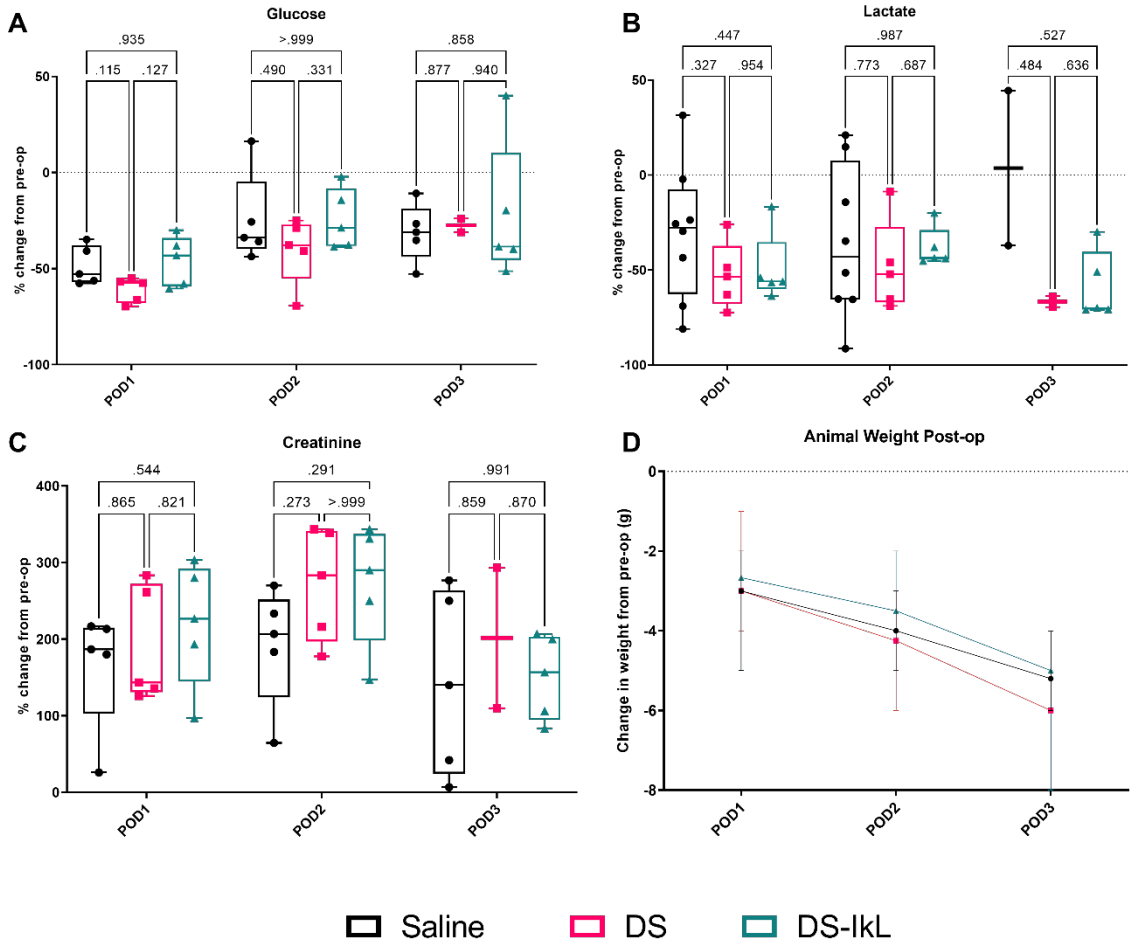

Figure B-2 Change in serum biomarkers and animal weight. Glucose (**A**), lactate (**B**), and creatinine (**C**) levels were measured in saline, DS, or DS-IkL treated mice over a 3-day reperfusion time. Serum biomarkers were statistically similar among all groups. Animal weights were similar over the course of reperfusion for all treatment groups (**D**).

B.3.3 Pulmonary edema reduced in DS-IkL treated mice

Respiratory complications such as pulmonary edema are a common complication of acute kidney injury (39, 40). To test the effect of DS-IkL on pulmonary edema, the wet to dry ratio (wet:dry) and percent weight change of lungs was taken in saline and DS-IkL treated mice at POD3. DS-IkL treated mice had

significantly less water retention in lungs compared to saline mice (**Figure B-3**). Similarly, visual reductions in peripheral edema in the animal hindlimbs over the course of recovery were observed (data not shown). Further exploration into these phenomena, including a potentially protective effect of DS-IkL against pulmonary and peripheral edema and the underlying mechanisms, is needed.

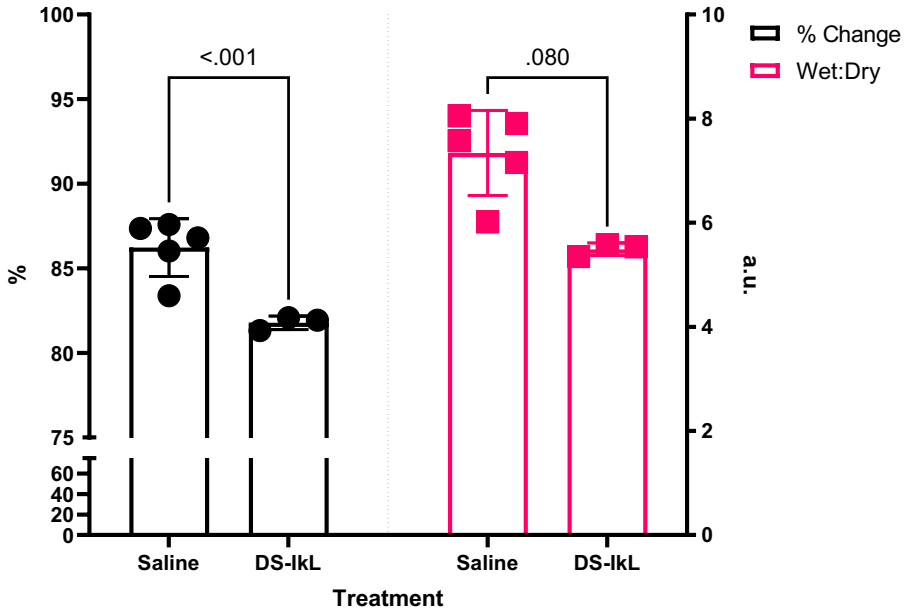

Figure B-3 Pulmonary edema. Treatment with DS-IkL resulted in a reduction in pulmonary edema, as assessed by % change in lung weight and wet to dry ratio. P-values shown are from a one-way ANOVA with post-hoc Tukey test.

B.3.4 Blood urea nitrogen levels elevated in DS-IkL treated mice

To investigate if DS-IkL affects kidney function after AKI, we quantified the levels of urea in the serum of afflicted mice two- or three-days post-op using a blood urea nitrogen (BUN) assay (**Figure B-4**). Data is displayed as both BUN and BUN/creatinine ratio, two methods of clinical reporting for potential AKI (41, 42). DS-IkL treated mice exhibited increased BUN at POD3 compared to saline treated mice

(**Figure B-4 A**). BUN and BUN/creatinine levels were similar for DS-IkL and saline treated mice at POD2. DS-IkL treated sham mice likewise exhibited a high BUN/creatinine ratio at POD3 (**Figure B-4 B**).

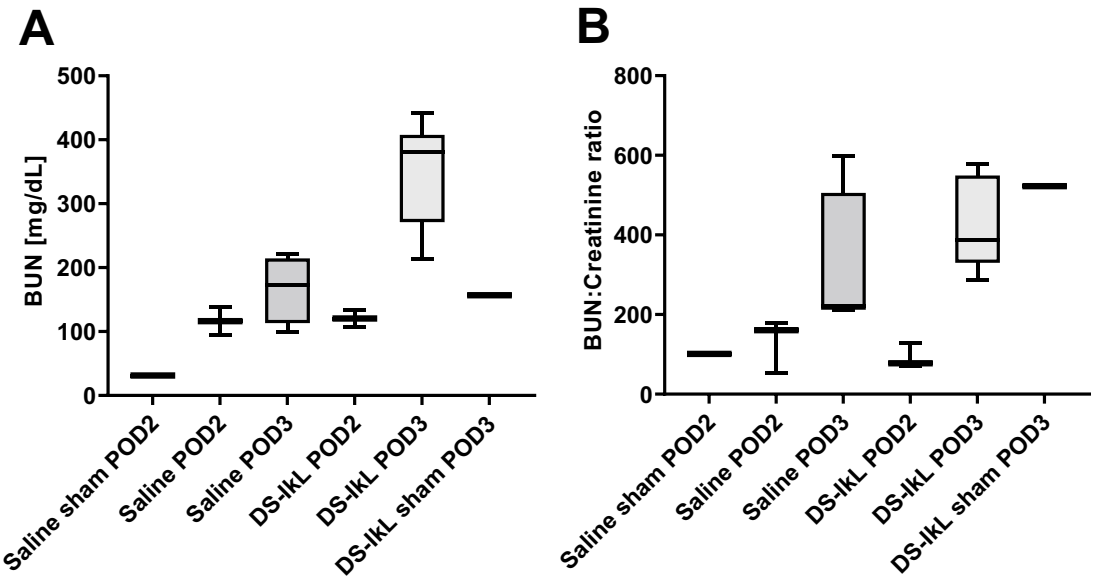

Figure B-4 Blood urea nitrogen (BUN) levels. Treatment with DS-IkL did not protect against elevations in BUN levels (**A**) or BUN/creatinine ratios (**B**) at POD2 or POD3.

B.4 Discussion

Vascular complications make up a significant percentage of postoperative renal transplant complications (43). Downstream consequences of ischemia and ischemia reperfusion injury (IRI) can occur for both the donor kidney and the recipients, thereby playing a role in short- and long-term vascular complications related to transplant. Here we describe a molecule, DS-IkL, as a potential therapeutic after acute renal ischemia reperfusion injury. Previous work with this molecule has shown it is cardioprotective after cardiac IRI in a murine model of ST-elevation myocardial infarction (11). We were therefore interested

in testing the molecule's efficacy in a renal IRI model that recapitulates warm ischemia time experienced by transplant kidneys.

We first set out to optimize warm ischemia time (WIT), recovery time, and time points for serum biomarkers. After several iterations of surgery parameters, we settled on 21 minutes of WIT due to insufficient creatinine elevation after 18 minutes of WIT, and high mortality after 23 minutes WIT. Mice received a single injection of treatment *via* the IVC two minutes before reperfusion such that treatments would immediately circulate into the kidney once the clamp was removed. Since the contralateral kidney was removed prior to injection, we did not anticipate large molecule clearance or loss during the latency time.

Initially, wire mesh metabolic cages were used to collect urine from post-op mice to assess changes in urea excretion after kidney injury. However, urine collection was halted after observing detrimental effects on animal recovery. Metabolic cages put excessive stress on the animals at POD1, leading to increased dehydration, slower recovery time, and increased mortality. This may be in part due to the mouse's inability to thermoregulate properly after long-term isoflurane exposure (38), therefore leading to animals being cold and lethargic after overnight housing in the metabolic cages. In addition, urine collection was inconsistent from animal to animal, perhaps due to animal dehydration or evaporation of the small urine volumes on the large catch plate below the cage. Due to inconsistent urine collection, samples that had been collected were not processed.

When time points were extended past POD3, animal mortality and weight loss increased beyond acceptable levels (data not shown). Therefore, the study endpoint was chosen at POD3. High levels of variation, unpredictable animal survival, and indeterminant data suggest that further optimization of this model is required before conclusions can be made regarding the efficacy of DS-IkL. Future studies should adjust the study parameters until a desired level of endothelial injury is observed before assessing molecule efficacy. As is, the effect of DS-IkL on WIT and renal ischemia reperfusion injury remains undetermined.

B.5 Conclusions

In this study, we describe preliminary efforts at developing a model of severe acute renal injury in C57BL6/J mice and test the efficacy of a selectin-targeted glycan therapeutic designed in the lab, DS-IkL. We showed that, though DS-IkL may provide some protection against edema following AKI, it may not have therapeutic value in the model used here. Serum levels of creatinine, lactate, and glucose were unchanged compared to saline treated controls. Animal weights did not differ between groups over the course of the study. Finally, blood urea nitrogen levels were similarly elevated in all groups. Future studies should emphasize optimizing the study protocol to assess longer-term markers of organ damage and recovery.

C: NEUTROPHIL AND MOLECULE BINDING TO PLATELETS

C.1 Methods

C.1.1 Neutrophil binding to platelets

Ibidi sticky slides VI$^{0.4}$ were adhered to standard microscope slides and channels coated with 75 µg/mL rat tail collagen type-1 at 37°C for 1 hour. During this time, platelet-rich plasma and neutrophils were isolated from whole blood from healthy donors as described previously. Wells were rinsed 3x with DPBS then incubated with 100 µL platelet rich plasma at 37°C for 1 hour. Meanwhile, neutrophils were stained with CellTracker Green (ThermoFisher; final concentration of 3 µM for 30 minutes at RT with end-over-end rotation). Platelet-coated wells were rinsed 3x with DPBS and stained with CellTracker Red (3 µM for 30 minutes at RT), then fixed for 10 minutes at RT with 4% PFA in PBS. After 3 washes, 100 µL of stained neutrophil suspensions were added to individual channels at increasing concentrations (0-400,000 cells/mL). Chips were left rocking at RT for 30 minutes, washed 3x with HBSS$^{+/+}$ with 0.4% HSA and 20 mM HEPES, then imaged on a Keyence BZ-X700 microscope. Neutrophil binding was quantified in ImageJ as mean fluorescence intensity (mean grey value) over a 45.059 square inch area.

C.1.2 Molecule binding to platelets

Ibidi µ-slides VI$^{0.1}$ were coated with fibrillar collagen type-1 (50 µg/ml in saline) for at least 30 minutes at room temperature then washed 3x with DPBS. Platelets were isolated according to standard Abcam protocols. Briefly, citrate-buffered whole blood was centrifuged at 200 x g for 20-25 minutes at RT with no brake. The top platelet-rich plasma layer was collected and diluted 1:1 with HEP buffer (140 mM NaCl, 2.7 mM KCl, 3.8 mM HEPES, 5 mM EGTA, pH 7.4) with 1 µM prostaglandin E1 and further centrifuged at 100 x g for 15 minutes at RT with no brake. The supernatant was collected and centrifuged at 800 x g for 15 minutes at RT with no brake. The supernatant was aspirated and the remaining platelet pellet was resuspended in Tyrode's buffer (134 mM NaCl, 12 mM $NaHCO_3$, 2.9 mM KCl, 0.34 mM

Na_2HPO_4, 1 mM $MgCl_2$, 1 mM $CaCl_2$, 10 mM HEPES, pH 7.4). and stained with 3 μM calcein-AM (ThermoFisher) for 30-45 minutes at 37°C. Calcein-labeled platelet suspensions were further diluted to 10^8 cells/ml and 60 μL added to each microchannel. Chips were incubated for 1 hour in a cell culture incubator then carefully washed 3x with 50 μL HEPES-buffered Tyrode's Buffer with calcium and magnesium. CF633-tagged molecules were dissolved at 60 μM in Tyrode's buffer with ions and added to individual wells (40 μL per channel), then incubated for 1 hour in a cell culture incubator. Channels were washed 3x with Tyrode's buffer, fixed for 20 minutes at RT with 4% PFA in PBS, then rinsed 3x in DPBS before overnight storage. The next day, channels were rinsed an additional time and imaged on a Keyence BZ-X700 all-in-one fluorescence microscope (Keyence). Images were analyzed in ImageJ by quantifying median CF633 fluorescence that colocalized with calcein-AM (platelet)-positive regions of interest. Values were normalized to vehicle treated groups. Experiments were repeated three independent times for an n=3. Statistics were conducted using a one-way ANOVA with post-hoc Tukey's test. P-values less than 0.05 were considered significant.

C.2 Results

C.2.1 Neutrophils binding to platelets

During severe inflammatory injury the vascular endothelial lining can be denuded, exposing the underlying collagen-rich extracellular matrix. Circulating platelets adhere to this collagen-rich surface and activate, leading to the upregulation of P-selectin molecules on the platelet surface. As discussed in Chapter 4, platelet P-selectin can facilitate neutrophil tethering and additional thromboinflammatory events. To first validate that isolated human neutrophils tether to collagen-bound platelets, fluorescently tagged neutrophils were incubated with immobilized platelets in microfluidic channels. Bidirectional shear was used to create an environment that enables neutrophil rolling. After one hour, channels were

rinsed with cell-free buffer and overall cell binding visualized using a fluorescence microscope. **Figure C-1A** shows that neutrophil binding to platelet surfaces increased with neutrophil concentration.

C.2.2 Molecule binding to platelets

To test molecule binding to collagen-activated platelets, we immobilized platelets on microfluidic channels pre-coated with fibrillar collagen type-1 prior to incubation with fluorescently tagged molecules. In these preliminary experiments, we observed a significant increase in DS-IkL binding to regions with immobilized platelets compared to both vehicle-treated controls and DS-treated channels (**Figure C-1B**). Additional studies investigating the effect of our molecule on neutrophil binding to platelet-rich surfaces are needed to determine the efficacy of DS-IkL in reducing neutrophil-platelet complex formation under flow.

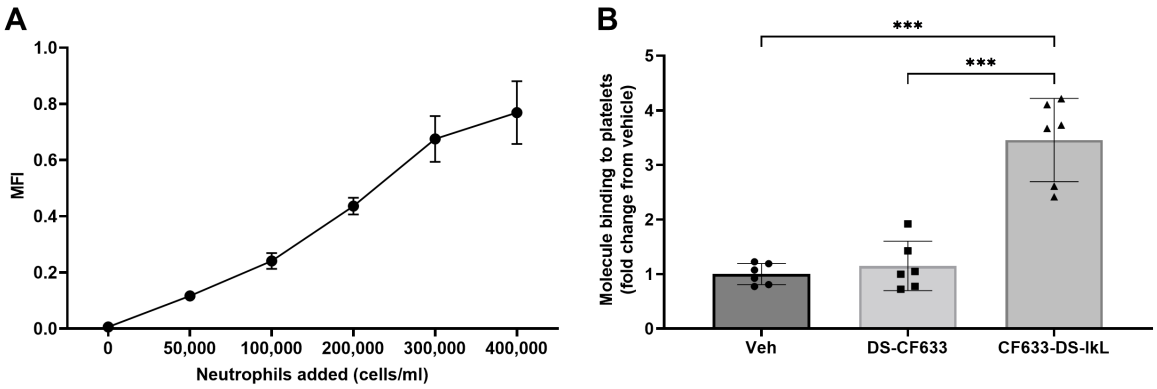

Figure C-1 Neutrophil and molecule binding to platelets. Neutrophil binding to platelet-rich channels increased with neutrophil concentration (**A**). DS-IkL exhibited significantly more binding to platelet-rich channels compared to Vehicle or DS-treated groups (**B**). Data represented as means ± SD for 2-4 independent experiments. *** $p < 0.001$.

D: References

1. Jha P, Ramasundarahettige C, Landsman V, Rostron B, Thun M, Anderson RN, et al. 21st-Century Hazards of Smoking and Benefits of Cessation in the United States. New England Journal of Medicine. 2013;368(4):341-50.
2. Speaks M. Health United States Report 2016. 2016.
3. Hurst JR, Donaldson GC, Quint JK, Goldring JJP, Baghai-Ravary R, Wedzicha JA. Temporal Clustering of Exacerbations in Chronic Obstructive Pulmonary Disease. American Journal of Respiratory and Critical Care Medicine. 2009;179(5):369-74.
4. McDonald VM, Higgins I, Wood LG, Gibson PG. Multidimensional assessment and tailored interventions for COPD: respiratory utopia or common sense? Thorax. 2013;68(7):691 LP-4.
5. Zuo W, Zhang T, Wu DZA, Guan SP, Liew A-A, Yamamoto Y, et al. p63+Krt5+ distal airway stem cells are essential for lung regeneration. Nature. 2014;517(7536):616-20.
6. Lapperre TS, Postma DS, Gosman MME, Snoeck-Stroband JB, ten Hacken NHT, Hiemstra PS, et al. Relation between duration of smoking cessation and bronchial inflammation in COPD. Thorax. 2006;61(2):115 LP-21.
7. Sinden NJ, Stockley RA. Systemic inflammation and comorbidity in COPD: a result of 'overspill' of inflammatory mediators from the lungs? Review of the evidence. Thorax. 2010;65(10):930 LP-6.
8. Yang Q, Underwood M, Hsin M, Liu X-C, He G-W. Dysfunction of Pulmonary Vascular Endothelium in Chronic Obstructive Pulmonary Disease: Basic Considerations for Future Drug Development. Current Drug Metabolism. 2008;9(7):661-7.
9. Stockley RA. Neutrophils and the Pathogenesis of COPD. Chest. 2002;121(5):151S-5S.
10. Wodicka JR, Morikis VA, Dehghani T, Simon SI, Panitch A. Selectin-Targeting Peptide-Glycosaminoglycan Conjugates Modulate Neutrophil-Endothelial Interactions. Cell Mol Bioeng. 2019;12(1):121-30.
11. Dehghani T, Thai PN, Sodhi H, Ren L, Sirish P, Nader CE, et al. Selectin-Targeting Glycosaminoglycan-Peptide Conjugate Limits Neutrophil Mediated Cardiac Reperfusion Injury. Cardiovasc Res. 2020.
12. Wiedeman JA, Kaul R, Heuer LS, Thao NN, Pinkerton KE, Wenman WM. Tobacco smoke induces persistent infection of Chlamydophila pneumoniae in HEp-2 cells. Microb Pathog. 2004;37(3):141-8.
13. Wiegman Coen H, Li F, Clarke Colin J, Jazrawi E, Kirkham P, Barnes Peter J, et al. A comprehensive analysis of oxidative stress in the ozone-induced lung inflammation mouse model. Clinical Science. 2013;126(6):425-40.
14. Teague SV, Pinkerton KE, Goldsmith M, Gebremichael A, Chang S, Jenkins RA, et al. Sidestream cigarette smoke generation and exposure system for environmental tobacco smoke studies. Inhalation Toxicology. 1994;6(1):79-93.
15. Lu Q, Gottlieb E, Rounds S. Effects of cigarette smoke on pulmonary endothelial cells. American Journal of Physiology-Lung Cellular and Molecular Physiology. 2018;314(5):L743-L56.
16. Morris A, Kinnear G, Wan W-YH, Wyss D, Bahra P, Stevenson CS. Comparison of cigarette smoke-induced acute inflammation in multiple strains of mice and the effect of a matrix metalloproteinase inhibitor on these responses. The Journal of pharmacology and experimental therapeutics. 2008;327(3):851-62.
17. Vlahos R, Bozinovski S, Jones JE, Powell J, Gras J, Lilja A, et al. Differential protease, innate immunity, and NF-κB induction profiles during lung inflammation induced by subchronic cigarette smoke exposure in mice. American Journal of Physiology-Lung Cellular and Molecular Physiology. 2006;290(5):L931-L45.
18. Gotsch U, Jäger U, Dominis M, Vestweber D. Expression of P-selectin on endothelial cells is upregulated by LPS and TNF-alpha in vivo. Cell Adhes Commun. 1994;2(1):7-14.
19. Wyble CW, Hynes KL, Kuchibhotla J, Marcus BC, Hallahan D, Gewertz BL. TNF-alpha and IL-1 upregulate membrane-bound and soluble E-selectin through a common pathway. J Surg Res. 1997;73(2):107-12.
20. Sokolowska M, Quesniaux VFJ, Akdis CA, Chung KF, Ryffel B, Togbe D. Acute Respiratory Barrier Disruption by Ozone Exposure in Mice. Frontiers in Immunology. 2019;10(2169).
21. Gross KB, White HJ, Sargent NE. The effect of ozone inhalation on metabolic functioning of vascular endothelium and on ventilatory function. Toxicology and Applied Pharmacology. 1991;109(2):336-51.
22. Robertson S, Colombo ES, Lucas SN, Hall PR, Febbraio M, Paffett ML, et al. CD36 Mediates Endothelial Dysfunction Downstream of Circulating Factors Induced by O3 Exposure. Toxicological Sciences. 2013;134(2):304-11.

23. Hillas G, Perlikos F, Tzanakis N. Acute exacerbation of COPD: is it the "stroke of the lungs"? International journal of chronic obstructive pulmonary disease. 2016;11:1579-86.
24. Hoenderdos K, Condliffe A. The Neutrophil in Chronic Obstructive Pulmonary Disease. Too Little, Too Late or Too Much, Too Soon? American Journal of Respiratory Cell and Molecular Biology. 2013;48(5):531-9.
25. Viniol C, Vogelmeier CF. Exacerbations of COPD. European respiratory review : an official journal of the European Respiratory Society. 2018;27(147):170103-.
26. Wedzicha JA, Mackay AJ, Singh R. COPD exacerbations: impact and prevention. Breathe. 2013;9(6):434-40.
27. Kierstein S, Poulain FR, Cao Y, Grous M, Mathias R, Kierstein G, et al. Susceptibility to ozone-induced airway inflammation is associated with decreased levels of surfactant protein D. Respiratory research. 2006;7(1):85-.
28. Harris KK, Zopey M, Friedman TC. Metabolic effects of smoking cessation. Nat Rev Endocrinol. 2016;12(5):299-308.
29. Mizgerd JP, Meek BB, Kutkoski GJ, Bullard DC, Beaudet AL, Doerschuk CM. Selectins and neutrophil traffic: margination and Streptococcus pneumoniae-induced emigration in murine lungs. J Exp Med. 1996;184(2):639-45.
30. Curley GF, Laffey JG, Zhang H, Slutsky AS. Biotrauma and Ventilator-Induced Lung Injury: Clinical Implications. Chest. 2016;150(5):1109-17.
31. Li H, Pan P, Su X, Liu S, Zhang L, Wu D, et al. Neutrophil Extracellular Traps Are Pathogenic in Ventilator-Induced Lung Injury and Partially Dependent on TLR4. BioMed research international. 2017;2017:8272504-.
32. Kabagambe SK, Palma IP, Smolin Y, Boyer T, Palma I, Sageshima J, et al. Combined Ex Vivo Hypothermic and Normothermic Perfusion for Assessment of High-risk Deceased Donor Human Kidneys for Transplantation. Transplantation. 2019;103(2):392-400.
33. Irish WD, Ilsley JN, Schnitzler MA, Feng S, Brennan DC. A risk prediction model for delayed graft function in the current era of deceased donor renal transplantation. Am J Transplant. 2010;10(10):2279-86.
34. Kaminska D, Koscielska-Kasprzak K, Chudoba P, Halon A, Mazanowska O, Gomolkiewicz A, et al. The influence of warm ischemia elimination on kidney injury during transplantation - clinical and molecular study. Sci Rep. 2016;6:36118.
35. Salvadori M, Rosso G, Bertoni E. Update on ischemia-reperfusion injury in kidney transplantation: Pathogenesis and treatment. World J Transplant. 2015;5(2):52-67.
36. Palmisano A, Gandolfini I, Delsante M, Cantarelli C, Fiaccadori E, Cravedi P, et al. Acute Kidney Injury (AKI) before and after Kidney Transplantation: Causes, Medical Approach, and Implications for the Long-Term Outcomes. J Clin Med. 2021;10(7):1484.
37. Munshi R, Hsu C, Himmelfarb J. Advances in understanding ischemic acute kidney injury. BMC Med. 2011;9:11-.
38. Au - Hesketh EE, Au - Czopek A, Au - Clay M, Au - Borthwick G, Au - Ferenbach D, Au - Kluth D, et al. Renal Ischaemia Reperfusion Injury: A Mouse Model of Injury and Regeneration. JoVE. 2014(88):e51816.
39. Faubel S. Pulmonary complications after acute kidney injury. Adv Chronic Kidney Dis. 2008;15(3):284-96.
40. Faubel S, Edelstein CL. Mechanisms and mediators of lung injury after acute kidney injury. Nature Reviews Nephrology. 2016;12(1):48-60.
41. Manoeuvrier G, Bach-Ngohou K, Batard E, Masson D, Trewick D. Diagnostic performance of serum blood urea nitrogen to creatinine ratio for distinguishing prerenal from intrinsic acute kidney injury in the emergency department. BMC Nephrology. 2017;18(1):173.
42. Uchino S, Bellomo R, Goldsmith D. The meaning of the blood urea nitrogen/creatinine ratio in acute kidney injury. Clinical kidney journal. 2012;5(2):187-91.
43. Reyna-Sepúlveda F, Ponce-Escobedo A, Guevara-Charles A, Escobedo-Villarreal M, Pérez-Rodríguez E, Muñoz-Maldonado G, et al. Outcomes and Surgical Complications in Kidney Transplantation. Int J Organ Transplant Med. 2017;8(2):78-84.